UNIVERSIDADE ESTADUAL PAULISTA
"JÚLIO DE MESQUITA FILHO"
Câmpus de São José do Rio Preto

Gabriela Miranda Ayusso

Síntese e Avaliação de Análogos Monocetônicos de Curcumina como Potenciais Agentes contra a Tuberculose

São José do Rio Preto
2019

Gabriela Miranda Ayusso

Síntese e Avaliação de Análogos Monocetônicos de Curcumina como Potenciais Agentes contra a Tuberculose

Dissertação apresentada como parte dos requisitos para obtenção do título de Mestre em Microbiologia, junto ao Programa de Pós-Graduação em Microbiologia, do Instituto de Biociências, Letras e Ciências Exatas da Universidade Estadual Paulista "Júlio de Mesquita Filho", Câmpus de São José do Rio Preto.

Financiadora: FAPESP – Proc. 2017/08383-7
CAPES

Orientador: Prof. Dr. Luis Octávio Regasini

Coorientador: Prof. Dr. Fernando Rogério Pavan

São José do Rio Preto

2019

Ayusso, Gabriela Miranda.
Síntese e avaliação de análogos monocetônicos de curcumina como potenciais agentes contra a tuberculose / Gabriela Miranda Ayusso. – São José do Rio Preto, 2019
171 f.: il., tabs.

Orientador: Luis Octávio Regasini
Coorientador: Fernando Rogério Pavan
Dissertação (mestrado) – Universidade Estadual Paulista (Unesp), Instituto de Biociências, Letras e Ciências Exatas, São José do Rio Preto

1. Microbiologia. 2. Tuberculose. 3. Mycobacterium tuberculosis. 4. Curcumina. 5. Antibacterianos. I. Título.

CDU – 576.8

Ficha catalográfica elaborada pela Biblioteca do IBILCE
UNESP - Câmpus de São José do Rio Preto

Gabriela Miranda Ayusso

Síntese e Avaliação de Análogos Monocetônicos de Curcumina como Potenciais Agentes contra a Tuberculose

Dissertação apresentada como parte dos requisitos para obtenção do título de Mestre em Microbiologia, junto ao Programa de Pós-Graduação em Microbiologia, do Instituto de Biociências, Letras e Ciências Exatas da Universidade Estadual Paulista "Júlio de Mesquita Filho", Câmpus de São José do Rio Preto.

Financiadora: FAPESP – Proc. 2017/08383-7
CAPES

Comissão Examinadora

Prof. Dr. Luis Octávio Regasini
UNESP – Câmpus de São José do Rio Preto
Orientador

Profa. Dra. Katiany Rizzieri Caleffi Ferracioli
UEM – Maringá

Profa. Dra. Carolina Colombelli Pacca Mazaro
UNESP – Câmpus de São José do Rio Preto

São José do Rio Preto

13 de fevereiro de 2019

DEDICATÓRIA

Dedico esse trabalho aos meus pais, ***Sueli Benedita Miranda Ayusso*** *e* ***Benedito Donizetti de Jesus Ayusso****, que, durante toda a minha vida, depositaram grande esforço na minha formação. São eles que sempre me incentivaram a lutar pelos meu sonhos, me ensinando a dar o melhor de mim em tudo que faço.*

AGRADECIMENTOS

À **Deus**, pela vida, pelas conquistas, por me dar força nos momentos mais difíceis e por me proporcionar o convívio com pessoas tão especiais. Agradeço por me dar a força necessária para lutar pelos meus sonhos, mesmo com as dificuldades.

Ao meu orientador, **Prof. Dr. Luis Octávio Regasini**, por me acolher desde do primeiro ano de Graduação e por ter acreditado e confiado no meu trabalho. Agradeço pelas lições e ensinamentos sobre a ciência e sobre a vida e por sempre nos incentivar a utilizar nosso conhecimento em prol da sociedade. Obrigada por ser, além de orientador, um amigo e um pai acadêmico durante esses anos.

Ao meu coorientador, **Prof. Dr. Fernando Rogério Pavan**, por me receber em seu laboratório e por me fornecer todo o suporte necessário para a realização dos experimentos biológicos. Agradeço pela contribuição no meu conhecimento científico acerca da tuberculose.

Aos meus pais, **Sueli** e **Benedito**, pelo amor, pelo carinho, por apoiarem as minhas decisões, pelas lições e ensinamentos sobre a vida e por me segurarem nos momentos mais difíceis. Agradeço imensamente por todo o esforço que depositaram na minha formação, por sempre me incentivarem a lutar pelos meus objetivos e por sempre acreditarem e confiarem em mim. Obrigada por tudo!

Ao meu namorado, **Caique**, pelo companheirismo, pelo amor, pelas conversas sobre a vida e pelas palavras de conforto nesses oito anos. Agradeço por estar ao meu lado tanto nos momentos bons quanto ruins, por apoiar e entender as minhas decisões e por me proporcionar tantos momentos felizes. Obrigada por ser, além de namorado, um amigo.

À minha tia, **Izilda**, e aos meus primos, **Graziela** e **Gabriel**, pelo apoio, pelo amor, pelo carinho e por todo o auxílio que sempre me proporcionaram. Agradeço principalmente por todo o amparo que me deram quando cheguei em São José do Rio Preto para iniciar a graduação no IBILCE e por serem tão atenciosos quando preciso de ajuda. Obrigada por estarem sempre ao meu lado.

À todas as pessoas que estão e já passaram pelo **Laboratório de Antibióticos e Quimioterápicos (LAQ)**, por todo o auxílio no cotidiano laboratorial e pela contribuição no meu conhecimento científico. Agradeço, em especial, à **Mariana**, **Carlos**, **Beatriz**,

Mayara, **Éder**, **Guilherme**, **Ana**, **Daiane**, **Caroline**, **Thaíse**, **Valéria**, **Isabelle**, **Matheus** e **Ricardo**, pela amizade, pelo apoio, pela ajuda, pelas conversas e pelos momentos de diversão. Jamais esquecerei vocês!

Às minhas amigas de graduação, **Gabrielle** e **Beatriz**, por me proporcionarem tantos momentos bons durante a graduação e por estarmos sempre juntas, principalmente nos momentos difíceis. Agradeço pelo companheirismo e pelos momentos de descontração. Obrigada pela amizade, meninas.

Às minhas amigas e colegas de quarto, **Mayara**, **Adriana**, **Amanda** e **Sandyelle**, pelo carinho, pelo zelo e pela cumplicidade. Agradeço por serem uma família para mim e por fazerem os meus dias de semana melhores. Estarei sempre torcendo pela felicidade de vocês.

À **Ma. Débora L. Campos**, **Ma. Mariana C. Solcia** e **Ma. Camila M. Ribeiro**, pelo acolhimento durante minha estadia no Laboratório de Tuberculose, Faculdade de Ciências Farmacêuticas, UNESP/Araraquara. Agradeço pelos ensinamentos e por toda a assistência durante a realização dos ensaios de atividade antimicobacteriana e citotóxica.

Ao **Prof. Dr. Pedro L. Rosalen**, por ceder seu laboratório e fornecer o suporte necessário para a realização do ensaio de toxicidade *in vivo* em *Galleria mellonella*. À **Dra. Janaina C. O. Sardi**, pela realização do experimento e por mostrar-se sempre solicita.

À **Profa. Dra. Eleni Gomes**, por todo suporte oferecido nas análises de Cromatografia Líquida de Alta Eficiência com Detecção por Arranjo de Fotodiodos (CLAE-DAD). Ao **Me. Diego A. Monteiro**, pelo auxílio durante o experimento.

Ao **Centro Multiusuário de Inovação Biomolecular**, Instituto de Biociências, Letras e Ciências Exatas, UNESP/São José do Rio Preto (FAPESP – Processo nº 2009/53989-4), pela utilização dos espectrômetros Bruker Avance III 9,397 T (400 MHz) e 14,095 T (600 MHz). Ao **Laboratório-II de Ressonância Magnética Nuclear**, Instituto de Química, UNESP/Araraquara, pela utilização do espectrômetro Bruker Fourier (300 MHz).

Ao **Instituto de Biociências, Letras e Ciências Exatas (IBILCE)**, por fazer parte da minha história e por ser minha segunda casa durante todos esses anos. Agradeço, em especial, à todos os **docentes** do IBILCE e do **Programa de Pós-graduação em**

Microbiologia que fizeram parte da minha formação, por transmitirem seus conhecimentos com dedicação e por sempre estarem preocupados com a aprendizagem dos discentes. Obrigada por contribuirem no conhecimento que tenho hoje.

À **Fundação de Amparo à Pesquisa do Estado de São Paulo (FAPESP)**, pelas duas bolsas de Iniciação Científica concedidas durante a graduação (Processo nº 2014/18719-4 e 2016/07108-0) e pela bolsa concedida durante o Mestrado (Processo nº 2017/08383-7) para a realização do presente trabalho.

O presente trabalho foi realizado com apoio da **Coordenação de Aperfeiçoamento de Pessoal de Nível Superior – Brasil (CAPES)** – Código de Financiamento 001.

À **Comissão Examinadora**, pela disponibilidade e aceite em tornar esse trabalho mais completo.

“A tarefa não é tanto ver aquilo que ninguém viu, mas pensar o que ninguém ainda pensou sobre aquilo que todo mundo vê.” (Arthur Schopenhauer)

RESUMO

A tuberculose (TB) é a décima principal causa de morte no mundo. As características morfo-fisiológicas peculiares de *Mycobacterium tuberculosis*, o principal agente etiológico da TB, e o surgimento de cepas resistentes aos fármacos atuais representam grandes desafios no desenvolvimento de fármacos contra a TB. Os produtos naturais desempenham um importante papel na descoberta de novos fármacos. A curcumina está presente nos rizomas do açafrão e demonstra diversas bioatividades, incluindo antibacteriana. Essa substância apresenta limitações que impedem o seu uso como agente terâpeutico, relacionadas principalmente à subunidade β-dicêtonica de sua estrutura. O objetivo do presente trabalho foi sintetizar e avaliar a atividade anti-TB, a toxicidade e as propriedades farmacocinéticas *in silico* de análogos monocetônicos de curcumina. Duas séries de análogos de curcumina com a subunidade β-dicêtonica substituída por um grupo monocarbonílico foram sintetizadas. A curcumina e seus análogos foram avaliados contra *M. tuberculosis* H37Rv. A substituição da subunidade β-dicêtonica por um grupo monocarbonílico e a presença de heteroátomos e do grupo nitro potencializou o efeito antimicobacteriano. As substâncias que demonstraram concentração inibitória mínima para 90% (CIM_{90}) < 85 μM foram submetidas a ensaios de toxicidade contra fibroblastos de pulmão humano MRC-5 e macrófagos murinos J774A.1 para determinação da concentração inibitória para 50% (CI_{50}) e do índice de seletividade (IS). De modo geral, os análogos exibiram menor toxicidade e maior seletividade para macrófagos do que fibroblastos de pulmão. As substâncias que apresentaram IS ≥ 10 foram analisadas contra isolados clínicos de *M. tuberculosis* com resistência a diferentes fármacos anti-TB. A atividade dos análogos **7**, **8**, **13**, **15–17**, **27** e **28** contra três isolados clínicos sugeriu que essas substâncias provavelmente apresentam mecanismo de ação diferenciado. Além de demonstrar maior atividade anti-TB contra *M. tuberculosis* H37Rv, o análogo **28** foi o mais seletivo para fibroblastos de pulmão e macrófagos. Essa substância não apresentou antagonismo com a rifampicina e a moxifloxacina e não demonstrou toxicidade *in vivo* significativa em *Galleria mellonella*, indicando seu potencial uso seguro no cenário clínico. Estudos *in silico* indicaram que os análogos bioativos são potenciais candidatos a fármacos por administração oral. Portanto, nosso estudo estabeleceu dados preliminares de relação estrutura-atividade, além de identificar análogos monocetônicos de curcumina como promissores candidatos a fármacos contra a TB.

Palavras-chave: tuberculose, curcumina, análogos, anti-TB, seletividade

ABSTRACT

Tuberculosis (TB) is the tenth leading cause of death in the world. The peculiar morpho-physiological features of *Mycobacterium tuberculosis*, the main etiological agent of TB, and the emergence of drug resistant strains represent major challenges in the development of drugs against TB. Natural products play an important role in the discovery of new drugs. Curcumin is present in the turmeric rhizomes and demonstrates several bioactivities, including antibacterial. This compound has limitations that prevent its use as therapeutical agent, mainly related to the β-diketone moiety of its structure. The aim of present study was to synthesize and evaluate the anti-TB activity, the toxicity and the *in silico* pharmacokinetic properties of monocarbonyl analogues of curcumin. Two series of curcumin analogues with the β-diketone moiety replaced by a monocarbonyl group were synthesized. The curcumin and its analogues were evaluated against *M. tuberculosis* H37Rv. The replacement of β-diketone moiety by a monocarbonyl group and the presence of heteroatoms and the nitro group improved the antimycobacterial effect. The compounds which demonstrated minimum inhibitory concentration for 90% (MIC_{90}) < 85 μM were subjected to toxicity tests against human lung fibroblasts MRC-5 and murine macrophages J774A.1 to determine the inhibitory concentration for 50% (IC_{50}) and the selectivity index (SI). In general, the analogues displayed lower toxicity and higher selectivity for macrophages than lung fibroblasts. The compounds with SI ≥ 10 were analysed against clinical isolates of *M. tuberculosis* with resistance to different anti-TB drugs. The activity of analogues **7**, **8**, **13**, **15–17**, **27** and **28** against three clinical isolates suggested that these compounds probably have a differentiated action mechanism. In addition to demonstrate highest anti-TB activity against *M. tuberculosis* H37Rv, the analogue **28** was the most selective for lung fibroblasts and macrophages. This compound did not present antagonism with rifampicin and moxifloxacin and did not demonstrate significant *in vivo* toxicity in *Galleria mellonella*, indicating its potential safe use in the clinical setting. *In silico* studies indicated that bioactive analogues are potential drugs candidates by oral administration. Therefore, our study established preliminary structure-activity relationship data, besides to identify monocarbonyl analogues of curcumin as promising drugs candidates against TB.

Keywords: tuberculosis, curcumin, analogues, anti-TB, selectivity

LISTA DE FIGURAS

Capítulo I

Capítulo II

LISTA DE ESQUEMAS

Capítulo II

LISTA DE TABELAS

Capítulo II

LISTA DE ABREVIATURAS E SIGLAS

λ_{max}: wavelength with maximum absorption

^{1}H NMR: nuclear magnetic resonance of hydrogen

^{13}C NMR: nuclear magnetic resonance of thirteen carbon

AIDS: acquired immunodeficiency syndrome

ADME: absorption, distribution, metabolism and excretion

ATP: adenosina trifosfato

BBB: blood-brain barrier

BCG: *Bacilo de Calmette-Guérin*

br s: broad singlet

$CDCl_3$: deuterated chloroform

CF: Clemente Ferreira

CFU/mL: colony-forming unities per mL

CI_{50}: concentração inibitória para 50%

CIM: concentração inibitória mínima

CIM_{90}: concentração inibitória mínima para 90%

d: doublet

dd: doublet of doublets

ddd: doublet of doublet of doublets

DMEM: *Dulbecco's Modified Eagle's Medium*

DMSO: dimethylsulfoxide

DMSO-d_6: hexadeuterated dimethylsulfoxide

DZG: dehydrozingerone

EMA: *European Medicines Agency*

FDA: *Food and Drug Administration*

FICI: fractional inhibitory concentration index

HBA: number of hydrogen bond acceptors

HBD: number of hydrogen bond donors

HIA: human intestinal absorption

HIV: human immunodeficiency virus

HPLC-PAD: high performance liquid chromatography with photodiode array detection

IC_{50}: inhibitory concentration for 50%

IFN-γ: interferon-γ

IS: índice de seletividade

J: constante de acoplamento

LD_{50}: lethal dose for 50%

log *K*: capacity factor

log $P_{o/a}$: coeficiente de partição *n*-octanol/água

log $P_{o/w}$: partition coefficient *n*-octanol/water

m: multiplet

MDR: multi drug resistant

MIC_{90}: minimum inhibitory concentration for 90%

MRSA: methicilin resistant *Staphylococcus aureus*

MSSA: methicilin susceptible *Staphylococcus aureus*

MW: molecular weight

NROTB: number of routable bonds

OADC: oleic acid, albumin, dextrose and catalase

OMS: Organização Mundial de Saúde

ONU: Organização das Nações Unidas

REDCA: *Resazurin Drugs Combination Microtiter Assay*

REMA: *Resazurin Microtiter Assay*

RPMI: *Roswell Park Memorial Institute*

s: singlet

SI: selectivity index

TB: tuberculose

TDR: totally drug resistant

TLC: thin-layer chromatography

TNF-α: tumor necrosis factor-α

WHO: World Health Organization

XDR: extensively drug resistant

SUMÁRIO

Capítulo I

1. INTRODUÇÃO E REVISÃO BIBLIOGRÁFICA

1.1. Epidemiologia da Tuberculose (TB)

A tuberculose (TB) é uma doença que afeta os seres humanos há milhares de anos, sendo considerada um grave problema de saúde pública. No ano de 1993, a Organização Mundial de Saúde (OMS) declarou que a TB deveria ser tratada como um problema emergencial de saúde global. Atualmente, a TB é a décima principal causa de morte no mundo e, desde 2011, a doença causada por um único agente infeccioso que promove a mais alta mortalidade no mundo, ultrapassando a Síndrome da Imunodeficiência Adquirida (AIDS) (WHO, 2018).

De acordo com a OMS, 10 milhões de novos casos mundiais de TB foram relatados no ano de 2017, sendo 90% adultos (idade igual ou superior a 15 anos), 64% homens e 9% pessoas soropositivas ao vírus da imunodeficiência humana (HIV). No mesmo ano, foram registrados 1,6 milhões de óbitos causados por TB, dos quais cerca de 300 mil foram de pacientes co-infectados pelo HIV (WHO, 2018).

As maiores taxas de incidência de TB, em 2017, foram relacionadas ao sudeste asiático (44%), ao continente africano (25%) e ao Pacífico Ocidental (18%). Trinta países, incluindo o Brasil, foram responsáveis por 87% dos casos incidentes de TB. Entre esses países, aproximadamente 2/3 dos novos casos de TB ocorreram na Índia (27%), China (9%), Indonésia (8%), Filipinas (6%), Paquistão (5%), Nigéria (4%), Bangladesh (4%) e África do Sul (3%) (Figura 1, p. 27). A maioria dos casos de TB com co-infecção por HIV concentraram-se em países do continente africano, ultrapassando 50% em regiões da África do Sul (WHO, 2018).

Figura 1. Número de casos mundiais incidentes de TB no ano de 2017. Fonte: WHO, 2018

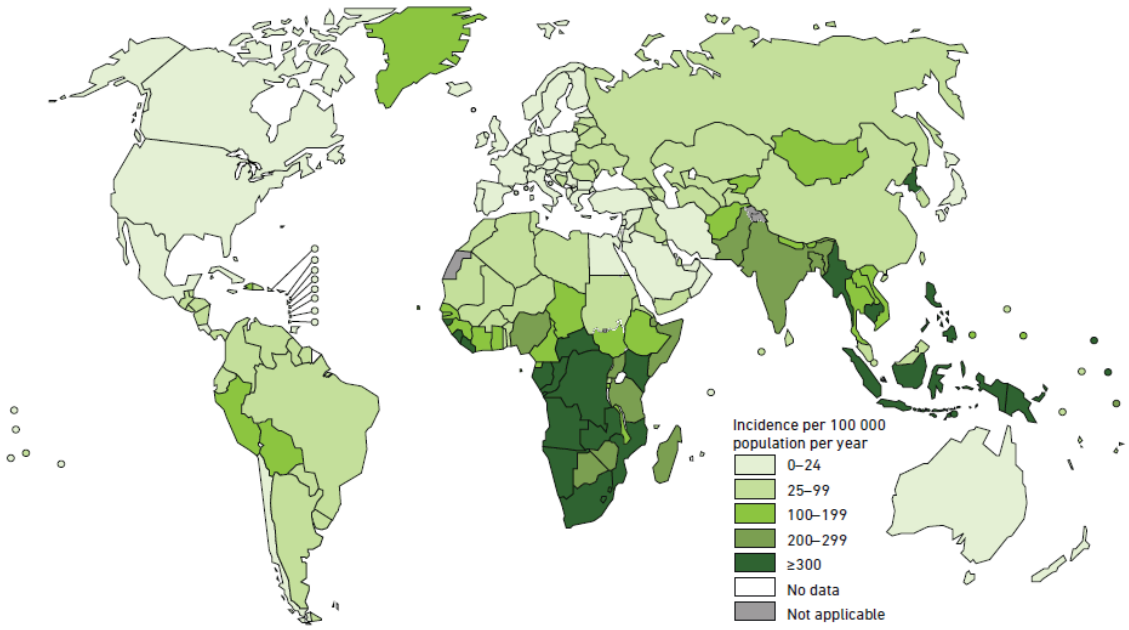

De acordo com a OMS, muitos casos incidentes de TB, no ano de 2017, foram atribuídos à cinco principais fatores de risco: desnutrição (1,9 milhões), infecção por HIV (0,88 milhões), tabagismo (0,83 milhões), diabetes (0,79 milhões) e abuso de álcool (0,49 milhões). A pobreza também é considerada uma condição favorável para o estabelecimento de epidemias de TB, sendo que a eliminação da pobreza extrema e o fornecimento de proteção social poderiam reduzir significativamente o número de novos casos de TB (WHO, 2018).

Em 2014 e 2015, a OMS e a Organização das Nações Unidas (ONU) propuseram o "End TB Strategy" que tem como objetivo eliminar a epidemia global de TB. Esse programa é sustentado por três pilares principais: (1) cuidados e prevenção integrados e centrados no paciente; (2) políticas ousadas e sistemas de apoio às pessoas afetadas pela TB; e (3) intensificação da inovação e da pesquisa. A principal meta da OMS e da ONU é que ocorra, até 2030, uma redução de 80 e 90% nos casos incidentes e na mortalidade, respectivamente, por TB comparado com as taxas registradas no ano de 2015 (WHO, 2018).

1.2. Agente Etiológico da TB

Mycobacterium tuberculosis, pertencente à família *Mycobacteriaceae* da ordem *Actinomycetales*, é o principal agente etiológico da TB (KOCH; MIZRAHI, 2018). A doença também pode ser causada por *M. africanum*, *M. microti*, *M. pinnipedii*, *M. orygis*, *M. mungii*, *M. caprae* e *M. bovis* (complexo *M. tuberculosis*). O principal patógeno da TB foi descoberto por Robert Koch em 24 de março de 1882, sendo essa data instituída pela OMS e a União Internacional como o Dia Mundial da TB (GORDON; PARISH, 2018).

M. tuberculosis apresenta a morfologia de bacilo com um tamanho aproximado de 0,2 a 0,4 µm por 1 a 10 µm. Trata-se de uma bactéria quimiorganotrófica e aeróbica obrigatória de crescimento lento. O tempo de geração varia de 15 a 20 horas sendo que o surgimento de colônias ocorre após 4 a 6 semanas. Além de ser imóvel, essa bactéria não apresenta capacidade de formar esporos (IQBAL et al., 2017; GORDON; PARISH, 2018).

Um dos grandes desafios no desenvolvimento de fármacos contra a TB refere-se às características morfo-fisiológicas peculiares de *M. tuberculosis*. A parede micobacteriana é estruturalmente e quimicamente diferente das demais bactérias (QUIGLEY et al., 2017). Na superfície externa da célula, uma espessa camada de ácidos micólicos (ácidos graxos ramificados de cadeia longa) está associada a uma camada de arabinogalactano que, por sua vez, está ligado covalentemente ao peptideoglicano (Figura 2) (BROWN et al., 2015; VASAVA et al., 2017; GORDON; PARISH, 2018).

Figura 2. Estrutura e composição da parede micobacteriana. Fonte: BROWN et al., 2015

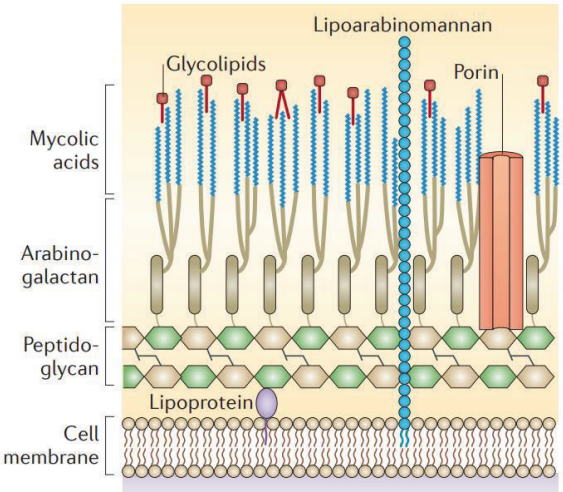

A parede das micobactérias confere diversas características importantes para esse patógeno, como a relativa impermeabilidade aos antibióticos e a presença de diversas moléculas imunomoduladoras. A biossíntese da parede micobacteriana é alvo de muitos fármacos contra a TB por apresentar uma composição e estrutura específica e diferencial, conferindo seletividade aos fármacos (GORDON; PARISH, 2018).

A composição química e estrutural da parede desse microrganismo impossibilita sua classificação em bactéria Gram-positiva ou Gram-negativa (IQBAL et al., 2017; KOCH & MIZRAHI, 2018). *M. tuberculosis* pode ser visualizado por microscopia óptica por meio da coloração de *Ziehl-Neelsen*. Os ácidos micólicos presentes na parede micobacteriana formam um complexo com a carbolfucsina (corante vermelho). As micobactérias são classificadas como microrganismos ácido-álcool resistentes. Dessa forma, a calbolfucsina é retida pela parede da micobactéria frente a lavagens ácido-álcool. Em bactérias que não apresentam essa propriedade, soluções diluídas de ácido-álcool extraem a carbolfucsina da célula, sendo esta contracorada com um segundo corante, geralmente o azul de metileno (GORDON; PARISH, 2018).

1.3. Patogênese da TB

M. tuberculosis afeta principalmente os pulmões, causando a forma mais conhecida da doença, a TB pulmonar. Porém, esse patógeno também pode atingir outros órgãos ao se espalhar através da extensão linfática, hematogênica ou direta de um foco infeccioso, caracterizando a TB extrapulmonar. Nesse último caso, a micobactéria pode infectar gânglios linfáticos, trato gastrointestinal, ossos, articulações, pele e até mesmo meninges (LEE, 2015; ANKRAH et al., 2017). De acordo com a OMS, a TB pulmonar representou 86% dos casos incidentes em 2017 (WHO, 2018).

A transmissão de *M. tuberculosis* ocorre por meio da inalação de perdigotas com bacilos expelidos pela tosse, fala ou espirro de um indivíduo infectado (CHIN et al., 2017). A resposta frente à infecção é variável em cada indivíduo, dependendo do estado imunológico do hospedeiro. O microrganismo pode ser eliminado pelo sistema imunológico, iniciar uma infecção ativa ou permanecer em um estado latente (ANKRAH et al., 2017).

Ao alcançar os alvéolos pulmonares, *M. tuberculosis* é fagocitado por macrófagos, produzindo uma resposta inflamatória local com liberação de citocinas e quimiocinas, que iniciam o processo de recrutamento de leucócitos dos vasos sanguíneos

vizinhos (NUNES-ALVES et al., 2014; EVANGELOPOULOS; MCHUGH, 2015; NILLER et al., 2017; PEDDIREDDY; DODDAM; AHMED, 2017; TURNER et al., 2017; YUAN; SAMPSON, 2018). Alguns bacilos podem bloquear o processo de maturação fagossômica que consiste na fusão do fagossomo com o lisossomo, acidificação do fagolisossomo e ativação de hidrolases lisossômicas. Dessa forma, esses microrganismos conseguem escapar da imunidade inata do hospedeiro e sobreviver dentro do ambiente hostil do macrófago (WELIN et al., 2011; YUAN; SAMPSON, 2018).

A resposta imune adaptativa do hospedeiro ocorre por meio da apresentação de antígenos micobacterianos por células dendríticas a células T nos linfonodos. Esse processo desencadeia a migração dessas células para o local da infecção no qual, juntamente com outros leucócitos, estimulam a formação de um granuloma (NUNES-ALVES et al., 2014). As células T ativam os macrófagos por meio da secreção de interferon- γ (IFN- γ) e do fator de necrose tumoral-α (TNF-α) que restringem a dispersão e a replicação de *M. tuberculosis* (NUNES-ALVES et al., 2014; YUAN; SAMPSON, 2018).

Os granulomas são constituídos por macrófagos infectados com *M. tuberculosis* no centro, rodeados por diferentes células imunes, principalmente macrófagos e células T (Figura 3, p. 31) (PIETERS, 2008). As micobactérias podem permanecer dentro dos macrófagos ou em um núcleo de *caseum* rico em lipídeos presente nos granulomas. Ambos os nichos apresentam hipóxia, pH ácido, privação de nutrientes, nitrogênio reativo e espécies de oxigênio, impedindo a replicação desse microrganismo (WELLINGTON; HUNG, 2018).

Figura 3. Estrutura de um granuloma. Fonte: PIETERS, 2008

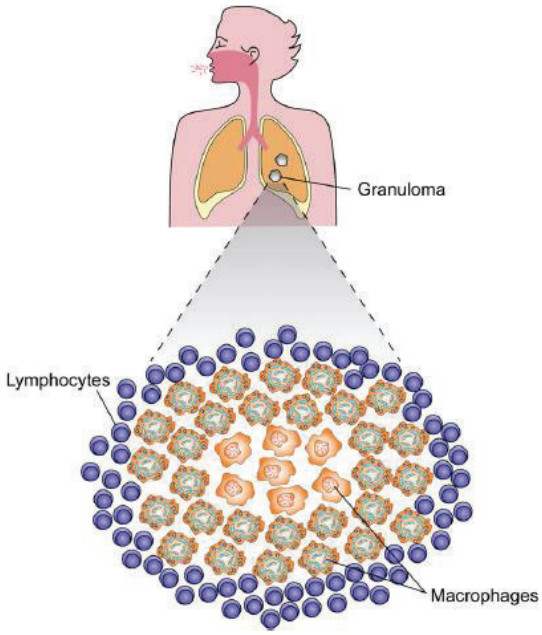

M. tuberculosis pode persistir por décadas no granuloma em um estado latente, não sendo infeccioso nessa fase (NUNES-ALVES et al., 2014; EVANGELOPOULOS; MCHUGH, 2015; PEDDIREDDY; DODDAM; AHMED, 2017; TANG; JOHNSTON, 2017; YUAN; SAMPSON, 2018). Estima-se que 23% da população mundial, aproximadamente 1,7 bilhões de pessoas, esteja infectada com a forma latente desse patógeno (WHO, 2018).

Em aproximadamente 10% dos casos de TB latente, a micobactéria pode sofrer reativação, após anos de latência, em situações em que há comprometimento do sistema imunológico, como durante um tratamento com imunossupressores, em doenças como o diabetes associado a deficiência imune e na co-infecção com HIV (EVANGELOPOULOS; MCHUGH, 2015; TOUSIF et al., 2017). A quebra de latência ocorre por meio da ruptura do granuloma e escape de bacilos infecciosos, resultando na TB ativa (EVANGELOPOULOS & MCHUGH, 2015; YUAN & SAMPSON, 2018). Esse processo pode resultar na dispersão de micobactérias viáveis para a circulação sanguínea, gerando focos de infecção à distância em diversos órgãos ou os bacilos podem ser liberados para as vias aéreas onde podem ser expelidos dos pulmões e infectar outros indivíduos (KIM; KIM, 2018).

Embora a TB latente seja caracterizada pela ausência de sintomas, os indivíduos infectados pela forma latente de *M. tuberculosis* representam um reservatório global para

o patógeno (TOUSIF et al., 2017; GORDON; PARISH, 2018). As principais intervenções no ramo da saúde para prevenir novos casos de TB ativa são o tratamento da TB latente e a vacinação de crianças com a vacina *Bacilo de Calmette-Guérin* (BCG). A OMS recomenda o tratamento de TB latente em dois grupos prioritários: pessoas soropositivas ao HIV e crianças com idade inferior a 5 anos que tiveram contato com indivíduos que apresentem TB pulmonar (WHO, 2018). Portanto, o tratamento de indivíduos com TB latente reduz o risco de desenvolvimento de TB ativa bem como o tempo de duração do tratamento e seleção de bacilos resistentes aos fármacos (HALEY, 2017).

1.4. Tratamento da TB e Resistência Micobacteriana

O tratamento da TB preconizado pela OMS inclui a associação de quatro fármacos, denominados agentes de primeira linha. A fase inicial do tratamento é representada pela associação entre isoniazida, pirazinamida, etambutol e rifampicina (Figura 4) com duração de dois meses. Com quatro meses de duração, a fase de manutenção é constituída pela associação entre isoniazida e rifampicina (WHO, 2018).

Figura 4. Fármacos de primeira linha utilizados no tratamento da TB

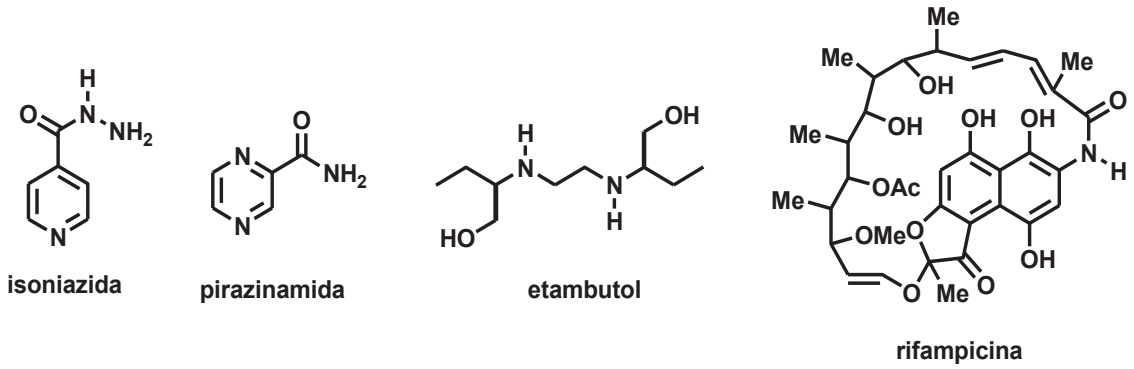

Apesar do estabelecimento precoce de combinação de fármacos no tratamento da TB, as cepas de *M. tuberculosis* resistentes à fármacos continuaram a evoluir (GYGLI et al., 2017). Em casos de TB causada por cepas resistentes, o tratamento recomendado pela OMS, com duração que varia entre 18 a 24 meses, inclui os agentes de segunda linha: aminoglicosídeos (estreptomicina, canamicina ou amicacina), capreomicina, cicloserina, ácido *para*-aminosalicilico, tioamidas (etionamida ou protionamida), e fluoroquinolonas (moxifloxacina, gatifloxacina ou levofloxacina) (WHO, 2018).

Apesar de apresentar alta eficácia, o tratamento com os agentes de primeira linha demonstra diversas limitações, como o longo tempo de duração, totalizando, no mínimo,

6 meses. A terapia prolongada reduz a adesão do paciente ao tratamento devido principalmente à toxicidade dos fármacos utilizados. Entre os efeitos adversos, destacam-se erupções cutâneas, intolerância gastrointestinal, insuficiência renal e hepatotoxicidade (PAI et al., 2016). Os fármacos de segunda linha, por sua vez, são menos efetivos e acessíveis e mais onerosos e tóxicos que os agentes de primeira linha (ZIGNOL et al., 2016).

Segundo a OMS, a TB é a principal causa de morte por resistência antimicrobiana (WHO, 2018). A forma multi-fármaco resistente (MDR) é resistente a pelo menos rifampicina e isoniazida. A forma extensivamente resistente à fármacos (XDR) possui resistência adicional a fluoroquinolonas e, pelo menos, a um dos antimicobacterianos injetáveis, tais como: amicacina, canamicina e capreomicina (PRASAD; SRIVASTAVA, 2013; CHAUDHARI et al., 2016). A forma totalmente resistente (TDR) é caracterizada por demonstrar uma resistência além da cepa XDR, sendo resistente à todos os fármacos de primeira e segunda linha (MATTEELLI; ROGGI; CARVALHO, 2014). A recrudescência de cepas resistentes aos fármacos representa um desafio na erradicação da TB (ABDELRAHMAN et al., 2017).

Em 2017, dentre os casos incidentes de TB no mundo, aproximadamente 19% demonstraram resistência a todos os fármacos de primeira linha. A OMS também estimou que 8,5% das pessoas infectadas por cepas MDR demonstraram resistência aos fármacos de segunda linha, apresentando infecção por cepas XDR. Dentre os indivíduos que tiveram acesso ao tratamento da TB, apenas 55% dos pacientes infectados por formas MDR e 34% infectados por cepas XDR obtiveram sucesso no tratamento (WHO, 2018).

As pessoas contraem bacilos resistentes aos fármacos por meio da resistência primária ou secundária. A resistência primária ocorre quando cepas resistentes são transmitidas a um novo hospedeiro enquanto a resistência secundária ou adquirida ocorre quando os bacilos adquirem mutações de resistência aos fármacos, ou seja, uma resistência que se desenvolve durante o tratamento. *M. tuberculosis* pode adquirir resistência principalmente pela indução de bombas de efluxo que expulsam os fármacos da célula micobacteriana ou por mutações em genes que codificam os alvos dos fármacos ou as enzimas ativadoras de pró-fármacos (DHEDA et al., 2017; DOOKIE et al., 2018).

Apesar da existência da vacina BCG para prevenir o desenvolvimento da TB em crianças e jovens, sua eficácia de imunização contra a TB pulmonar em adultos vem sendo

questionada, sendo a quimioterapia com fármacos a estratégia principal para o controle da disseminação da TB. Contudo, após 40 anos do surgimento da rifampicina, somente dois novos fármacos foram aprovados para o tratamento específico de casos da forma MDR: a bedaquilina, aprovada em 2012 pela *Food and Drug Administration* (FDA), e a delamanida, aprovada em 2014 pela *European Medicines Agency* (EMA) (Figura 5) (WHO, 2018).

Figura 5. Fármacos modernos para tratamento de cepas MDR

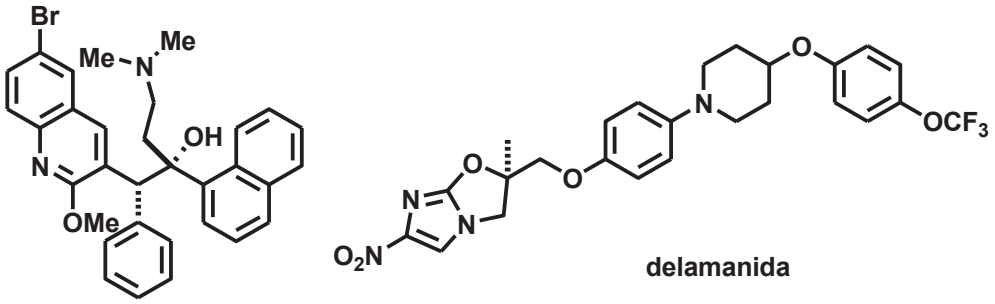

bedaquilina

A bedaquilina desempenha sua atividade antimicobacteriana ao se ligar à subunidade C da enzima ATP sintase micobacteriana. Essa ligação promove inibição da bomba de prótons e consequente inibição da biossíntese de ATP. Portanto, a bedaquilina atua na inibição da produção de ATP micobacteriano (MAHAJAN, 2013).

A delamanida é um pró-fármaco que sofre ação da enzima deazaflavina nitroredutase dependente (Rv3547). O metabólito ativo promove a inibição da biossíntese de ácido micólico, mais especificamente ácido metoximicólico e ácido cetomicólico. Dessa forma, a delamanida atua na inibição da biossíntese da parede micobacteriana (XAVIER; LAKSHMANAN, 2014).

Atualmente, há cinco candidatos a fármacos contra a TB que estão em fases clínicas I ou II: pretomanida (nitroimidazol), delpazolida e sutezolida (oxazolidinonas), SQ109 (etilenodiamina) e PBTZ169 (benzotiazolinona) (Figura 6, p. 35). O alvo terapêutico da pretomanida, delpazolida e sutezolida é a biossíntese proteica, enquanto o SQ-109 e o PBTZ169 atuam na biossíntese da parede micobacteriana (VJECHA; TIBERI; ZUMLA, 2018).

Figura 6. Candidatos a fármacos contra a TB

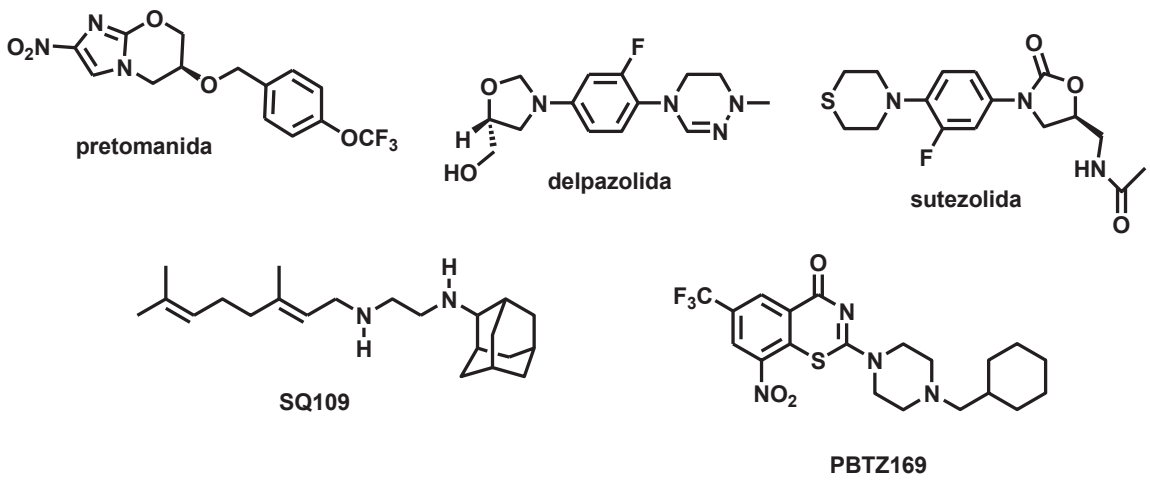

O surgimento de cepas de *M. tuberculosis* resistentes aos fármacos atuais e a co-infecção por HIV conduzem à busca por fármacos inovadores mais eficientes e seguros, os quais permitam maior adesão dos pacientes ao tratamento (PAI et al. 2016). Espera-se que um fármaco contra a TB possa reduzir a duração do tratamento, demonstrar menor toxicidade, ser ativo contra cepas resistentes, bem como não interferir com os principais fármacos anti-HIV (EVANGELOPOULOS; MCHUGH, 2015; VJECHA; TIBERI; ZUMLA, 2018).

1.5. Produtos Naturais

Os produtos naturais desempenham um importante papel na descoberta de novos fármacos, particularmente antimicrobianos e antineoplásicos (HARVEY; EDRADA-EBEL; QUINN, 2015; NEWMAN; CRAGG, 2016). Dentre os novos fármacos aprovados pela FDA entre 1981 e 2010, 34% eram produtos naturais ou baseados na estrutura de produtos naturais. As principais classes de antibióticos tiveram produtos naturais como ponto de partida, tais como: β-lactâmicos, aminoglicosídeos, macrolídeos, tetraciclinas e rifamicinas (HARVEY; EDRADA-EBEL; QUINN, 2015).

Há milhares de anos, as plantas já eram utilizadas por populações para fins medicinais. Atualmente, várias plantas utilizadas na alimentação ou como especiarias tem sido amplamente estudadas devido suas propriedades terapêuticas (HAMPANNAVAR et al., 2016; IZAH; ASEIBAI, 2018; NETO et al., 2018). O açafrão (*Curcuma longa*), pertencente à família Zingiberaceae da ordem Zingiberales, é uma planta perene herbácea nativa do Sudeste Asiático. Os rizomas de *C. longa* são frequentemente utilizados para o

tratamento de úlceras gástricas, infecções parasitárias, doenças de pele, inflamações articulares, gripes e resfriados (HEWLINGS; KALMAN, 2017). O extrato dos rizomas dessa planta contém três componentes majoritários: curcumina (60–70%), dimetoxicurcumina (20–27%) e bisdimetoxicurcumina (10–15%), sendo a curcumina a principal responsável pelas propriedades terapêuticas do açafrão (KOCAADAM; SAMLIER, 2015; XU et al., 2018).

1.6. Curcumina e seus Análogos

A curcumina (diferuloilmetano) (Figura 7) está presente nos rizomas do açafrão. Essa substância demonstra diversas bioatividades, tais como: antibacteriana, antifúngica, antiviral, antitumoral, antioxidante, anti-inflamatória, antidiabetes, neuroprotetora, cardioprotetora e hepatoprotetora (MOGHADAMTOUSI et al., 2014; STANIC, 2017; KOCAADAM; SANLIER, 2017; XU et al., 2018).

Figura 7. Curcumina (diferuloilmetano)

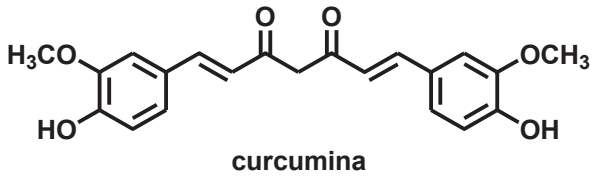

curcumina

Apesar do efeito antitumoral ser a atividade da curcumina mais estudada nos últimos 10 anos, o primeiro trabalho que relatou a ação biológica dessa substância abordou sua atividade antibacteriana (TEOW et al., 2016). Mourão e colaboradores (2018) avaliaram a porcentagem de inibição de crescimento bacteriano da curcumina na concentração de 100 µg/mL contra *Staphylococcus aureus*, *Enterococcus faecalis*, *Bacillus subtilis*, *Xanthomonas citri*, *Pseudomonas aeruginosa*, *Salmonella typhimurium* e *Escherichia coli*. A curcumina foi ativa contra seis das sete bactérias testadas, demonstrando uma porcentagem de inibição de crescimento que variou de 52 a 98%. A substância não demonstrou ação somente contra *X. citri*.

A atividade antibacteriana da curcumina também foi investigada contra outras espécies e cepas resistentes à fármacos. No trabalho de De e colaboradores (2009), a curcumina apresentou atividade antibacteriana significativa contra 65 isolados clínicos de *Helicobacter pylori*, demonstrando valores de concentração inibitória mínima (CIM) que variaram de 5 a 50 µg/mL. A curcumina apresentou atividade bactericida contra *S. aureus*, matando 50 e 100% das bactérias na concentração de 25 e 50 µM, respectivamente

(TYAGI et al., 2015). Outros trabalhos também relataram o efeito antibacteriano sinérgico da curcumina contra cepas de *S. aureus* sensíveis (MSSA) e resistentes (MRSA) à meticilina quando utilizada em combinação com antibióticos relevantes, como penicilina, eritromicina, amicacina, gentamicina, vancomicina, tetracicilina, ampicilina e ciprofloxacina (MOGHADDAM et al., 2009; MUN et al., 2013; TEOW et al., 2016).

Apesar de demonstrar diversas bioatividades, a curcumina apresenta diversas limitações que impedem o seu uso como agente terâpeutico. Essa substância demonstra baixa solubilidade em água, baixa biodisponibilidade e instabilidade elevada em condições fisiológicas, sofrendo degradação prematura por administração oral (MOGHADAMTOUSI et al., 2014; HAMPANNAVAR et al., 2016; TEOW et al., 2016; HEWLINGS; KALMAN, 2017; XU et al., 2018). As instabilidades farmacocinéticas da curcumina estão relacionadas principalmente à subunidade β-dicêtonica de sua estrutura (HEGER et al., 2014; HAMPANNAVAR et al., 2016).

Uma das estratégias utilizadas para superar as limitações da curcumina é o desenvolvimento de análogos estruturais que apresentem a substituição da subunidade β-dicêtonica por um grupo monocarbonílico. Estudos farmacocinéticos indicam que esses análogos são mais ativos e demonstram maior estabilidade *in vivo* do que a curcumina (SUBHEDAR et al., 2017).

Mourão e colaboradores (2018) analisaram a atividade antibacteriana de um análogo simplificado da curcumina (**1**) (Figura 8) no qual um grupo monocarbonílico substituiu a subunidade β-dicêtonica, preservando as duplas ligações bem como as subunidades guaiacol. Essa substância foi ativa contra *X. citri*, *S. typhimurium*, *E. faecalis* e *B. subtilis* com valores de porcentagem de inibição de crescimento que variaram de 59 a 93% na concentração de 100 μg/mL. Os resultados demonstraram que o análogo **1** exerce sua atividade antibacteriana por meio da permeabilização da membrana bacteriana e disrupção do septo divisional bacteriano.

Figura 8. Estrutura do análogo monocetônico de curcumina **1**

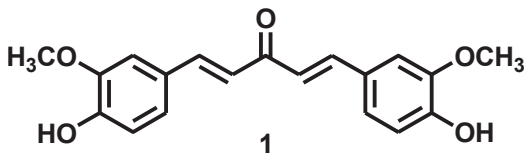

1

Além da subunidade β-dicêtonica, outra subunidade estrutural da curcumina que pode ser alvo de modificação para o planejamento de análogos são os anéis aromáticos (BALDWIN et al., 2015). No presente trabalho, planejou-se duas séries de análogos de curcumina com a subunidade β-dicêtonica substituída por um grupo monocarbonílico. A série I constituiu-se de análogos com o anel B substituído por grupos eletroatratores/eletrodoadores e lipofílicos/hidrofílicos e a série II foi composta por análogos com bioisósteros do grupo fenila (anel B) (Figura 9).

Figura 9. Planejamento dos análogos monocetônicos de curcumina

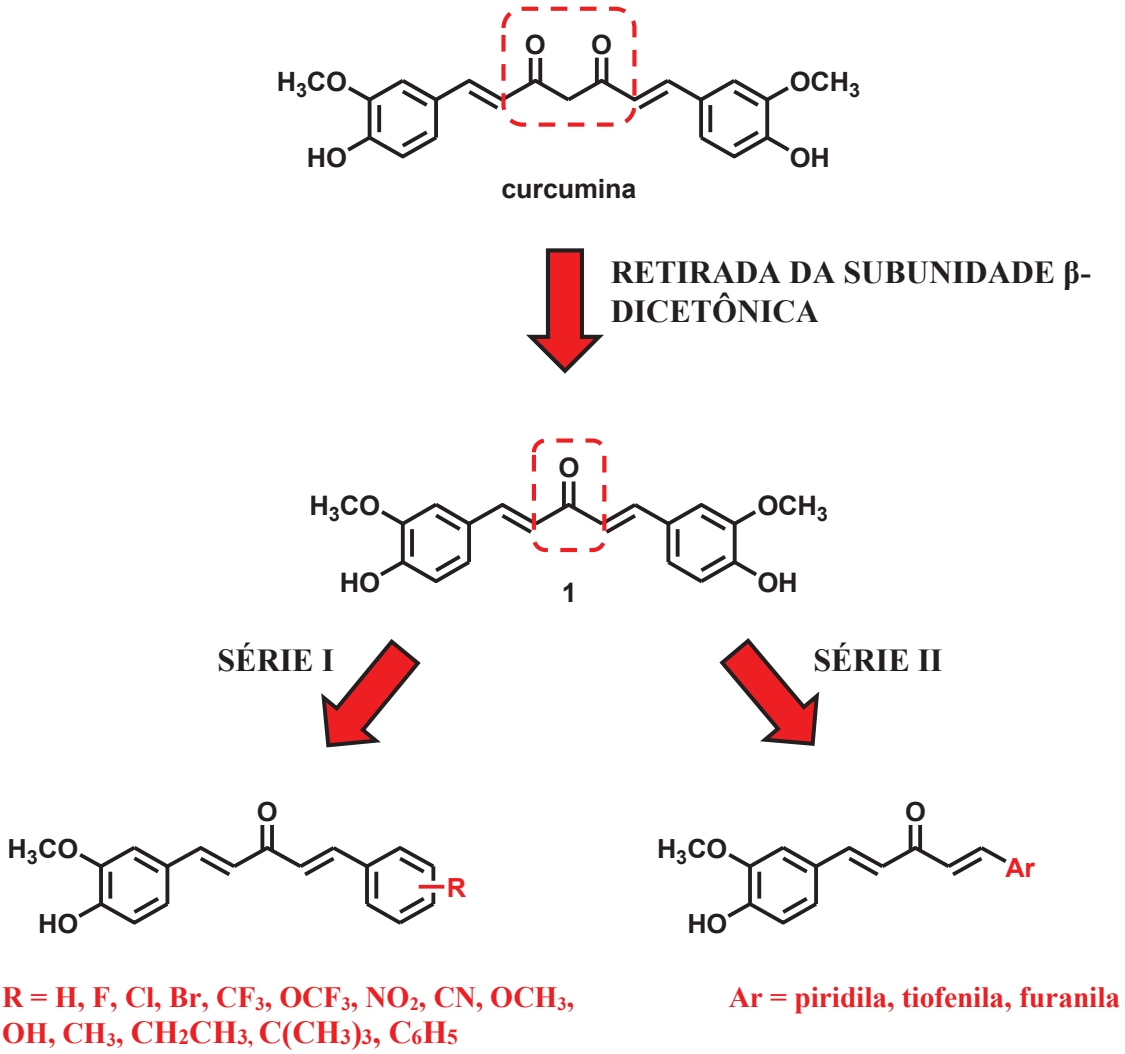

2. OBJETIVOS

2.1. Objetivo Geral

Sintetizar e avaliar a atividade antimicobacteriana, a toxicidade e as propriedades farmacocinéticas *in silico* de análogos monocetônicos de curcumina.

2.2. Objetivos Específicos

A) Sintetizar, purificar e identificar 28 análogos monocetônicos de curcumina;

B) Determinar o coeficiente de partição *n*-octanol/água (log $P_{o/a}$) dos análogos monocetônicos de curcumina, correlacionando a lipofilicidade com a atividade anti-TB;

C) Avaliar a atividade antimicobacteriana das substâncias contra *M. tuberculosis* H37Rv;

D) Avaliar a toxicidade dos análogos bioativos contra fibroblastos de pulmão humano MRC-5 e macrófagos murinos J774A.1;

E) Avaliar a atividade antimicobacteriana dos análogos seletivos contra isolados clínicos de *M. tuberculosis* com resistência a diferentes fármacos anti-TB;

F) Avaliar os efeitos da associação do análogo mais ativo e seletivo com a rifampicina e a moxifloxacina;

G) Avaliar a toxicidade do análogo mais ativo e seletivo no modelo invertebrado alternativo de *G. mellonella*;

H) Avaliar as propriedades *drug-likeness* e farmacocinéticas *in silico* das substâncias bioativas.

3. REFERÊNCIAS BIBLIOGRÁFICAS

ABDELRAHMAN, M. A.; SALAMA, I.; GOMAA, M. S.; ELAASSER, M. M.; ABDEL-AZIZ, M. M.; SOLIMAN, D. H. Design, synthesis and 2D QSAR study of novel pyridine and quinolone hydrazone derivatives as potential antimicrobial and antitubercular agents. **Eur. J. Med. Chem.**, v. 138, p. 698–714, 2017.

ANKRAH, A. O.; GLAUDEMANS, A. W. J. M.; MAES, A.; VAN DE WIELE, C.; DIERCKX, R. A. J. O.; VORSTER, M.; SATHEKGE, M. M. Tuberculosis. **Semin. Nucl. Med.**, v. 48, p. 108–130, 2017.

BALDWIN, P. R.; REEVES, A. Z.; POWELL, K. R.; NAPIER, R. J.; SWIMM, A. I.; SUN, A.; GIESLER, K.; BOMMARIUS, B.; SHINNICK, T. M.; SNYDER, J. P.; LIOTTA, D. C.; KALMAN, D. Monocarbonyl analogs of curcumin inhibit growth of antibiotic sensitive and resistant strains of *Mycobacterium tuberculosis*. **Eur. J. Med. Chem.**, v. 92, p. 693–699, 2015.

CHAUDHARI, K.; SURANA, S.; JAIN, P.; PATEL, H. M. *Mycobacterium tuberculosis* (MTB) GyrB inhibitors: An attractive approach for developing novel drugs against TB. **Eur. J. Med. Chem.**, v. 124, p. 160–185, 2016.

CHIN, K. L.; ANIS, F. Z.; SARMIENTO, M. E.; NORAZMI, M. N.; ACOSTA, A. Role of interferons in the development of diagnostics, vaccines, and therapy for tuberculosis. **J. Immunol. Res.**, v. 2017, p. 1–10, 2017.

DE, R.; KUNDU, P.; SWARNAKAR, S.; RAMAMURTHY, T.; CHOWDHURY, A.; NAIR, G. B.; MUKHOPADHYAY, A. K. Antimicrobial activity of curcumin against *Helicobacter pylori* isolates from India and during infections in mice. **Antimicrob. Agents Chemother.**, v. 53, p. 1592–1597, 2009.

DHEDA, K.; GUMBO, T.; MAARTENS, G.; DOOLEY, K. E.; MCNERNEY, R.; MURRAY, M.; FURIN, J.; NARDELL, E. A.; LONDON, L.; LESSEM, E.; THERON, G.; VAN HELDEN, P.; NIEMANN, S.; MERKER, M.; DOWDY, D.; VAN RIE, A.; SIU, G. K. H.; PASIPANODYA, J. G.; RODRIGUES, C.; CLARK, T. G.; SIRGEL, F. A.; ESMAIL, A.; LIN, H. H.; ATRE, S. R.; SCHAAF, H. S.; CHANG, K. C.; LANGE, C.; NAHID, P.; UDWADIA, Z. F.; HORSBURGH, C. R.; CHURCHYARD, G. J.; MENZIES, D.; HESSELING, A. C.; NUERMBERGER, E.; MCILLERON, H.; FENNELLY, K. P.; GOEMAERE, E.; JARAMILLO, E.; LOW, M.; JARA, C. M.;

PADAYATCHI, N.; WARREN, R. M. The epidemiology, pathogenesis, transmission, diagnosis, and management of multidrug-resistant, extensively drug-resistant, and incurable tuberculosis. **Lancet Respir. Med.**, v. 5, p. 291–360, 2017.

DOOKIE, N.; RAMBARAN, S.; PADAYATCHI, N.; MAHOMED, S.; NAIDOO, K. Evolution of drug resistance in *Mycobacterium tuberculosis*: a review on the molecular determinants of resistance and implications for personalized care. **J. Antimicrob. Chemother.**, v. 73, p. 1138–1151, 2018.

EVANGELOPOULOS, D.; MCHUGH, T. D. Improving the tuberculosis drug development pipeline. **Chem. Biol. Drug. Des.**, v. 86, p. 951−960, 2015.

GORDON, S. V.; PARISH, T. Microbe Profile: M*ycobacterium tuberculosis*: Humanity's deadly microbial foe. **Microbiol.**, v. 164, p. 437–439, 2018.

GYGLI, S. M.; BORRELL, S.; TRAUNER, A.; GAGNEUX, S. Antimicrobial resistance in *Mycobacterium tuberculosis*: Mechanistic and evolutionary perspectives. **FEMS Microbiol. Rev.**, v. 41, p. 354–373, 2017.

HALEY, C. A. Treatment of latent tuberculosis infection. **Microbiol. Spectr.**, v. 5, p. 1–32, 2017.

HAMPANNAVAR, G. A.; KARPOORMATH, R.; PALKAR, M. B.; SHAIKH, M. S. An appraisal on recent medicinal perspective of curcumin degradant: Dehydrozingerone (DZG). **Bioorg. Med. Chem.**, v. 24, p. 501–520, 2016.

HARVEY, A. L.; EDRADA-EBEL, R.; QUINN, R. J. The re-emergence of natural products for drug discovery in the genomics era. **Nat. Rev. Drug Discov.**, v. 14, p. 111–129, 2015.

HEGER, M.; VAN GOLEN, R. F.; BROEKGAARDEN, M.; MICHEL, M. C. The molecular basis for the pharmacokinetics and pharmacodynamics of curcumin and its metabolites in relation to cancer. **Pharmacol. Rev.**, v. 66, p. 222–307, 2014.

HEWLINGS, S. J.; KALMAN, D. S. Curcumin: A review of its' effects on human health. **Foods**, v. 6, p. 1–11, 2017.

IQBAL, Z.; ULLAH, I.; REHMAN, H. U.; WALI, N.; AHMAD, R.; ZAMAN, H.; KAMAL, R.; JADOON, M. A.; REHMAN, H.; REHMAN, M. U.; ULLAH, R.; ZEB,

A.; WAQAS, M.; HAMEED, M. F. *Mycobacterium tuberculosis* & its recent vaccine approach: A review. **J. Entomol. Zool. Studies**, v. 5, p. 360–365, 2017.

IZAH, S. C.; ASEIBAI, E. R. Antibacterial and synergistic activities of methanolic leaves extract of lemon grass (*Cymbopogon citratus*) and rhizomes of ginger (*Zingiber officinale*) against *Escherichia coli*, *Staphylococcus aureus* and *Bacillus subtilis*. **Acta Sci. Microbiol.**, v. 1, p. 26–30, 2018.

KIM, H. W.; KIM, J. S. Treatment of latent tuberculosis infection and its clinical efficacy. **Tuberc. Respir. Dis.**, v. 81, p. 6–12, 2018.

KOCAADAM, B.; SANLIER, N. Curcumin, an active component of turmeric (*Curcuma longa*), and its effects on health. **Crit. Rev. Food Sci. Nutr.**, v. 57, p. 2889–2895, 2017.

KOCH, A.; MIZRAHI, V. *Mycobacterium tuberculosis*. **Trends Microbiol.**, v. 26, p. 555–556, 2018.

LEE, J. Y. Diagnosis and treatment of extrapulmonary tuberculosis. **Tuberc. Respir. Dis.**, v. 78, p. 47–55, 2015.

MAHAJAN, R. Bedaquiline: First FDA-approved tuberculosis drug in 40 years. **Int. J. Basic Med. Res.**, v. 3, p. 1–2, 2013.

MATTEELLI, A.; ROGGI, A.; CARVALHO, A. C. Extensively drug-resistant tuberculosis: epidemiology and management. **Clin. Epidemiol.**, v. 6, p. 111–118, 2014.

MOGHADAMTOUSI, S.Z.; KADIR, H.A.; HASSANDARVISH, P.; TAJIK, H.; ABUBAKAR, S.; ZANDI, K. A review on antibacterial, antiviral, and antifungal activity of curcumin. **Biomed Res. Int.**, p. 1–12, 2014. [doi: 10.1155/2014/186864]

MOGHADDAM, K.; IRANSHAHI, M.; YAZDI, M.; SHAHVERDI, A. The combination effect of curcumin with different antibiotics against *Staphylococcus aureus*. **Int. J. Green Pharm.**, vol. 3, p. 141–143, 2009.

MOURÃO, L. G.; POLAQUINI, C. R.; KOPACZ, M.; TORREZAN, G. S.; AYUSSO, G. M.; DILARRI, G.; CAVALCA, L. B.; ZIELINSKA, A.; SCHEFFERS, D.; REGASINI, L. O.; FERREIRA, H. A simplified curcumin targets the membrane of *Bacillus subtilis*. **MicrobiologyOpen**, p. 1–12, 2018. [doi: 10.1002/mbo3.683]

MUN, S. H.; JOUNG, D. K.; KIM, Y. S.; KANG, O. H.; KIM, S. B.; SEO, Y. S.; KIM, Y.C.; LEE, D. S.; SHIN, D. W.; KWEON, K. T.; KWON, D. Y. Synergistic antibacterial effect of curcumin against methicillin-resistant *Staphylococcus aureus*. **Phytomedicine**, vol. 20, p. 714–718, 2013.

NETO, F. C.; MARTON, L. T.; MARQUI, S. V.; LIMA, T. A.; BARBALHO, S. M. Curcuminoids From *Curcuma longa*: New adjuvants for the treatment of crohn's disease and ulcerative colitis? **Crit. Rev. Food Sci. Nutr.**, p. 1–36, 2018. [doi: 10.1080/10408398.2018.1456403]

NEWMAN, D. J.; CRAGG, G. M. Natural products as sources of new drugs from 1981 to 2014. **J. Nat. Prod.**, v. 79, p. 629–661, 2016.

NILLER, H. H.; MASA, R.; VENKEI, A.; MÉSZÁROS, S.; MINAROVITS, J. Pathogenic mechanisms of intracellular bacteria. **Curr. Opin. Infect. Dis.**, v. 30, p. 309–315, 2017.

NUNES-ALVES, C.; BOOTY, M. G.; CARPENTER, S. M.; JAYARAMAN, P.; ROTHCHILD, A. C.; BEHAR, S. M. In search of a new paradigm for protective immunity to TB. **Nat. Rev. Microbiol.**, v. 12, p. 289–299, 2014.

PAI, M.; BEHR, M. A.; DOWDY, D.; DHEDA, K.; DIVANGAHI, M.; BOEHME, C. C.; GINSBERG, A.; SWAMINATHAN, S.; SPIGELMAN, M.; GETAHUN, H.; MENZIE, D.; RAVIGLIONE, M. Tuberculosis. **Nat. Rev.**, v. 2, p. 1–23, 2016.

PEDDIREDDY, V.; DODDAM, S. N.; AHMED, N. Mycobacterial dormancy systems and host responses in tuberculosis. **Front. Immunol.**, v. 8, p. 1–19, 2017.

PIETERS, J. *Mycobacterium tuberculosis* and the macrophage: Maintaining a balance. **Cell Host Microbe**, v. 3, p. 399–407, 2008.

PRASAD, R.; SRIVASTAVA, D. K. Multi drug and extensively drug-resistant TB (M/XDR-TB) management: Current issues. **Clin. Epidemiol. Glob. Health**, v. 1, p. 124–128, 2013.

QUIGLEY, J.; HUGHITT, V. K.; VELIKOVSKY, C. A.; MARIUZZA, R. A.; EL-SAYED, N. M.; BRIKEN, V. The cell wall lipid PDIM contributes to phagosomal escape and host cell exit of *Mycobacterium tuberculosis*. **mBio**, v. 8, p. 1–12, 2017.

STANIC, Z. Curcumin, a compound from natural sources, a true scientific challenge – A review. **Plant Foods Hum. Nutr.**, v.72, p. 1-12, 2017.

SUBHEDAR, D. D.; SHAIKH, M. H.; NAWALE, L.; SARKAR, D.; KHEDKAR, V. M.; SHINGATE, B. B. Quinolidene based monocarbonyl curcumin analogues as promising antimycobacterial agents: Synthesis and molecular docking study. **Bioorg. Med. Chem. Lett.**, v. 27, p. 922–928, 2017.

TANG, P.; JOHNSTON, J. Treatment of latent tuberculosis infection. **Curr. Treat. Options Infect. Dis.**, v. 9, p. 371–379, 2017.

TEOW, S. Y.; LIEW, K.; ALI, S. A.; KHOO, A. S. B.; PEH, S. C. Antibacterial action of curcumin against *Staphylococcus aureus*: A brief review. **J. Trop. Med.,** v. 2016, p. 1–10, 2016.

TOUSIF, S.; SINGH, D. K.; MUKHERJEE, S.; AHMAD, S.; ARYA, R.; NANDA, R.; RANGANATHAN, A.; BHATTACHARYYA, M.; KAER, L. Van; KAR, S. K.; DAS, G. Nanoparticle-formulated curcumin prevents posttherapeutic disease reactivation and reinfection with *Mycobacterium tuberculosis* following isoniazid therapy. **Front. Immun.**, v. 8, p. 1–12, 2017.

TURNER, R. D.; CHIU, C.; CHURCHYARD, G. J.; ESMAIL, H.; LEWINSOHN, D. M.; GANDHI, N. R.; FENNELLY, K. P. Tuberculosis infectiousness and host susceptibility. **J. Infect. Dis.**, v. 216, p. S636–S643, 2017.

TYAGI, P.; SINGH, M.; KUMARI, H.; KUMARI, A.; MUKHOPADHYAY, K. Bactericidal activity of curcumin I is associated with damaging of bacterial membrane. **PLOS ONE**, v. 10, p. 1–15, 2015.

VJECHA, M. J.; TIBERI, S.; ZUMLA, A. Accelerating the development of therapeutic strategies for drug-resistant tuberculosis. **Nat. Rev. Drug Discov.**, v. 17, p. 607–608, 2018.

WELIN, A.; RAFFETSEDER, J.; EKLUND, D.; STENDAHL, O.; LERM, M. Importance of phagosomal functionality for growth restriction of *Mycobacterium tuberculosis* in primary human macrophages. **J. Innate Immun.**, v. 3, p. 508–518, 2011.

WELLINGTON, S.; HUNG, D. T. The expanding diversity of *Mycobacterium tuberculosis* drug targets. **ACS Infect. Dis.**, v. 4, p. 696–714, 2018.

WHO. World Health Organization. Global Tuberculosis Report. Geneva: 2018. Disponível em: <http://www.who.int/tb/publications/global_report/en/> Acesso em: 15 jan 2019.

XAVIER, A. S.; LAKSHMANAN, M. Delamanid: A new armor in combating drug-resistant tuberculosis. **J. Pharmacol. Pharmacother.**, v. 5, p. 222–224, 2014.

XU, X. Y.; MENG, X.; LI, S.; GAN, R. Y.; LI, Y.; LI, H. B. Bioactivity, health benefits, and related molecular mechanisms of curcumin: Current progress, challenges, and perspectives. **Nutrients**, v. 10, p. 1–33, 2018.

YUAN, T.; SAMPSON, N. S. Hit generation in TB drug discovery: From genome to granuloma. **Chem. Rev.**, v. 118, p. 1887–1916, 2017.

ZIGNOL, M.; DEAN, A. S.; PH, D.; FALZON, D.; GEMERT, W. V.; WRIGHT, A.; DEUN, A. V.; PORTAELS, F.; PH, D.; LASZLO, A.; PH, D.; ESPINAL, M. A.; MÉNDEZ, A. P.; BLOOM, A.; AZIZ, M. A.; WEYER, K.; SC, D.; JARAMILLO, E.; NUNN, P.; FLOYD, K.; PH, D.; RAVIGLIONE, M. C. Special report twenty years of global surveillance of antituberculosis-drug resistance. **N. Engl. J. Med.**, v. 375, p. 1081–1089, 2016.

Capítulo II

European Journal of Medicinal Chemistry

Molecular Simplification and Ring Bioisosterism Improved Antitubercular Activity of Monocarbonyl Analogues of Curcumin

Gabriela M. Ayusso [a], Débora L. Campos [b], Mariana B. Santos [a], Carlos R. Polaquini [a], Valéria K. Almeida [a], Camila M. Ribeiro [b], Mariana C. Solcia [b], Diego A. Monteiro [c], Eleni Gomes [c], Janaina C. O. Sardi [d], Pedro L. Rosalen [d], Fernando R. Pavan [b,*], Luis O. Regasini [a,**]

[a] *Department of Chemistry and Environmental Sciences, Institute of Biosciences, Humanities and Exact Sciences (IBILCE), São Paulo State University (UNESP), São José do Rio Preto, SP, Brazil.*

[b] *Department of Biological Sciences, School of Pharmaceutical Sciences (FCFAR), São Paulo State University (UNESP), Araraquara, SP, Brazil.*

[c] *Department of Biology, Institute of Biosciences, Humanities and Exact Sciences (IBILCE), São Paulo State University (UNESP), São José do Rio Preto, SP, Brazil.*

[d] *Department of Physiological Sciences, Piracicaba Dental School, University of Campinas (UNICAMP), Piracicaba, SP, Brazil.*

*** Corresponding author.**

**** Corresponding author.**

E-mail addresses: regasini@ibilce.unesp.br (LO Regasini) and fernandopavan@fcfar.unesp.br (FR Pavan).

ABSTRACT

In the present study, two series of curcumin analogues with the β-diketone moiety replaced by a monocarbonyl group were synthesized and their antitubercular activity, toxicity and *in silico* pharmacokinetic properties were evaluated. The curcumin and its analogues (**1–28**) were analysed against *Mycobacterium tuberculosis* H37Rv. The replacement of β-diketone moiety by a monocarbonyl group and the presence of heteroatoms and the nitro group improved the antimycobacterial effect. The bioactive compounds (**1–18** and **20–28**) were subjected to cytotoxicity tests. The analogues displayed lower toxicity and higher selectivity for murine macrophages J774A.1 than human lung fibroblasts MRC-5. The activity of selective analogues **7**, **8**, **13**, **15–17**, **27** and **28** against three clinical isolates of *M. tuberculosis* with resistance to different clinically used drugs, including an extensively drug resistant (XDR) strain, suggested that these compounds probably have a differentiated action mechanism. In addition to demonstrate highest antitubercular activity against *M. tuberculosis* H37Rv, the analogue **28** was the most selective for lung fibroblasts and macrophages. This compound did not present antagonism with rifampicin and moxifloxacin and did not demonstrate significant *in vivo* toxicity in *Galleria mellonella*, indicating its potential safe use in the clinical setting. *In silico* studies indicated that bioactive analogues (**1–18** and **20–28**) are potential drugs candidates by oral administration and may be used in the treatment of tuberculous meningitis. Therefore, our study established preliminary structure-activity relationship data, besides to identify monocarbonyl analogues of curcumin as promising drugs candidates against tuberculosis.

Keywords: tuberculosis, curcumin, analogue, antitubercular, selectivity, pharmacokinetic

1. Introduction

According to World Health Organization (WHO), tuberculosis (TB) is the tenth leading cause of death and the disease caused by a single infectious agent that promotes the highest mortality in the world, overcoming the Acquired Immunodeficiency Syndrome (AIDS). In 2017, 10 million new TB cases and 1.6 million deaths caused by TB were reported worldwide [1]. One of major challenges in the development of drugs against TB refers to the peculiar morpho-physiological features of *Mycobacterium tuberculosis*, the main etiological agent of TB. The mycobacterial wall is structurally and chemically different from the other bacteria [2], conferring several important features for this pathogen, such as the relative impermeability to antibiotics [3]. This bacterium can be eliminated by the host immune system, start an active infection or remain in a latent state in host [4]. It was estimated that 23% of world's population is infected with non-infectious form of *M. tuberculosis*, of which approximately 10% will likely develop active TB [1].

The TB treatment demonstrates several limitations, such as the long duration, totalizing at least 6 months. The prolonged therapy reduces patient adherence to treatment due mainly to the toxicity and consequently adverse effects of drugs [5]. Another problem associated with TB is the increase of multi drug resistant (MDR), extensively drug resistant (XDR) and totally drug resistant (TDR) strains of *M. tuberculosis* [6,7,8]. Among the individuals who had access to TB treatment, only 55% of patients infected with MDR strains and 34% of those infected with XDR strains were successful in treatment. According to WHO, TB is the leading cause of death by antimicrobial resistance [1]. Therefore, the co-infection by HIV and the existence of drug resistant strains of *M. tuberculosis* lead to search more efficient and safe innovative drugs, which allow greater adherence of patients to treatment [5].

Natural products play an important role in the discovery of new drugs. Curcumin (Figure 1A) is present in the turmeric rhizomes and demonstrates several bioactivities, including antibacterial [9,10,11,12]. This compound has several limitations that prevent its use as therapeutical agent, such as low solubility in water, poor bioavailability and high instability under physiological conditions [9,12,13,14,15]. The pharmacokinetic instabilities of curcumin are mainly related to the β-diketone moiety of its structure [13,16]. One of strategies used to overcome the limitations of curcumin is the development of structural analogues with the β-diketone replaced by a monocarbonyl group [17]. Mourão and collaborators evaluated antibacterial activity of a simplified analogue of curcumin (**1**) (Figure 1B), in which a monocarbonyl group replaced the β-diketone moiety. This analogue was active against Gram-positive and Gram-negative bacteria, causing membrane permeabilization and divisional septum disruption of *Bacillus subtilis* [18].

In our search for new antitubercular agents, we designed and synthesized two series of curcumin analogues with the β-diketone replaced by a monocarbonyl group. These analogues were evaluated against *M. tuberculosis* H37Rv to derive preliminary structure-activity relationships. The cytotoxicity of bioactive compounds was determined against human lung fibroblasts MRC-5 and murine macrophages J774A.1 to analyse selective toxicity between eukaryotic and prokaryotic cells. The selective analogues were evaluated against clinical isolates of *M. tuberculosis* with resistance to different clinically used anti-TB drugs. Additionally, the most active and selective compound were investigated regarding their interaction effect with rifampicin and moxifloxacin and their toxicity in *Galleria mellonella*, an alternative invertebrate model. Finally, the bioactive analogues were subjected to *in silico* studies to evaluate their drug-likeness and pharmacokinetic properties.

2. Results and Discussion

2.1. Chemistry

Monocarbonyl analogues of curcumin were synthesized by two steps. The first step was characterized by the synthesis of dehydrozingerone (DZG). The synthesis of DZG was performed by the aldol condensation reaction between vanillin and acetone under basic catalysis, resulting in yield of 51% (Scheme 1). The second step involved the synthesis of two series of curcumin analogues, in which a monocarbonyl group replaced the β-diketone moiety. The synthesis of monocarbonyl analogues of curcumin was performed by aldol condensation reactions between DZG and corresponding aryl aldehydes under basic catalysis, resulting in yields which ranged from 8–90% (Scheme 2).

In the series I, phenyl ring B exhibited electron-withdrawing/electron-donating and lipophilic/hydrophilic substituents. In the series II, phenyl ring B was replaced by pyridinyl, thiophenyl and furanyl rings (Table 1).

The structure of compounds was confirmed by their melting point, UV-Vis and Nuclear Magnetic Resonance of Hydrogen (^{1}H NMR) and Thirteen Carbon (^{13}C NMR) spectra analysis. Detailed spectral analysis were presented in the supplementary material. According to Scifinder database, the analogues **3**, **4**, **7**, **12**, **15-18**, **21-23**, **25**, **27** and **28** were identified as new chemical entities [19].

2.2. Biological Activity

2.2.1. Antimycobacterial Activity against *M. tuberculosis* H37Rv

The antimycobacterial activity of curcumin and its analogues **1–28** was evaluated against *M. tuberculosis* H37Rv. The influence of lipophilicity on the

antitubercular action was investigated by determination of partition coefficient *n*-octanol/water (log $P_{o/w}$). The minimum inhibitory concentration for 90% (MIC_{90}) against *M. tuberculosis* H37Rv and the log $P_{o/w}$ values found for compounds were shown in Table 2.

First, we compared the antimycobacterial activity of curcumin and its simplified analogue **1**. Curcumin was not active against *M. tuberculosis* (MIC_{90} > 85 μM) while its analogue **1** demonstrated antitubercular activity (MIC_{90} = 24.5 μM), corroborating that replacement of β-diketone moiety by a monocarbonyl group improves bioactivity (17). Second, the analogue with unsubstituted ring B (**2**) was compared with substituted analogues **3–23**.

Analysing the influence of electronic parameter of substituents in relation to inhibition of mycobacteria growth, the presence of substitutions on ring B by electron-withdrawing atoms and groups (fluor, chloro, bromo, trifluoromethyl, trifluoromethoxyl, nitro and nitril) increased the antitubercular activity when compared to substitutions by electron-donating groups (methoxyl, hydroxyl, methyl, ethyl, *terc*-butyl and biphenyl). The comparison of MIC_{90} values of regioisomers **3/4/5**, **6/7/8**, **9/10/11** and **12/13** demonstrated the relevance of position of fluor, chloro, bromo and trifluoromethyl, respectively, for anti-*M. tuberculosis* activity. For chloro, bromo and trifluoromethyl, the position 4''' exhibited highest antimycobacterial activity whereas the most active position was 3''' for fluor.

The mycobacterial wall is rich in lipids, mainly mycolic acids [20]. The lipophilicity is a relevant physicochemical property in the discovery of drugs against TB, since lipophilic compounds cross the mycobacterial wall more easily. In addition, the interaction of lipophilic compounds with mycobacterial membrane can promote disruption of proton-motive force, altering its stability and functionality, resulting in a

lethal effect [21]. Thus, besides the electronic parameter, we also evaluated the influence of lipophilic parameter of substituents in antitubercular activity. Except analogues **1** (log $P_{o/w}$ = 1.9) and **17** (log $P_{o/w}$ = 2.4), active compounds against *M. tuberculosis* exhibited log $P_{o/w} \geq 3.0$. These data suggested that lipophilic substituents on ring B improve the antimycobacterial activity, corroborating that lipophilic compounds are generally more active against *M. tuberculosis* than hydrophilic compounds [21].

Third, in order to investigate hypothetical ring bioisosterism, comparisons were made to determine the effect of replacement of phenyl ring B in **2** by equivalent heteroaryl rings with six π-electrons, including 3-pyridinyl (**24**), 4-pyridinyl (**25**), thiophenyl (**26**) and furanyl (**27**). The analogues **24**, **25**, **26** and **27** exhibited higher activity against *M. tuberculosis* than **2**, indicating that presence of heteroatoms improved antitubercular activity.

Fourth, we proposed a monocarbonyl analogue of curcumin with furanyl ring containing nitro group (**28**) since the most active compounds in the series I present nitro group (**15** and **16**) and the analogue with lowest antitubercular action in the series II exhibit furanyl ring (**27**). The compound **28** (MIC_{90} = 0.3 μM) was approximately 17 times more active than **27** (MIC_{90} = 5.2 μM), indicating that the insertion of nitro group in furanyl ring potentiated antimycobacterial effect. This result demonstrates the relevance of nitro group for anti-*M. tuberculosis* activity.

The TB treatment includes the association of four drugs, called first-line agents. The initial phase of treatment (two months) is represented by the association between rifampicin, isoniazid, pyrazinamide and ethambutol. The maintenance phase (four months) consists of association between rifampicin and isoniazid [1]. Among monocarbonyl analogues of curcumin of series I and II, compound **28** exhibited highest activity against *M. tuberculosis*. This analogue presented the same MIC_{90} value of

isoniazid and it was only three times less active than rifampicin (MIC_{90} = 0.1 μM). In relation to other drugs used in TB treatment, the MIC_{90} value of analogue **28** was considerably better than pyrazinamide and ethambutol [22], demonstrating that MIC_{90} value obtained are sufficient to use this compound in TB therapy.

2.2.2. Cytotoxicity and Selectivity

The cytotoxic activity of bioactive analogues **1–18** and **20–28** was investigated against human lung fibroblasts MRC-5 and murine macrophages J774A.1. The comparison of differential toxic effect of analogues on eukaryotic and prokaryotic cells was determined by calculating selectivity index (SI), which was obtained by the ratio of inhibitory concentration for 50% (IC_{50}) against lung fibroblasts or macrophages and MIC_{90} against *M. tuberculosis* H37Rv. The IC_{50} and SI values of monocarbonyl analogues of curcumin for human lung fibroblasts and murine macrophages were summarized in Table 3.

The transmission of *M. tuberculosis* occurs by airways. When this mycobacterium crosses the respiratory system and reaches the pulmonary alveoli, it begins the infection process [23]. Thus, the evaluation of toxicity of compounds with anti-TB action against lung fibroblasts is relevant since *M. tuberculosis* mainly affects the lungs, causing TB pulmonary [24] which accounted for 86% of incident cases in 2017 [1]. In the pulmonary alveoli, *M. tuberculosis* is phagocytosed by macrophages. However, some mycobacteria may interrupt phagolysosome formation and persist in latency in the intramacrophagic environment for a long period of time [23]. Therefore, the evaluation of toxic action of compounds with antitubercular activity against macrophages is important since *M. tuberculosis* is a facultative intramacrophagic pathogen [20,24]. The IC_{50} values of analogues ranged from 28.0 to 277.2 μM against lung fibroblasts and from 71.5 to 328.0 μM against macrophages.

The safety of a compound for preclinical tests may be investigated by SI, a parameter that expresses the selectivity between eukaryotic and prokaryotic cells [25,26]. According to Orme and collaborators [27], drugs candidates must have a SI equal or higher than 10. The analogues **7**, **8**, **13**, **15–17** and **24–28** were selective for both lung fibroblasts and macrophages (SI > 10.0). Thus, our study identified monocarbonyl analogues of curcumin as very promising new anti-TB drugs candidates. The compound **23** exhibited selectivity for only lung fibroblasts (SI = 18.7) and the analogues **2–4**, **6**, **10**, **11**, **14** and **18** demonstrated SI > 10.0 for only macrophages. Except **13** and **23**, all analogues presented lower toxicity and higher selectivity for macrophages than lung fibroblasts.

In addition to demonstrate highest antitubercular activity against *M. tuberculosis* H37Rv, analogue **28** was also the most selective for both lung fibroblasts and macrophages, displaying SI value of 116.7 and 743.7, respectively.

2.2.3. Antimycobacterial Activity against Clinical Isolates of *M. tuberculosis* with Drug Resistance

The antimycobacterial activity of selective compounds **7**, **8**, **13**, **15–17** and **24–28** was performed against four clinical isolates of *M. tuberculosis* with resistance to different anti-TB drugs. The clinical isolates were collected at Clemente Ferreira (CF) hospital, located in São Paulo city, São Paulo State, Brazil. The critical concentration to determine antibiotic resistance of clinical isolates was previously reported [22]. In determination of MIC_{90}, clinical isolates CF 44 and CF 184 were mono-resistant to isoniazid; CF 48 demonstrated resistance to isoniazid, gatifloxacin and amikacin; and CF 61 was classified as XDR strain, exhibiting resistance to all drugs. The MIC_{90} values obtained for each monocarbonyl analogue of curcumin were listed in Table 4.

In TB caused by drug resistant strains, treatment includes the second-line agents: aminoglycosides (streptomycin, kanamycin or amikacin), capreomycin, cycloserine, *para*-aminosalicylic acid, thioamides (ethionamide or protionamide) and fluoroquinolones (moxifloxacin, gatifloxacin or levofloxacin) [1]. Second-line drugs are less effective and accessible and more costly and toxic than first-line drugs [28]. Thus, the resurgence of *M. tuberculosis* strains with resistance to clinically used drugs leads to the search for more efficient and safe innovative anti-TB drugs [5].

In our study, CF 48 was not susceptible to any compound. All monocarbonyl analogues of curcumin of series I were able to inhibit growth of other clinical isolates of *M. tuberculosis*, displaying MIC_{90} values which ranged from 2.5 to 21.0 μM. The compounds **7** and **13** were more active against clinical isolates with drug resistance than H37Rv strain. The analogue **15** demonstrated the same MIC_{90} value for both CF 61 and H37Rv strain (MIC_{90} = 2.5 μM).

Among compounds of series II, only analogues **27** and **28** exhibited significant antimycobacterial activity against clinical isolates of *M. tuberculosis* with MIC_{90} values ranging from 6.3 to 30.4 μM. Comparisons of MIC_{90} values of monocarbonyl analogues of curcumin indicated that compounds of series I displayed higher anti-TB activity than analogues of series II, demonstrating that heteroatoms decreased activity against clinical isolates.

Among clinical isolates of *M. tuberculosis*, XDR strain (CF 61) was the most susceptible to the major compounds. While MDR strains are resistant to at least rifampicin and isoniazid, XDR strains has additional resistance to fluoroquinolones and to at least one of injectable anti-TB drugs, such as amikacin, kanamycin and capreomycin [6,8]. In 2017, among worldwide TB incident cases, approximately 19% demonstrated

resistance to all first-line drugs and 8.5% of people infected with MDR strains exhibited resistance to second-line drugs, presenting infection with XDR strains [1].

The monocarbonyl analogues of curcumin **7**, **8**, **13**, **15–17**, **27** and **28** were active against clinical isolates of *M. tuberculosis* with resistance profiles to different drugs. These data suggested that action mechanism of these compounds probably differs from the drugs used in TB therapy. Among active compounds, **13** and **15** displayed the highest antitubercular activity against all clinical isolates. Therefore, we identified monocarbonyl analogues of curcumin as promising new second-line drugs candidates. Once the drug resistant TB rates were declared a global threat by WHO [1], new compounds that exhibit activity against *M. tuberculosis* strains with resistance to clinically used drugs represent advance in the control and treatment of TB.

2.2.4. Effects of Associations with Clinically Used Anti-TB Drugs

Monocarbonyl analogue of curcumin **28** was the most active against *M. tuberculosis* H37Rv, being equipotent with isoniazid (MIC_{90} = 0.3 μM). In addition, this compound was the most selective for human lung fibroblasts (SI = 116.7) and murine macrophages (SI = 743.7), besides to demonstrate antitubercular activity against three clinical isolates of *M. tuberculosis* with drug resistance, including a XDR strain (MIC_{90} = 6.3 μM). These data encouraged us to investigate the effects of association between analogue **28** and rifampicin (first-line drug) or moxifloxacin (second-line drug) against *M. tuberculosis* H37Rv by determination of fractional inhibitory concentration index (FICI). The effects of combinations were classified as synergistic ($FICI \leq 0.5$), indifferent ($0.5 < FICI < 4$) and antagonistic ($FICI \geq 4$) [29].

Drug combinations are essential for TB treatment due to their better performance than with single drug. The multidrug therapy against TB prevents the emergence of *M.*

tuberculosis strains with drug resistance. Thus, the association between new drugs candidates and clinically used drugs should be evaluated to determine the potential of interactions and avoid antagonistic effects, preventing the selection of drug resistant strains [30,31]. The analysis of FICI values indicated no interaction between analogue **28** and rifampicin or moxifloxacin (FICI = 0.6) (Table 5), demonstrating that this compound and these drugs act independently of each other against *M. tuberculosis* H37Rv. Importantly, no association of analogue **28** with rifampicin or moxifloxacin displayed antagonistic effect.

2.2.5. *In vivo* Toxicity in *G. mellonella*

In addition to the interactions with rifampicin and moxifloxacin, the *in vivo* toxicity of analogue **28** was evaluated in the alternative invertebrate model of *G. mellonella* by determination of lethal dose for 50% (LD_{50}). Successful drugs candidates might to be tested in an animal model (preclinical phase) before their application in humans (clinical phase) in order to investigate responsive doses, drug toxicity, pharmacokinetics and pharmacodynamics. The use of alternative animals models increased over the last 25 years in parallel with decline in the use of mammals, which are time-consuming, expensive and require complex ethical considerations [32,33]. The *G. mellonella* insect larvae has been used increasingly as an alternative invertebrate model for scientific experimentation. When compared with conventional mammalians models, *G. mellonella* larvae demonstrates some advantages, including lower costs to establish, easier to maintain and manipulate and not require ethical approval, being ethically more acceptable. Additionally, the innate immune system of larvae displays high structural and functional similarity to that of mammals and their short-life makes them ideal for high-throughput screening of active compounds, allowing fast data acquisition [32,34,35].

As shown in Figure 2, the LD_{50} of analogue **28** in *G. mellonella* was estimated to be 60 mg/Kg. In doses below 60 mg/Kg, the compound did not exert considerable acute toxic effects in the larvae over a period of 96 h. The analogue **28** were safer than ethambutol (LD_{50} = 2.21 and 4.0 mg/Kg in mices and rats, respectively) [22], first-line drug used in initial phase of TB therapy. Besides, the LD_{50} found for analogue **28** over the larvae is greatly far from the MIC_{90} values of this compound against *M. tuberculosis* H37Rv and clinical isolates of *M. tuberculosis* with drug resistance. Thus, the results of this study demonstrated that compound **28** has no significant *in vivo* toxic effects, indicating its potential safe use in the clinical setting. However, further toxicity tests are required to confirm these data.

2.3. *In silico* Drug-likeness and Pharmacokinetic Predictions

In order to assess drug-likeness and pharmacokinetic properties, bioactive analogues **1–18** and **20–28** were subjected to an *in silico* study. Approximately 30% of oral drugs candidates fail in the development phase due to poor absorption, distribution, metabolism and excretion (ADME) properties [36]. Lipinski established four rules that determine good absorption for drugs candidates with oral administration: (1) log $P_{o/w} \leq$ 5.0; (2) molecular weight (MW) ≤ 500.0 g/mol; (3) number of hydrogen bond donors (HBD) ≤ 5.0; and (4) number of hydrogen bond acceptors (HBA) ≤ 10.0 [37]. Only analogue **22** violated one rule with log $P_{o/w}$ = 5.1 (Table 6). Bedaquiline, approved in 2012 by *Food and Drug Administration*, has two violations of Lipinski's rules, exhibiting log $P_{o/w}$ = 7.1 and MW = 555.5 g/mol. Delamanid, approved in 2014 by *European Medicines Agency*, violates one rule of Lipinski, demonstrating MW = 534.5 g/mol. Nevertheless, these drugs reached the market and nowadays are used in the treatment of TB caused by MDR strains [38].

Veber and collaborators also reported two predictors for good oral bioavailability: (1) HBD + HBA ≤ 12; and (2) number of routable bonds (NROTB) ≤ 10 [39]. No compound violated the two criteria determined by Veber (Table 7). Thus, except **22**, all bioactive analogues did not violate Lipinski's and Veber's parameters, indicating their good oral drug-likeness properties.

Two main processes influence absorption of oral drugs: the dissolution in gastrointestine and the permeation through gastrointestinal membrane [40]. The percentage of human intestinal absorption (HIA) is a relevant pharmacokinetic property used in oral drug design [41]. Yee classified compounds according to their percentage of HIA in poorly absorbed (0–20%), moderately absorbed (20–70%) and well absorbed (70–100%) [42]. All bioactive analogues demonstrated percentage of HIA ranging from 87.2 to 96.6% (Table 8). Thus, these compounds were considered well absorbed in human intestine, which is relevant for their oral administration.

The blood-brain barrier (BBB) is composed of specialized endothelial cells connected by tight junctions. The BBB function is to control passage of molecules and cells from blood circulation to brain tissue [43,44]. The ability of drugs candidates to penetrate BBB is relevant mainly when infective agent is located in brain. Brito-Sánchez and collaborators reported that compounds with BBB ≥ 0 present high distribution in central nervous system while molecules with BBB < 0 are considered poor penetrators of BBB [45]. All bioactive analogues displayed good BBB penetration (BBB ≥ 0) (Table 9), which can be useful to threat meningitis caused by *M. tuberculosis*. Tuberculous meningitis is the most lethal form of TB, accounting for 1% of all cases. Approximately 20% of cases result in death and more than 50% of survivors demonstrate neurological sequels [44,46].

3. Conclusion

Our study demonstrated that replacement of β-diketone moiety by a monocarbonyl group and the presence of heteroatoms and the nitro group improve activity against *M. tuberculosis* H37Rv. In general, all compounds displayed lower toxicity and higher selectivity for macrophages than lung fibroblasts. The selective analogues **7**, **8**, **13**, **15–17**, **27** and **28** were active against clinical isolates of *M. tuberculosis* with resistance to different anti-TB drugs, suggesting that these compounds probably have a differentiated action mechanism. The monocarbonyl analogue of curcumin **28** was the most active against *M. tuberculosis* H37Rv, being equipotent with isoniazid. This compound was the most selective for lung fibroblasts and macrophages, besides to demonstrate antitubercular activity against three clinical isolates with drug resistance, including a XDR strain. The analogue **28** did not exhibit antagonism with rifampicin and moxifloxacin and did not demonstrate significant *in vivo* toxicity, indicating its potential safe use in clinical studies. *In silico* predictions indicated that all bioactive analogues exhibit good oral drug-likeness and pharmacokinetic properties. Taken together, our results identified monocarbonyl analogues of curcumin as very promising new antitubercular drugs candidates.

4. Experimental

4.1. Chemistry

Curcumin and all starting reagents were purchased from SigmaAldrich®. The DZG and monocarbonyl analogues of curcumin were synthesized by aldol condensation reactions. In order to synthesize DZG, vanillin (2 mmol) were solubilized in acetone (50 mL) in a reaction flask. For the synthesis of monocarbonyl analogues of curcumin, DZG (1 mmol) and respective aryl aldehydes (1 mmol) were added in a reaction flask. The pH

10 was obtained by adding the ethanolic solution of NaOH. Reactions were maintained under constant stirring at room temperature. The progress of reactions was checked by thin-layer chromatography (TLC) analysis. When significant consumption of reagents was verified, the reaction medium was poured into crushed ice. Precipitated crude products were filtered and dried at room temperature. Soluble crude products were partitioned with ethyl acetate. Organic phase was concentrated under reduced pressure.

The purification of DZG was performed by liquid-liquid extraction, followed by normal phase column chromatography. Monocarbonyl analogues of curcumin were purified by precipitation, liquid-liquid extraction, gel permeation chromatography, normal phase column chromatography and reverse phase column chromatography. Details of spectral analysis data were provided in the supplementary material.

4.2. Determination of Partition Coefficient *n*-Octanol/Water (log $P_{o/w}$)

The log $P_{o/w}$ values were determined by high performance liquid chromatography with photodiode array detection (HPLC-PAD) following standard procedures described in OECD Guidelines [47], on system equipped with binary pump, automatic sampler (Agilent Technologies® Model 1220 Infinity), photodiode array system and Zorbax Eclipse Plus C-18 column (4.6 × 250 mm, 5 μm, Agilent® Technologies). The analysis were performed on isocratic elution in methanol and water (3:1) at a flow of 1.0 mL/min. The injected sample volume was 20.0 μL and the wavelength was 254 nm. Thiourea, phenol, acetophenone, benzoic acid, benzene, toluene, biphenyl, fluoranthene and triphenylamine were used as standards to construct the curve log K × log P. The capacity factor (log K) of compounds was determined from the retention times and linearization of curve log K × log P. The data were analysed by LC Solution Agilent Technologies® software. The experiments were performed in duplicate.

4.3. Biological Procedures

4.3.1. *M. tuberculosis* Strains and Cell Lines

M. tuberculosis H37Rv (ATCC 27294), human lung fibroblasts MRC-5 (ATCC CCL-171) and murine macrophages J774A.1 (ATCC TIB-67) were purchased from ATCC®. Clinical isolates of *M. tuberculosis* with drug resistance (CF 44, CF 184, CF 61 and CF 48) were collected between 2007 and 2009 at Clemente Ferreira hospital, located in São Paulo city, São Paulo State, Brazil.

All *M. tuberculosis* strains were cultivated in Middlebrook 7H9 medium (Difco®) enriched with 10% OADC (oleic acid, albumin, dextrose and catalase). Lung fibroblasts and macrophages were cultivated in *Dulbecco's Modified Eagle's Medium* (DMEM) and *Roswell Park Memorial Institute* (RPMI) medium (Vitrocell®), respectively, enriched with 10% bovine fetal serum, gentamicin sulfate (50 mg/L) and amphotericin B (2 mg/L).

4.3.2. Antimycobacterial Activity Assay

The antimycobacterial activity of compounds was determined by *Resazurin Microtiter Assay* (REMA), as previously described with minor modifications [48,49]. Stock solutions of compounds were prepared in dimethylsulfoxide (DMSO) (10 mg/mL) and diluted in growth medium to obtain a final concentration range of 0.09–25.0 µg/mL. The mycobacterial inoculum was incubated on *shaker* at 37 °C and 120 rpm for seven days until reaching a turbidity of 1.0 in McFarland standard. The bacterial suspension was adjusted to 3×10^5 colony-forming unities per mL (CFU/mL) and 100 µL of inoculum was added to each well of a 96-well plate (Kasvi®) together with 100 µL of compounds solution. The plate was incubated for seven days at 37 °C with 5% CO_2. After this period, 30 µL of resazurin (SigmaAldrich®) solubilized in sterile water (0.01%) was added. After

24 hours, the fluorescence of wells was read using the Cytation 3 equipment (Biotek®) with excitation and emission filters at wavelengths of 530 and 590 nm, respectively. Rifampicin, isoniazid, gatifloxacin and amikacin were used as reference drugs against TB. The tests were performed in three independent assays.

4.3.3. Cytotoxicity Assay

The cytotoxic activity of monocarbonyl analogues of curcumin was performed, as recommended by Pavan and collaborators with minor modifications [49]. Cells were incubated at 37 °C with 5% CO_2 until reaching cell confluence. The lung fibroblasts and macrophages suspension was adjusted to 2.5 × 10^5 CFU/mL and 1 × 10^6 CFU/mL, respectively, and 100 µL of cell suspensions was added to each well of a 96-well plate (Kasvi®). The plate was incubated for 24 hours at 37 °C with 5% CO_2. Stock solutions of compounds were prepared in DMSO (10 mg/mL) and diluted in growth medium to obtain a final concentration ranging from 0.4 to 100 µg/mL. After 24 hours of exposure of the cells to compounds, 50 µL of resazurin (SigmaAldrich®) solubilized in growth medium (0.01%) was added to the plate. After 3 hours, the fluorescence of wells was read using the Cytation 3 equipment (Biotek®) with excitation and emission filters at wavelengths of 530 and 590 nm, respectively. Doxorubicin was used as reference cytotoxic drug. The tests were performed in three independent assays.

4.3.4. Determination of Selectivity Index (SI)

The SI of monocarbonyl analogues of curcumin was determined by the ratio of IC_{50} values against lung fibroblasts or macrophages and MIC_{90} values against *M. tuberculosis* H37Rv. Two SI's were calculated: SI (lung fibroblasts) = IC_{50} (lung fibroblasts) / MIC_{90} (H37Rv); and SI (macrophages) = IC_{50} (macrophages) / MIC_{90} (H37Rv).

4.3.5. *Resazurin Drugs Combination Microtiter Assay* (REDCA)

The interactions between analogue **28** and rifampicin or moxifloxacin were analysed in two-drug combinations against *M. tuberculosis* H37Rv by *Resazurin Drugs Combination Microtiter Assay* (REDCA), a modified checkerboard method [29]. The assay was performed in 96-well plates (Kasvi®), in which the combinations were tested two-dimensionally. Anti-TB drugs (rifampicin or moxifloxacin) and compound **28** were diluted in growth medium at *x*-axis and *y*-axis, respectively, to obtain a final concentration range of 0.002–0.5 µg/mL. The mycobacterial inoculum was incubated on *shaker* at 37 °C and 120 rpm for seven days until reaching a turbidity of 1.0 in McFarland standard. The bacterial suspension was adjusted to 3×10^5 CFU/mL and 100 µL of inoculum was added to each well. The plate was incubated for seven days at 37 °C with 5% CO_2. After this period, 30 µL of resazurin (SigmaAldrich®) solubilized in sterile water (0.01%) was added. After 24 hours, the fluorescence of wells was read using the Cytation 3 equipment (Biotek®) with excitation and emission filters at wavelengths of 530 and 590 nm, respectively. The tests were performed in three independent assays. In order to evaluate the effects of interactions, the FICI was calculated: FICI = (MIC_{90} A+B / MIC_{90} A) + (MIC_{90} B+A / MIC_{90} B), in which MIC_{90} A + B represents the MIC_{90} of drug A combined with drug B and MIC_{90} B + A represents the MIC_{90} of drug B combined with drug A. The MIC_{90} A and MIC_{90} B represent the MIC_{90} of drug A and B tested alone, respectively [29].

4.3.6. *In vivo* Toxicity Assay

The acute toxicity of analogue **28** was assessed *in vivo* in the alternative invertebrate model of *G. mellonella*, as previously described with minor modifications [50]. A total of 10 larvae were randomly selected for each group, weighing between 0.2 and 0.3 g with no or few signs of melanization. The larvae were chilled on ice for 20 min

and 10 μL of compound (2.0 mg/mL, 1.5 mg/mL, 1.0 mg/mL, 0.5 mg/mL and 0.25 mg/mL) or controls (12.5% DMSO and saline) were injected into the hemocoel of each larva via the last left proleg by a trained operator using a 25-μL Hamilton syringe (Hamilton, Reno, NV). After injection, the larvae were incubated in the dark at 37 °C in an incubator and their survival was recorded at selected intervals for 96 h. Larvae displaying no movements upon touch and high levels of melanization were counted as dead. The tests were performed in three independent assays. Kaplan-Meier killing curves were plotted and estimations of differences in survival were compared using the log rank test. In all tests, type one error (α) was set at 0.05.

4.4. *In silico* Studies

In silico investigations about drug-likeness and pharmacokinetic properties of monocarbonyl analogues of curcumin were performed using Molinspiration and PreADMET toolkits, respectively [51,52]. The log $P_{o/w}$, WM, HBA, HBD and NROTB were determined according to Lipinski's and Veber's rules [37,39]. Pharmacokinetic parameters were also computed, including percentage of HIA and BBB penetration.

Acknowledgments

The authors gratefully acknowledge financial support from Fundação de Amparo à Pesquisa do Estado de São Paulo (FAPESP) (2013/14957-5, 2014/18330-0 and 2017/08383-7), Coordenação de Aperfeiçoamento de Pessoal de Nível Superior (CAPES) (Financing Code 001) and Conselho Nacional de Desenvolvimento Científico e Tecnológico (CNPq) (429322/2018-6, 306251/2016-7 and 471129/2013-5). Also, we would like to thank Centro Multiusuário de Inovação Biomolecular (FAPESP 2009/53989-4) for the use of Bruker Avance III 9.397 T (400 MHz) and 14.095 T (600

MHz) spectrometers and Laboratório-II de Ressonância Magnética Nuclear for the use of Bruker Fourier (300 MHz) spectrometer.

References

[1] WHO. World Health Organization. Global Tuberculosis Report. Geneva: 2018. Available in: <http://www.who.int/tb/publications/global_report/en/> Access in: jan 2019.

[2] J. Quigley, V. K. Hughitt, C. A. Velikovsky, R. A. Mariuzza, N. M. El-Sayed, V. Briken, The cell wall lipid PDIM contributes to phagosomal escape and host cell exit of *Mycobacterium tuberculosis*, mBio, 8 (2017) 1–12.

[3] S. V. Gordon, T. Parish, Microbe Profile: M*ycobacterium tuberculosis*: Humanity's deadly microbial foe, Microbiol., 164 (2018) 437–439.

[4] A. O. Ankrah, A. W. J. M. Glaudemans, A. Maes, C. Van de Wiele, R. A. J. O. Dierckx, M. Vorster, M . M. Sathekge, Tuberculosis, Semin. Nucl. Med., 48 (2017) 108–130.

[5] M. Pai, M. A. Behr, D. Dowdy, K. Dheda, M. Divangahi, C. C. Boehme, A. Ginsberg, S. Swaminathan, M. Spigelman, H. Getahun, D. Menzie, M. Raviglione, Tuberculosis, Nat. Rev., 2 (2016) 1–23.

[6] R. Prasad, D. K. Srivastava, Multi drug and extensively drug-resistant TB (M/XDR-TB) management: Current issues, Clin. Epidemiol. Glob. Health, 1 (2013) 124–128.

[7] A. Matteelli, A. Roggi, A. C. Carvalho, Extensively drug-resistant tuberculosis: epidemiology and management, Clin. Epidemiol., 6 (2014) 111–118.

[8] K. Chaudhari, S. Surana, P. Jain, H. M. Patel, *Mycobacterium Tuberculosis* (MTB) GyrB inhibitors: An attractive approach for developing novel drugs against TB, Eur. J. Med. Chem., 124 (2016) 160–185.

[9] S. Z. Moghadamtousi, H. A. Kadir, P. Hassandarvish, H. Tajik, S. Abubakar, K. Zandi, A review on antibacterial, antiviral, and antifungal activity of curcumin, Biomed Res. Int., (2014) 1–12 [doi: 10.1155/2014/186864].

[10] Z. Stanic, Curcumin, a compound from natural sources, a true scientific challenge – A review, Plant Foods Hum. Nutr., 72 (2017) 1-12.

[11] B. Kocaadam, N. Sanlier, Curcumin, an active component of turmeric (*Curcuma longa*), and its effects on health, Crit. Rev. Food Sci. Nutr., 57 (2017) 2889–2895.

[12] X. Y. Xu, X. Meng, S. Li, R. Y. Gan, Y. Li, H. B. Li, Bioactivity, health benefits, and related molecular mechanisms of curcumin: Current progress, challenges, and perspectives, Nutrients, 10 (2018) 1–33.

[13] G. A. Hampannavar, R. Karpoormath, M. B. Palkar, M. S. Shaikh, An appraisal on recent medicinal perspective of curcumin degradant: Dehydrozingerone (DZG), Bioorg. Med. Chem., 24 (2016) 501–520.

[14] S. Y. Teow, K. Liew, S. A. Ali, A. S. B. Khoo, S. C. Peh, Antibacterial action of curcumin against *Staphylococcus aureus*: A brief review, J. Trop. Med., 2016 (2016) 1–10.

[15] S. J. Hewlings, D. S. Kalman, Curcumin: A review of its' effects on human health, Foods, 6 (2017) 1–11.

[16] M. Heger, R. F. Van Golen, M. Broekgaarden, M. C. Michel, The molecular basis for the pharmacokinetics and pharmacodynamics of curcumin and its metabolites in relation to cancer, Pharmacol. Rev., 66 (2014) 222–307.

[17] D. D. Subhedar, M. H. Shaikh, L. Nawale, D. Sarkar, V. M. Khedkar, B. B. Shingate, Quinolidene based monocarbonyl curcumin analogues as promising antimycobacterial agents: Synthesis and molecular docking study, Bioorg. Med. Chem. Lett., 27 (2017) 922–928.

[18] L. G. Mourão, C. R. Polaquini, M. Kopacz, G. S. Torrezan, G. M. Ayusso, G. Dilarri, L. B. Cavalca, A. Zielinska, D. Scheffers, L. O. Regasini, H. Ferreira, A simplified curcumin targets the membrane of *Bacillus subtilis*, MicrobiologyOpen, (2018) 1–12 [doi: 10.1002/mbo3.683].

[19] SciFinder. Available in: < https://scifinder.cas.org/> Access in: jan 2019.

[20] A. Koch, V. Mizrahi, *Mycobacterium tuberculosis*, Trends Microbiol., 26 (2018) 555–556.

[21] D. Machado, M. Girardini, M. Viveiros, M. Pieroni, Challenging the drug-likeness dogma for new drug discovery in tuberculosis, Front. Microbiol., 9 (2018) 1–23.

[22] P. J. Brennan, D. B. Young, B. D. Robertson, Handbook of anti-tuberculosis agents (Tuberculosis), Global Alliance for TB Drug Development - Elsevier Health, 82 (2008) 85–170.

[23] T. Yuan, N. S. Sampson, Hit generation in TB drug discovery: From genome to granuloma, Chem. Rev., 118 (2017) 1887–1916.

[24] Z. Iqbal, I. Ullah, H. U. Rehman, N. Wali, R. Ahmad, H. Zaman, R. Kamal, M. A. Jadoon, H. Rehman, M. U. Rehman, R. Ullah, A. Zeb, M. Waqas, M. F. Hameed,

Mycobacterium tuberculosis & its recent vaccine approach: A review. J. Entomol. Zool. Studies, 5 (2017) 360–365.

[25] Y. Kawasaki, E. Freire, Finding a better path to drug selectivity, Drug. Discov. Today, 15 (2011) 985–990.

[26] H. Lee, P. M. Giguere, B. L. Roth, DREADDs: novel tools for drug discovery and development, Drug Discov. Today, 19 (2014) 469–473.

[27] I. Orme, J. Secrist, S. Anathan, C. Kwong, J. Maddry, R. Reynolds, A. Poffenberger, M. Michael, L. Miller, J. Krahenbuh, L. Adams, A. Biswas, S. Franzblau, D. Rouse, D. Winfield, J. Brooks, Search for new drugs for treatment of tuberculosis, Antimicrob. Agents Chemother., 45 (2001) 1943–1946.

[28] M. Zignol, A. S. Dean, D. Ph, D. Falzon, W. V. Gemert, A. Wright, A. V. Deun, F. Portaels, D. Ph, A. Laszlo, D. Ph, M. A. Espinal, A. P. Méndez, A. Bloom, M. A. Aziz, K. Weyer, D. Sc, E. Jaramillo, P. Nunn, K. Floyd, D. Ph, M. C. Raviglione, Special report twenty years of global surveillance of antituberculosis-drug resistance, N. Engl. J. Med., 375 (2016) 1081–1089.

[29] K. R. Caleffi-Ferracioli, F. G. Maltempe, V. L. Siqueira, R. F. Cardoso, Fast detection of drug interaction in *Mycobacterium tuberculosis* by a checkerboard resazurin method, Tuberculosis, 93 (2013) 660–663.

[30] A. R. Barbosa, K. R. Caleffi-Ferracioli, C. Q. F. Leite, J. C. Garcia-Ramos, Y. Toledano-Magana, L. Ruiz-Azuara, V. L. D. Siqueira, F. R. Pavan, R. F. Cardoso, Potential of Casiopeínas® copper complexes and antituberculosis drug combination against *Mycobacterium tuberculosis*, Chemother., 61 (2016) 249–255.

[31] F. G. Maltempe, K. R. Caleffi-Ferracioli, R. C. R. Amaral, F. O. Demitto, V. L. D. Siqueira, R. B. L. Scodro, M. H. Hirata, F. R. Pavan, R. F. Cardoso, Activity of rifampicin and linezolid combination in *Mycobacterium tuberculosis*, Tuberculosis, 104 (2017) 24–29.

[32] C. J. Tsai, J. M. S. Loh, T. Proft, *Galleria mellonella* infection models for the study of bacterial diseases and for antimicrobial drug testing, Virulence, 7 (2016) 214–229.

[33] I. A. Freires, J. C. O. Sardi, R. D. Castro, P. L. Rosalen, Alternative animal and non-animal models for drug discovery and development: Bonus or burden?, Pharm. Res., 34 (2017) 681–686.

[34] U. Binder, E. Maurer, C. Lass-Florl, *Galleria mellonella*: An invertebrate model to study pathogenicity in correctly defined fungal species, Fungal Biol., 120 (2016) 288–295.

[35] Y. Li, J. Spiropoulos, W. Cooley, J. S. Khara, C. A. Gladstone, M. Asai, J. T., Bossé, B. D. Robertson, S. M. Newton, P. R. Langford, *Galleria mellonella* - a novel infection model for the *Mycobacterium tuberculosis* complex, Virulence, 9 (2018) 1126–1137.

[36] N. Polkam, V. R. Ramaswamy, P. Rayam, T. R. Allaka, H. S. Anantaraju, S. Dharmarajan, Y. Perumal, D. Gandamalla, N. R. Yellu, S. Balasubramanian, J. S. Anireddy, Synthesis, molecular properties prediction and anticancer, antioxidant evaluation of new edaravone derivatives, Bioorg. Med. Chem. Lett., 26 (2016) 2562–2568.

[37] C. A. Lipinski, Lead-and drug-like compounds: the rule-of-five revolution, Drug Discov. Today Technol., 1 (2004) 337–341.

[38] D. Machado, M. Girardini, M. Viveiros, M. Pieroni, Challenging the drug-likeness dogma for new drug discovery in tuberculosis, Front. Microbiol., 9 (2018) 1–23.

[39] D. F. Veber, S. R. Johnson, H. Y. Cheng, B. R. Smith, K. W. Ward, K. D. Kopple, Molecular properties that influence the oral bioavailability of drug candidates, J. Med. Chem., 45 (2002) 2615–2623.

[40] Y. Miyaji, Y. Fujii, S. Takeyama, Y. Kawai, M. Kataoka, M. Takahashi, S. Yamashita, Advantage of the dissolution/permeation system for estimating oral absorption of drug candidates in the drug discovery stage, Mol. Pharm., 13 (2016) 1564–1574.

[41] H. E. Selick, A. P. Beresford, M. H. Tarbit, The emerging importance of predictive ADME simulation in drug discovery, Drug. Discov. Today, 7 (2002) 109–116.

[42] S. Yee, *In vitro* permeability across Caco-2 cells (colonic) can predict *in vivo* (small intestinal) absorption in man – fact or myth, Pharm. Res., 14 (1997) 763–766.

[43] C. Saraiva, C. Praça, R. Ferreira, T. Santos, L. Ferreira, L. Bernardino, Nanoparticle-mediated brain drug delivery: Overcoming blood–brain barrier to treat neurodegenerative diseases, J. Control. Release, 235 (2016) 34–47.

[44] L. M. van Leeuwen, M. Boot, C. Kuijl, D. I. Picavet, G. van Stempvoort, S. M. A. van der Pol, H. E. Vries, N. N. van der Wel, M. van der Kuip, A. M. van Furth, A. M. van der Sar, W. Bitter, Mycobacteria employ two different mechanisms to cross the blood–brain barrier, Cell. Microbiol., 20 (2018) 1–17.

[45] Y. Brito-Sanchez, Y. Marrero-Ponce, S. J. Barigye, I. Yaber-Goenaga, C. M. Perez, H. Le-Thi-Thu, A. Cherkasov, Towards better BBB passage prediction using an extensive and curated data set, Mol. Inform., 34 (2015) 308–330.

[46] S. Mailankody, G. V. Dangeti, R. Soundravally, N. M. Joseph, J. Mandal, T. K. Dutta, T. Kadhiravan, Cerebrospinal fluid matrix metalloproteinase 9 levels, blood-brain barrier permeability, and treatment outcome in tuberculous meningitis, PLOS ONE, 12 (2017) 1–12.

[47] OECD. Test No. 117: Partition coefficient (*n*-octanol/water), HPLC method. In: OECD Guidelines for the Testing Chemicals; OECD Publishing: Paris, France, (2004) 1–11.

[48] J. C. Palomino, A. Martin, M. Camacho, H. Guerra, J. Swings, F. Portaels, *Resazurin Microtiter Assay* Plate: Simple and inexpensive method for detection of drug resistance in *Mycobacterium tuberculosis*, Antimicrob. Agents Chemother., 46 (2002) 2720–2722.

[49] F. R. Pavan, P. I. S. Maia, S. R. A. Leite, V. M. Deflon, A. A. Batista, D. N. Sato, S. G. Franzblau, C. Q. F. Leite, Thiosemicarbazones, semicarbazones, dithiocarbazates and hydrazide/ hydrazones: Anti-*Mycobacterium tuberculosis* activity and cytotoxicity, Eur. J. Med. Chem., 45 (2010) 1898–1905.

[50] J. Megaw, T. P. Thompson, R. A. Lafferty, B. F. Gilmore, *Galleria mellonella* as a novel *in vivo* model for assessment of the toxicity of 1-alkyl-3-methylimidazolium chloride ionic liquids, Chemosphere, 139, (2015) 197–201.

[51] Molinspiration Cheminformatics. Available in: <https://www.molinspiration.com/cgi-bin/properties> Access in: jan 2019.

[52] PreADMET. Available in: <https://preadmet.bmdrc.kr/adme/> Access in: jan 2019.

Figure 1. Structure of **(A)** curcumin and **(B)** analogue **1**

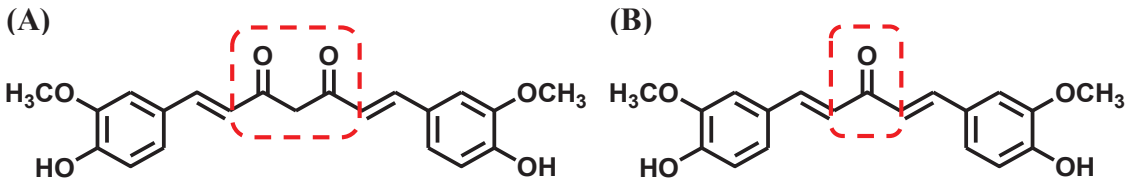

Scheme 1. Synthesis of dehydrozingerone (DZG)

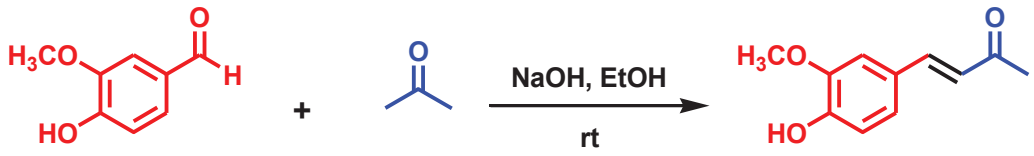

Scheme 2. Synthesis of monocarbonyl analogues of curcumin

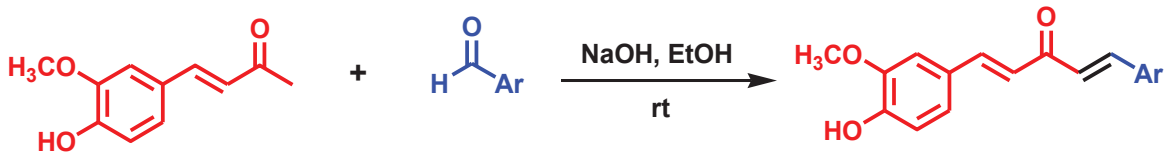

Table 1. Structures of monocarbonyl analogues of curcumin (**1–28**)

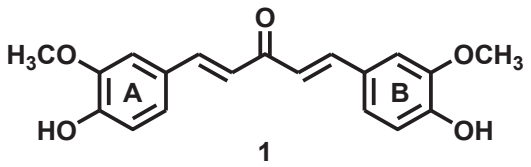

1

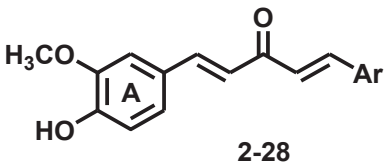

2-28

Monocarbonyl analogues of curcumin	Ar
Series I	
1	-
2	phenyl
3	2-fluorophenyl
4	3-fluorophenyl
5	4-fluorophenyl
6	2-chlorophenyl
7	3- chlorophenyl
8	4- chlorophenyl
9	2-bromophenyl
10	3-bromophenyl
11	4-bromophenyl
12	3-trifluoromethylphenyl
13	4- trifluoromethylphenyl
14	4-trifluoromethoxylphenyl
15	3-nitrophenyl
16	4-nitrophenyl
17	4-nitrilphenyl
18	3-methoxyphenyl
19	4-hydroxyphenyl
20	4-methylphenyl
21	4-ethylphenyl
22	4-*terc*-butylphenyl
23	biphenyl
Series II	
24	3-pyridinyl
25	4-pyridinyl
26	2-thiophenyl
27	2-furanyl
28	5-nitro-2-furanyl

Table 2. Antimycobacterial activity against *M. tuberculosis* H37Rv and log $P_{o/w}$ of curcumin and its analogues (**1–28**)

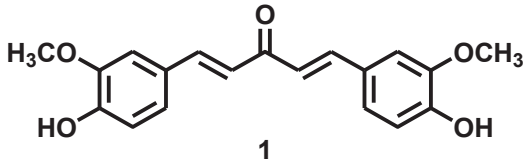

1

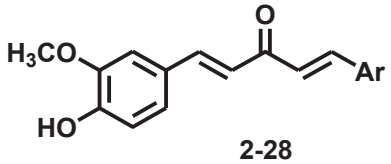

2-28

Compounds	Ar	MIC$_{90}$ (μM)	log $P_{o/w}$
Curcumin	-	> 85.0	nd
1	-	24.5	1.9
Series I			
2	phenyl	10.4	3.1
3	2-fluorophenyl	9.4	3.3
4	3-fluorophenyl	5.7	3.3
5	4-fluorophenyl	14.5	3.2
6	2-chlorophenyl	18.0	3.7
7	3- chlorophenyl	7.9	3.9
8	4- chlorophenyl	4.5	3.8
9	2-bromophenyl	10.7	3.8
10	3- bromophenyl	9.6	4.0
11	4- bromophenyl	7.9	4.0
12	3-trifluoromethylphenyl	23.6	3.9
13	4-trifluoromethylphenyl	6.9	4.0
14	4-trifluoromethoxylphenyl	7.2	4.1
15	3-nitrophenyl	2.5	3.0
16	4-nitrophenyl	2.7	3.0
17	4-nitrilphenyl	3.1	2.4
18	3-methoxylphenyl	8.3	3.2
19	4-hydroxyphenyl	> 85.0	1.9
20	4-methylphenyl	10.9	3.7
21	4-ethylphenyl	28.2	4.2
22	4-*terc*-butylphenyl	19.9	5.1
23	biphenyl	14.8	4.8
Series II			
24	3-pyridinyl	1.8	1.8
25	4-pyridinyl	2.0	1.9
26	2-thiophenyl	2.7	2.8
27	2-furanyl	5.2	2.4
28	5-nitro-2-furanyl	0.3	2.4
rifampicin	-	0.1	nd
isoniazid	-	0.3	nd

nd: no determined

Table 3. Cytotoxicity and selectivity of bioactive compounds for human lung fibroblasts MRC-5 and murine macrophages J774A.1

	Lung Fibroblasts MRC-5		Macrophages J774A.1	
Compounds	**IC_{50} (µM)**	**[a]SI**	**IC_{50} (µM)**	**[b]SI**
1	59.8	2.4	94.8	3.9
Series I				
2	78.4	7.5	194.2	18.7
3	74.1	7.9	178.7	19.0
4	49.3	8.6	160.3	28.1
5	112.3	7.7	124.5	8.6
6	113.7	6.3	189.4	10.5
7	91.6	11.6	161.6	20.5
8	86.6	19.2	153.7	34.2
9	75.1	7.0	75.5	7.1
10	77.5	8.1	133.7	13.9
11	73.3	9.3	165.0	20.9
12	64.4	2.7	149.7	6.3
13	80.5	11.7	71.5	10.4
14	45.0	6.3	147.8	20.5
15	74.1	29.6	161.2	64.5
16	81.0	30.0	168.4	62.4
17	72.9	23.5	197.2	63.6
18	81.6	9.8	204.1	24.6
20	85.9	7.9	105.5	9.7
21	84.4	3.0	177.2	6.3
22	72.4	3.6	167.3	8.4
23	277.2	18.7	118.6	8.0
Series II				
24	45.7	25.4	210.7	117.1
25	28.0	14.0	214.5	107.3
26	55.7	20.6	328.0	121.5
27	87.3	16.8	320.3	61.6
28	35.0	116.7	223.1	743.7
doxorubicin	0.002	nd	0.005	nd

nd: no determined

[a] SI (lung fibroblasts) = IC_{50} (lung fibroblasts) / MIC_{90} (*M. tuberculosis* H37Rv)

[b] SI (macrophages) = IC_{50} (macrophages) / MIC_{90} (*M. tuberculosis* H37Rv)

Table 4. Antimycobacterial activity of selective compounds against clinical isolates of *M. tuberculosis* with drug resistance

	MIC$_{90}$ (µM)			
Compounds	**[a]CF 44**	**[a]CF 184**	**[b]CF 61**	**[c]CF 48**
Series I				
7	11.0	4.1	6.2	> 93.0
8	9.0	21.0	6.7	76.8
13	4.1	2.6	2.5	62.7
15	3.3	3.6	2.5	> 93.0
16	6.4	19.0	3.6	> 93.0
17	7.1	35.8	4.3	> 93.0
Series II				
24	84.0	40.4	42.6	> 93.0
25	66.5	56.8	36.3	> 93.0
26	> 93.0	87.0	81.0	> 93.0
27	21.8	30.4	16.8	> 93.0
28	22.1	5.9	6.3	> 93.0
rifampicin	0.1	0,1	r	0.4
isoniazid	r	r	r	r
gatifloxacin	0.3	0.3	r	r
amikacin	1.5	0.6	r	r

r: resistant

[a] isoniazid-resistant

[b] rifampicin/isoniazid/gatifloxacin/amikacin-resistant (XDR strain)

[c] isoniazid/gatifloxacin/amikacin-resistant

Table 5. Evaluation of interactions between analogue **28** and clinically used anti-TB drugs in two-drug combinations against *M. tuberculosis* H37Rv

	FICI	[a]**Interaction effect**
rifampicin	0.6	indifferent
moxifloxacin	0.6	indifferent

[a] FICI ≤ 0.5: synergism, 0.5 < FICI < 4: indifference,

FICI ≥ 4: antagonism

Figure 2. Percentage of *G. mellonella* survival after treatment with analogue **28** for 96 hours

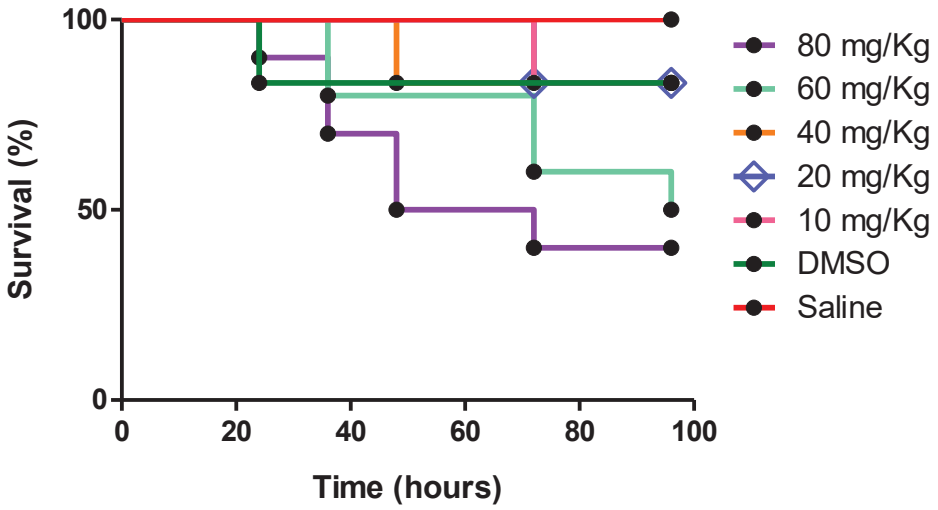

Table 6. *In silico* drug-likeness properties of bioactive compounds based on Lipinski's rules

Compounds	log $P_{o/w}$	MW	HBD	HBA	Lipinski's violations
1	1.9	326.4	2	5	0
Series I					
2	3.1	280.3	1	3	0
3	3.3	298.3	1	3	0
4	3.3	298.3	1	3	0
5	3.2	298.3	1	3	0
6	3.7	314.8	1	3	0
7	3.9	314.8	1	3	0
8	3.8	314.8	1	3	0
9	3.8	359.2	1	3	0
10	4.0	359.2	1	3	0
11	4.0	359.2	1	3	0
12	3.9	348.3	1	3	0
13	4.0	348.3	1	3	0
14	4.1	364.3	1	4	0
15	3.0	325.3	1	6	0
16	3.0	325.3	1	6	0
17	2.4	305.3	1	4	0
18	3.2	310.4	1	4	0
20	3.7	294.4	1	3	0
21	4.2	308.4	1	3	0
22	5.1	336.4	1	3	1
23	4.8	356.4	1	3	0
Series II					
24	1.8	281.3	1	4	0
25	1.9	281.3	1	4	0
26	2.8	286.4	1	3	0
27	2.4	270.3	1	4	0
28	2.4	315.3	1	7	0

log $P_{o/w}$: partition coefficient *n*-octanol/water, MW: molecular weight, HBD: number of hydrogen bond donors, HBA: number of hydrogen bond acceptors

Table 7. *In silico* drug-likeness properties of bioactive compounds based on Veber's rules

Compounds	HBD + HBA	NROTB	Veber's violations
1	7	6	0
Series I			
2	4	5	0
3	4	5	0
4	4	5	0
5	4	5	0
6	4	5	0
7	4	5	0
8	4	5	0
9	4	5	0
10	4	5	0
11	4	5	0
12	4	6	0
13	4	6	0
14	5	7	0
15	7	6	0
16	7	6	0
17	5	5	0
18	5	6	0
20	4	5	0
21	4	6	0
22	4	6	0
23	4	6	0
Series II			
24	5	5	0
25	5	5	0
26	4	5	0
27	5	5	0
28	8	6	0

HBD: number of hydrogen bond donors, HBA: number of hydrogen bond acceptors, NROTB: number of routable bonds

Table 8. *In silico* percentage of HIA of bioactive compounds

Compounds	HIA (%)
1	93.7
Series I	
2	95.7
3	95.7
4	95.7
5	95.7
6	96.2
7	96.2
8	96.2
9	96.5
10	96.5
11	96.5
12	95.9
13	95.9
14	95.8
15	89.9
16	89.9
17	96.2
18	95.8
20	95.8
21	95.9
22	96.1
23	96.6
Series II	
24	95.7
25	95.7
26	96.5
27	95.7
28	87.2

HIA: human intestinal absorption

Table 9. *In silico* BBB penetration of bioactive compounds

Compounds	BBB
1	0.5
Series I	
2	0.7
3	1.0
4	0.9
5	1.0
6	2.0
7	1.8
8	1.9
9	2.2
10	2.0
11	2.2
12	3.0
13	2.6
14	3.9
15	0.5
16	0.4
17	0.1
18	0.2
20	1.4
21	2.6
22	4.1
23	2.3
Series II	
24	0.03
25	0.04
26	0.04
27	0.1
28	0.2

BBB: blood-brain barrier

SUPPLEMENTARY MATERIAL

Molecular Simplification and Ring Bioisosterism Improved Antitubercular Activity of Monocarbonyl Analogues of Curcumin

Gabriela M. Ayusso [a], Débora L. Campos [b], Mariana B. Santos [a], Carlos R. Polaquini [a], Valéria K. Almeida [a], Camila M. Ribeiro [b], Mariana C. Solcia [b], Diego A. Monteiro [c], Eleni Gomes [c], Janaina C. O. Sardi [d], Pedro L. Rosalen [d], Fernando R. Pavan [b,*], Luis O. Regasini [a,**]

[a] *Department of Chemistry and Environmental Sciences, Institute of Biosciences, Humanities and Exact Sciences (IBILCE), São Paulo State University (UNESP), São José do Rio Preto, SP, Brazil.*

[b] *Department of Biological Sciences, School of Pharmaceutical Sciences (FCFAR), São Paulo State University (UNESP), Araraquara, SP, Brazil.*

[c] *Department of Biology, Institute of Biosciences, Humanities and Exact Sciences (IBILCE), São Paulo State University (UNESP), São José do Rio Preto, SP, Brazil.*

[d] *Department of Physiological Sciences, Piracicaba Dental School, University of Campinas (UNICAMP), Piracicaba, SP, Brazil.*

*** Corresponding author.**

**** Corresponding author.**

E-mail addresses: regasini@ibilce.unesp.br (LO Regasini) and fernandopavan@fcfar.unesp.br (FR Pavan).

1. SPECTROSCOPY DATA ANALYSIS

The melting points of compounds were determined on a capillary point apparatus with a digital thermometer. The UV-Vis spectrum and purity of compounds were recorded on HPLC-PAD analysis performed for determination of log $P_{o/w}$. The NMR spectra were obtained on Bruker® Avance III 9.397 T (400 MHz), Bruker® Avance III 14.095 T (600 MHz) and Bruker® Fourier (300 MHz) spectrometers. The compounds were solubilized in deuterated chloroform ($CDCl_3$) or hexadeuterated dimethylsulfoxide (DMSO-d_6). The NMR data are represented as chemical shifts (in ppm), coupling constants (J in Hz) and multiplicities: s = singlet; br s = broad singlet; d = doublet; m = multiplet; dd = doublet of doublets; and ddd = doublet of doublet of doublets.

The purity of compounds was measured by band area values, which ranged from 85.0 to 99.9%. The melting points of compounds ranged from 43 to 221 ºC. The UV-Vis spectra indicated λ_{max} values ranging from 314 to 386 nm. The ^{1}H NMR spectra presented a pair of doublets with coupling constants characteristics of carbon-carbon double bond with *trans* configuration ($J \approx 16$ Hz). The ^{13}C NMR spectra exhibited signals characteristics of α,β-unsaturated ketones ($\delta \approx 189$ ppm). The simultaneous presence of these signals in the NMR spectra confirmed the formation of an enone bridge in the structure of designed compounds.

1.1. Dehydrozingerone (DZG)

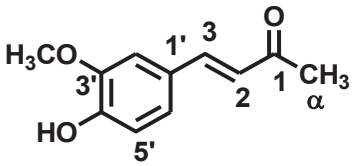

Yield: 51%

Purity: 99.9%

Melting point: 127–129 ºC

UV-Vis: λ_{max} 334 nm

^{1}H NMR (400 MHz, $CDCl_3$): 7.61 (d; 16.0; H-3), 7.47 (d; 16.0; H-2), 7.11 (dd; 2.0 and 8.0; H-6'), 7.02 (d; 2.0; H-2'), 6.95 (d; 8.0; H-5'), 5.97 (br s; 4'-OH), 3.96 (s; 3'-OCH_3), 2.39 (s; α-CH_3).

^{13}C NMR (100 MHz, $CDCl_3$): 198.4 (C-1), 148.3 (C-3'), 146.9 (C-4'), 143.8 (C-3), 126.9 (C-1'), 125.0 (C-2), 123.5 (C-5'), 114.8 (C-5'), 109.8 (C-2'), 56.0 (3'-OCH_3), 27.3 (α-CH_3).

1.2. Compound 1

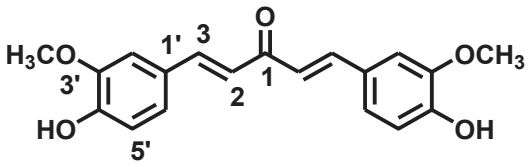

Yield: 47%

Purity: 99.1%

Melting point: 95–97 ºC

UV-Vis: λ_{max} 386 nm

^{1}H NMR (400 MHz, $CDCl_3$): 7.69 (d; 16.0; H-3), 7.20 (dd; 1.6 and 8.2; H-6'), 7.13 (d; 1.6; H-2'), 6.97 (d; 8.2; H-5'), 6.96 (d; 16.0; H-2), 5.98 (br s; 4'-OH), 3.98 (s; 3'-OCH_3).

^{13}C NMR (100 MHz, $CDCl_3$): 188.8 (C-1), 148.2 (C-3'), 146.8 (C-3), 143.2 (C-4'), 127.5 (C-1'), 123.4 (C-2 and C-6'), 114.9 (C-5'), 109.8 (C-2'), 56.0 (3'-OCH_3).

1.3. Compound 2

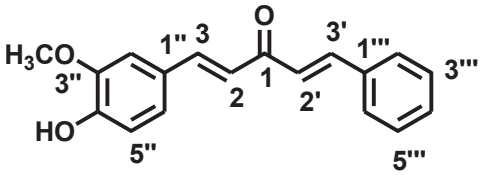

Yield: 72%

Purity: 99.7%

UV-Vis: λ_{max} 369 nm

^{1}H NMR (300 MHz, $CDCl_3$): 7.75 (d; 15.9; H-3'), 7.70 (d; 15.8; H-3), 7.64 (dd; 6.8 and 2.8, H-2''' and H-6'''), 7.43 (dd; 6.8 and 4.9; H-3''' and H-5'''), 7.43 (m; H-4'''), 7.20 (dd; 8.2 and 1.9; H-6''), 7.14 (d; 1.9; H-2''), 7.11 (d; 15.9; H-2'), 6.97 (d; 8.2; H-5''), 6.95 (d; 15.8; H-2), 3.98 (s; 3''-OCH_3).

^{13}C NMR (150 MHz, $CDCl_3$): 188.9 (C-1), 148.3 (C-3''), 146.8 (C-4''), 143.7 (C-3), 142.9 (C-3'), 134.9 (C-1'''), 130.4 (C-4'''), 129.0 (C-3''' and C-5'''), 128.4 (C-2''' and C-6'''), 127.4 (C-1''), 125.3 (C-6''), 123.5 (C-2'), 123.4 (C-2), 114.9 (C-5''), 109.7 (C-2''), 56.0 (3''-OCH_3).

1.4. Compound 3

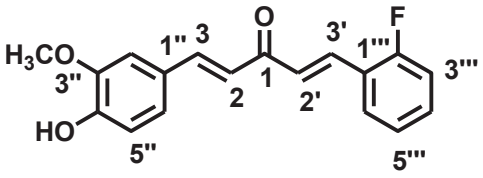

Yield: 8%

Purity: 97.9%

Melting point: 43–45 ºC

UV-Vis: λ_{max} 370 nm

^{1}H NMR (600 MHz, $CDCl_3$): 7.84 (d; 16.1; H-3'), 7.69 (d; 15.9; H-3), 7.63 (ddd; 7.6, 7.6 and 1,5; H-4'''), 7.40 – 7.36 (m; H-6'''), 7.19 (d; 16.1; H-2'), 7.21 – 7.18 (m; H-5'''), 7,19 (dd; 8.2 and 2.0; H-6''), 7.15 – 7.11 (m; H-3'''), 7.13 (d; 2.0; H-2''), 6.96 (d; 8.2; H-5''), 6.94 (d; 15.9; H-2), 3.97 (s; 3''-OCH_3).

^{13}C NMR (150 MHz, $CDCl_3$): 188.9 (C-1), 161.6 (d; J_{CF} 252, C-2'''), 148.3 (C-3''), 146.8 (C-4''), 143.9 (C-3), 135.5 (C-3'), 131.7 (d, J_{CF} 9.0, C-4'''), 129.5 (C-5'''), 127.8 (C-6'''), 127.7 (C-1''), 127.3 (C-6''), 124.5 (C-1'''), 123.6 (C-2'), 123.3 (C-2), 116.3 (d, J_{CF} 22.5, C-3'''), 114.8 (C-5''), 109.7 (C-2''), 56.0 (3''-OCH_3).

1.5. Compound 4

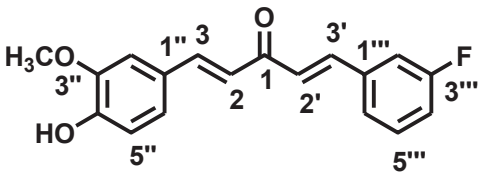

Yield: 75%

Purity: 99.0%

Melting point: 70–72 ºC

UV-Vis: λ_{max} 372 nm

^{1}H NMR (600 MHz, $CDCl_3$): 7.72 (d; 15.8; H-3'), 7.70 (d; 15.9; H-3), 7.42 – 7.38 (m; H-5''' and H-6'''), 7.36 – 7.33 (m; H-2'''), 7.21 (dd; 8.3 and 1.9; H-6''), 7.14 (d; 1.9; H-2''), 7.13 – 7.09 (m; H-4'''), 7.11 (d; 15.8; H-2'), 6.98 (d; 8.3; H-5'), 6.93 (d; 15.9; H-2), 3.99 (s; 3''-OCH_3).

^{13}C NMR (150 MHz, $CDCl_3$): 188.6 (C-1), 163.0 (d, J_{CF} 244, C-3'''), 148.5 (C-3''), 146.9 (C-4''), 144.1 (C-3), 141.4 (C-3'), 137.2 (d, J_{CF} 7.5, C-1'''), 130.5 (d, J_{CF} 7.5, C-5'''), 127.2 (C-1''), 126.3 (C-6''), 124.5 (d, J_{CF} 1.5, C-6'''), 123.7 (C-2'), 123.4 (C-2), 117.2 (d, J_{CF} 21.0, C-4'''), 114.9 (C-5''), 114.4 (d, J_{CF} 22.5, C-2'''), 109.7 (C-2''), 56.0 (3''-OCH_3).

1.6. Compound 5

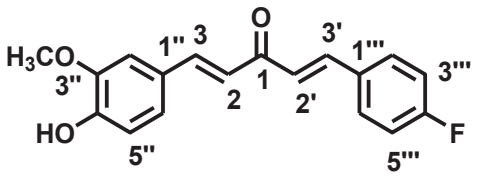

Yield: 84%

Purity: 94.8%

Melting point: 74–76 ºC

UV-Vis: λ_{max} 369 nm

^{1}H NMR (400 MHz, $CDCl_3$): 7.72 (d; 15.9; H-3), 7.71 (d; 15.9; H-3'), 7.63 (dd; 5.4 and 8.8; H-2''' and H-6'''), 7.20 (dd; 2.0 and 8.2; H-6''), 7.13 (m; H-2''), 7.04 (d; 15.9; H-2'), 6.98 (d; 8.2; H-5''), 6.94 (d; 15.9; H-2), 3.98 (s; 3''-OCH_3).

^{13}C NMR (150 MHz, $CDCl_3$): 188.9 (C-1), 164.0 (d, J_{CF} 249, C-4’’’), 148.3 (C-3’’), 146.8 (C-4’’), 143.8 (C-3), 141.7 (C-3’), 132.9 (C-1’’’), 130.2 (C-2’’’ and C-6’’’), 127.3 (C-1’’), 125.0 (C-6’’), 123.5 (C-2’), 123.4 (C-2), 116.1 (C-3’’’ and C-5’’’), 114.9 (C-5’’), 109.7 (C-2’’), 56.0 (3’’-OCH_3).

1.7. Compound 6

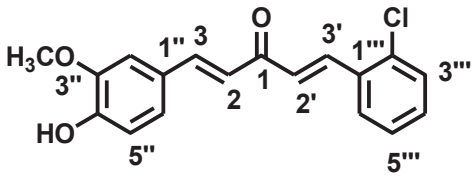

Yield: 9%

Purity: 85.0%

Melting point: 59–61 ºC

UV-Vis: λ_{max} 372 nm

^{1}H NMR (600 MHz, $CDCl_3$): 8.14 (d; 16.0; H-3’), 7.74 (dd; 7.4 and 2.1; H-6’’’), 7.72 (d; 15.9; H-3), 7.46 (dd; 7.7 and 1.6; H-3’’’), 7.34 (m; H-4’’’ and H-5’’’), 7.21 (dd; 8.2 and 1.8; H-6’’), 7.14 (d; 1.8; H-2’’), 7.08 (d; 16.0; H-2’), 6.98 (d; 15.9; H-2), 6.98 (d; 8.2; H-5’’), 3.98 (s; 3’’-OCH_3).

^{13}C NMR (150 MHz, $CDCl_3$): 188.8 (C-1), 148.4 (C-3’’), 146.9 (C-4’’), 144.1 (C-3), 138.6 (C-3’), 135.4 (C-2’’’), 133.2 (C-1’’’), 131.1 (C-4’’’), 130.3 (C-3’’’), 128.0 (C-6’’’), 127.7 (C-5’’’), 127.3 (C-1’’), 127.1 (C-6’’), 123.6 (C-2), 122.9 (C-2’), 114.9 (C-5’’), 109.8 (C-2’’), 56.0 (3’’-OCH_3).

1.8. Compound 7

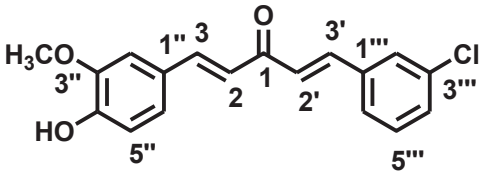

Yield: 10%

Purity: 98.3%

Melting point: 123–125 ºC

UV-Vis: λ_{max} 372 nm

^{1}H NMR (600 MHz, $CDCl_3$): 7.72 (d; 15.8; H-3'), 7.68 (d; 15.9; H-3), 7.64 (dd; 1.8 and 1.8; H-2'''), 7.50 (ddd; 1.4, 1.8 and 7.4; H-6'''), 7.39 – 7.36 (m; H-4''' and H-5'''), 7.21 (dd; 8.3 and 1.9; H-6''), 7.15 (d; 1.9; H-2''), 7.12 (d; 15.8; H-2'), 6.98 (d; 8.3; H-5''), 6.93 (d; 15.9; H-2), 3.99 (s; 3''-OCH_3).

^{13}C NMR (150 MHz, $CDCl_3$): 188.5 (C-1), 148.4 (C-3''), 146.8 (C-4''), 144.1 (C-3), 141.2 (C-3'), 136.8 (C-3'''), 134.9 (C-1'''), 130.2 (C-4'''), 131.1 (C-5'''), 127.8 (C-2'''), 127.2 (C-1''), 126.7 (C-6'''), 126.3 (C-6''), 123.7 (C-2'), 123.4 (C-2), 114.9 (C-5''), 109.7 (C-2''), 56.0 (3''-OCH_3).

1.9. Compound 8

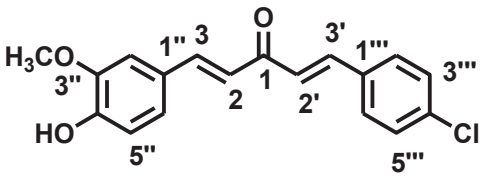

Yield: 63%

Purity: 98.8%

Melting point: 119–121 ºC

UV-Vis: λ_{max} 372 nm

^{1}H NMR (600 MHz, $CDCl_3$): 7.71 (d; 15.9; H-3'), 7.69 (d; 15.9; H-3), 7.56 (d; 8.4; H-2''' and H-6'''), 7.40 (d; 8.4; H-3''' and H-5'''), 7.20 (dd; 8.3 and 1.9; H-6''), 7.13 (d; 1.9; H-2''), 7.09 (d; 15.9; H-2'), 6.98 (d; 8.3; H-5''), 6.93 (d; 15.9; H-2), 3.98 (s; 3''-OCH_3).

^{13}C NMR (150 MHz, $CDCl_3$): 188.6 (C-1), 148.4 (C-3''), 146.9 (C-4''), 144.0 (C-3), 141.4 (C-3'), 136.3 (C-4'''), 133.4 (C-1'''), 129.5 (C-3''' and C-5'''), 129.2 (C-2''' and C-6'''), 127.2 (C-1''), 125.6 (C-6''), 123.6 (C-2'), 123.4 (C-2), 114.9 (C-5''), 109.7 (C-2''), 56.0 (3''-OCH_3).

1.10. Compound 9

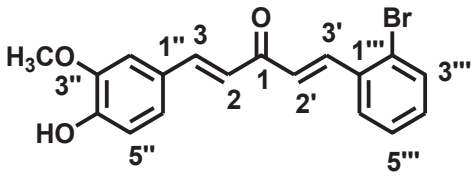

Yield: 43%

Purity: 96.7%

Melting point: 78–80 ºC

UV-Vis: λ_{max} 372 nm

^{1}H NMR (300 MHz, $CDCl_3$): 8.08 (d; 16.0; H-3'), 7.72 (dd; 8.0 and 1.8; H-3'''), 7.71 (d; 15.8; H-3), 7.65 (dd; 8.0 and 1.2; H-6'''), 7.37 (dd; 8.0 and 7.2; H-4'''), 7.30 – 7.24 (m; H-5'''), 7.21 (dd; 8.2 and 1.9; H-6''), 7.13 (d; 1.9; H-2''), 7.02 (d; 16.0; H-2'), 6.97 (d; 15.8; H-2), 6.97 (d; 8.2; H-5''), 3.98 (s; 3''-OCH_3).

^{13}C NMR (150 MHz, $CDCl_3$): 188.7 (C-1), 148.4 (C-3’’), 146.8 (C-4’’), 144.1 (C-3), 141.2 (C-3’), 135.0 (C-1’’’), 133.5 (C-3’’’), 131.2 (C-4’’’), 128.2 (C-6’’’), 127.8 (C-5’’’), 127.7 (C-6’’), 127.3 (C-1’’), 125.8 (C-2’’’), 123.6 (C-2), 122.9 (C-2’), 114.9 (C-5’’), 109.8 (C-2’’), 56.0 (3’’-OCH_3).

1.11. Compound 10

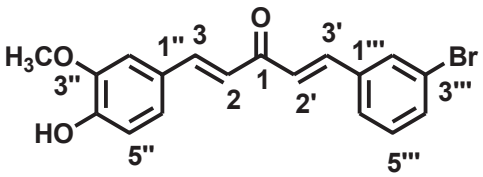

Yield: 40%

Purity: 98.9%

Melting point: 140–142 ºC

UV-Vis: λ_{max} 372 nm

^{1}H NMR (300 MHz, $CDCl_3$): 7.79 (dd; 1.7 and 1.8; H-2’’’), 7.70 (d; 16.0; H-3’), 7.65 (d; 15.9; H-3), 7.56 – 7.50 (m; H-4’’ and H-6’’), 7.31 (d; 7.8; H-5’’’), 7.20 (dd; 8.2 and 2.1; H-6’’), 7.13 (d; 2.1; H-2’’), 7.10 (d; 16.0; H-2’), 6.97 (d; 8.2; H-5’’), 6.91 (d; 15.9; H-2), 3.98 (s; 3’’-OCH_3).

^{13}C NMR (150 MHz, $CDCl_3$): 188.5 (C-1), 148.4 (C-3’’), 146.9 (C-4’’), 144.1 (C-3), 141.1 (C-3’), 137.1 (C-1’’’), 133.1 (C-2’’’), 130.7 (C-4’’’), 130.5 (C-5’’’), 127.2 (C-1’’ and C-6’’’), 126.3 (C-6’’), 123.7 (C-2’), 123.4 (C-2), 123.1 (C-3’’’), 114.9 (C-5’’), 109.7 (C-2’’), 56.0 (3’’-OCH_3).

1.12. Compound 11

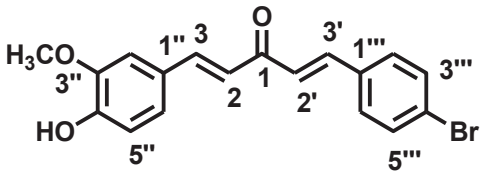

Yield: 10%

Purity: 93.1%

Melting point: 114–116 ºC

UV-Vis: λ_{max} 372 nm

^{1}H NMR (300 MHz, $CDCl_3$): 7.70 (d; 15.8; H-3'), 7.67 (d; 15.9; H-3), 7.56 (d; 8.6; H-3''' and H-5'''), 7.49 (d; 8.6; H-2''' and H-6'''), 7.20 (dd; 8.2 and 1.9; H-6''), 7.13 (d; 1.9; H-2''), 7.09 (d; 15.8; H-2'), 6.97 (d; 8.2; H-5''), 6.92 (d; 15.9; H-2), 3.98 (s; 3''-OCH_3).

^{13}C NMR (150 MHz, $CDCl_3$): 188.6 (C-1), 148.4 (C-3''), 146.8 (C-4''), 144.0 (C-3), 141.5 (C-3'), 133.8 (C-1'''), 132.2 (C-3''' and C-5'''), 129.7 (C-2''' and C-6'''), 127.3 (C-1''), 125.7 (C-6''), 124.6 (C-4'''), 123.6 (C-2'), 123.4 (C-2), 114.9 (C-5''), 109.7 (C-2''), 56.0 (3''-OCH_3).

1.13. Compound 12

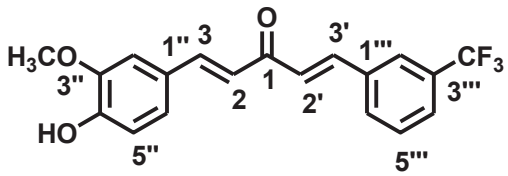

Yield: 50%

Purity: 98.0%

Melting point: 51–53 ºC

UV-Vis: λ_{max} 372 nm

^{1}H NMR (600 MHz, $CDCl_3$): 7.90 (s; H-2’’’), 7.80 (d; 7.7; H-3’’’), 7.76 (d; 15.7; H-3’), 7.74 (d; 15.8; H-3), 7.68 (d; 7.8; H-6’’’), 7.57 (dd; 7.7 and 7.8; H-5’’’), 7.22 (dd; 8.2 and 1.6; H-6’’), 7.18 (d; 15.7; H-2’), 7.15 (d; 1.6; H-2’’), 6.99 (d; 8.2; H-5’’), 6.95 (d; 15.8; H-2), 5.97 (s; 4’’-OH), 3.99 (s; 3’’-OCH_3).

^{13}C NMR (150 MHz, $CDCl_3$): 188.3 (C-1), 148.5 (C-3’’), 146.9 (C-4’’), 144.3 (C-3), 140.9 (C-3’), 135.7 (C-1’’’), 131.6 (C-3’’’), 129.5 (C-6’’’), 127.2 (C-1’’), 126.8 (C-6’’’), 126.6 (C-5’’’), 124.6 (C-4’’’), 123.7 (C-2’), 123.3 (C-2), 122.9 (3’’’-CF_3), 114.9 (C-5’’), 114.1 (C-2’’’), 109.7 (C-2’’), 56.0 (3’’-OCH_3).

1.14. Compound 13

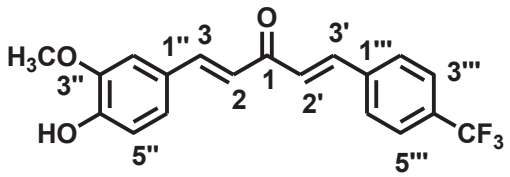

Yield: 90%

Purity: 96.6%

Melting point: 120–122 ºC

UV-Vis: λ_{max} 373 nm

^{1}H NMR (300 MHz, $CDCl_3$): 7.74 (d; 16.3; H-3’), 7.73 (d; 8.9; H-3’’’ and H-5’’’), 7.72 (d; 16.0; H-3), 7.68 (d; 8.9; H-2’’’ and H-6’’’), 7.23 – 7.12 (m; H-6’’), 7.14 (d; 1.9; H-2’’), 7.17 (d; 16.3; H-2’), 6.98 (d; 8.2; H-5’’), 6.94 (d; 16.0; H-2), 3.98 (s; 3’’-OCH_3).

^{13}C NMR (150 MHz, $CDCl_3$): 188.4 (C-1), 148.4 (C-3’’), 146.9 (C-4’’), 144.4 (C-3), 140.9 (C-3’), 138.3 (C-1’’’), 131.7 (d, J_{CF} 33.0, C-4’’’), 128.4 (C-2’’’ and C-6’’’), 127.3 (C-6’’), 127.1 (C-1’’), 125.9 (C-3’’’ and C-5’’’), 123.9 (d, J_{CF} 270, 4’’’-CF_3), 123.7 (C-2’), 123.4 (C-2), 114.9 (C-5’’), 109.7 (C-2’’), 56.0 (3’’-OCH_3).

1.15. Compound 14

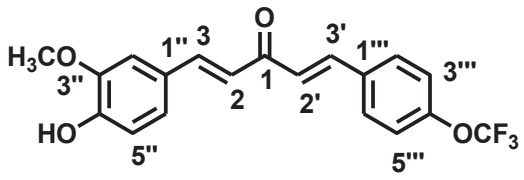

Yield: 45%

Purity: 99.5%

Melting point: 167–169 ºC

UV-Vis: λ_{max} 370 nm

^{1}H NMR (600 MHz, $CDCl_3$): 7.72 (d; 15.9; H-3), 7.72 (d; 15.8; H-3’), 7.67 (d; 8.3; H-2’’’ and H-6’’’), 7.28 (d; 8.3; H-3’’’ and H-5’’’), 7.21 (dd; 8.2 and 1.9; H-6’’), 7.14 (d; 1.9; H-2’’), 7.09 (d; 15.9; H-2), 6.98 (d; 8.2; H-5’’), 6.94 (d; 15.8; H-2’), 3.99 (s; 3’’-OCH_3).

^{13}C NMR (150 MHz, $CDCl_3$): 188.5 (C-1), 150.4 (C-4’’’), 148.4 (C-3’’), 146.9 (C-4’’), 144.0 (C-3), 141.1 (C-3’), 133.4 (C-1’’’), 129.7 (C-2’’’ and C-6’’’), 127.2 (C-1’’), 126.0 (C-6’’), 123.6 (C-2’), 123.3 (C-2), 121.2 (C-3’’’ and C-5’’’), 119.5 (4’’’-OCF_3), 114.9 (C-5’’), 109.7 (C-2’’), 56.0 (3’’-OCH_3).

1.16. Compound 15

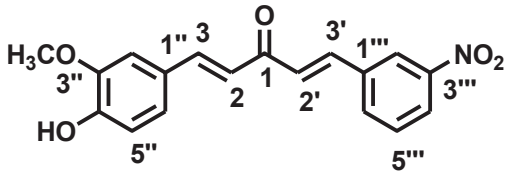

Yield: 65%

Purity: 99.4%

Melting point: 177–179 ºC

UV-Vis: λ_{max} 374 nm

^{1}H NMR (600 MHz, $CDCl_3$): 8.64 (dd; 1.8 and 1.7; H-2’’’), 8.26 (m; H-4’’’ and H-6’’’), 7.83 (d; 16.0; H-3’), 7.80 (d; 16.0; H-3), 7.75 (dd; 8.0 and 7.8; H-5’’’), 7.59 (d; 16.0; H-2’), 7.39 (d; 1.8; H-2’’), 7.24 (dd; 8.2 and 1.8; H-6’’), 7.16 (d; 16.0; H-2), 6.86 (d; 8.2; H-5’’), 3.86 (s; 3’’-OCH_3).

^{13}C NMR (150 MHz, $CDCl_3$): 188.6 (C-1), 150.4 (C-3’’’), 148.8 (C-3’’), 148.5 (C-4’’), 144.9 (C-3), 139.8 (C-3’), 137.2 (C-1’’’), 135.0 (C-6’’’), 130.9 (C-5’’’), 128.5 (C-2’’’), 126.5 (C-1’’), 124.9 (C-4’’’), 124.2 (C-6’’), 123.3 (C-2’), 123.2 (C-2), 116.2 (C-5’’), 111.9 (C-2’’), 56.1 (3’’-OCH_3).

1.17. Compound 16

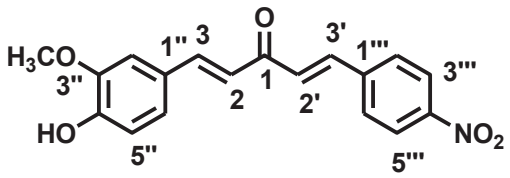

Yield: 10%

Purity: 95.7%

Melting point: 147–149 ºC

UV-Vis: λ_{max} 314 nm

^{1}H NMR (300 MHz, $CDCl_3$): 8.29 (d; 8.7; H-3’’’ and H-5’’’), 7.77 (d; 8.7; H-2’’’ and H-6’’’), 7.75 (d; 16.1; H-3’), 7.73 (d; 15.6; H-3), 7.22 (d; 16.1; H-2’), 7.22 (dd; 8.3 and 1.9; H-6’’), 7.14 (d; 1.9; H-2’’), 6.98 (d; 8.3; H-5’’), 6.93 (d; 15.6; H-2), 3.98 (s; 3’’-OCH_3).

^{13}C NMR (150 MHz, $CDCl_3$): 188.0 (C-1), 148.7 (C-3’’), 148.4 (C-4’’’), 146.9 (C-4’’), 144.8 (C-3), 141.2 (C-1’’’), 139.7 (C-3’), 128.8 (C-2’’’ and C-6’’’), 128.7 (C-6’’), 127.0 (C-1’’), 124.2 (C-3’’’ and C-5’’’), 123.9 (C-2’), 123.3 (C-2), 115.0 (C-5’’), 109.7 (C-2’’), 56.0 (3’’-OCH_3).

1.18. Compound 17

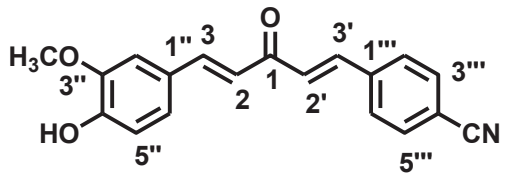

Yield: 14%

Purity: 97.5%

Melting point: 95–97 ºC

UV-Vis: λ_{max} 377 nm

^{1}H NMR (300 MHz, DMSO-d_6): 7.99 (d; 8.5; H-2’’’ and H-6’’’), 7.93 (d; 8.5; H-3’’’ and H-5’’’), 7.79 (d; 16.0; H-3’), 7.73 (d; 16.1; H-3), 7.55 (d; 16.0; H-2’), 7.38 (d; 1.8; H-2’’), 7.23 (dd; 8.2 and 1.8; H-6’’), 7.12 (d; 16.1; H-2), 6.85 (d; 8.2; H-5’’), 3.85 (s; 3’’-OCH_3).

^{13}C NMR (150 MHz, DMSO-*d*$_6$): 188.6 (C-1), 150.3 (C-3’’), 148.5 (C-4’’), 145.0 (C-3), 140.1 (C-3’), 140.0 (C-1’’’), 133.3 (C-3’’’ and C-5’’’), 129.5 (C-2’’’ and C-6’’’), 128.9 (C-1’’), 126.6 (C-6’’), 124.1 (C-2’), 123.5 (C-2), 119.1 (4’’’-CN), 116.2 (C-5’’), 112.5 (C-4’’’), 111.9 (C-2’’), 56.1 (3’’-OCH_3).

1.19. Compound 18

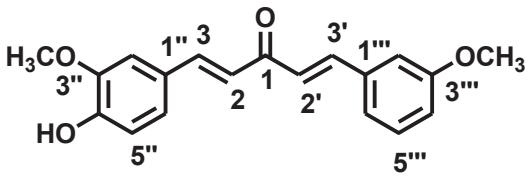

Yield: 45%

Purity: 96.7%

Melting point: 46–48 ºC

UV-Vis: λ_{max} 370 nm

^{1}H NMR (600 MHz, $CDCl_3$): 7.72 (d; 15.9; H-3), 7.71 (d; 15.9; H-3’), 7.36 (dd; 8.1 and 8.1; H-5’’’), 7.24 (d; 7.9; H-5’’), 7.21 (dd; 7.9 and 1.8; H-6’’), 7.16 (d; 1.8 and 2.8, H-2’’’), 7.15 (d; 1.8; H-2’’), 7.10 (d; 15.9; H-2), 6.98 (dd; 8.1 and 2.8; H-4’’’ and H-6’’’), 6.96 (d; 15.9; H-2’), 5.94 (s; 4’’-OH), 3.99 (s; 3’’-OCH_3), 3.88 (s, 3’’’-OCH_3).

^{13}C NMR (150 MHz, $CDCl_3$): 188.8 (C-1), 160.0 (C-3’’’), 148.3 (C-3’’), 146.8 (C-4’’), 143.7 (C-3), 142.8 (C-3’), 136.3 (C-1’’’), 129.9 (C-5’’’), 127.4 (C-1’’), 125.7 (C-6’’), 123.5 (C-2’), 123.4 (C-2), 121.1 (C-6’’’), 116.2 (C-4’’’), 114.9 (C-5’’), 113.3 (C-2’’’), 109.8 (C-2’’), 56.0 (3’’-OCH_3), 55.3 (3’’’-OCH_3).

1.20. Compound 19

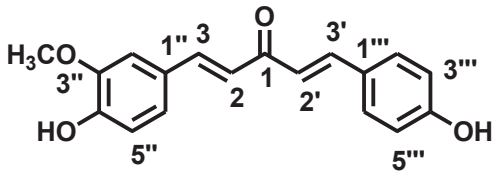

Yield: 15%

Purity: 97.0%

Melting point: 101–103 ºC

UV-Vis: λ_{max} 379 nm

^{1}H NMR (400 MHz, DMSO-*d*$_6$): 7.56 (d; 15.4; H-3), 7.52 (d; 15.6; H-3'), 7.51 (d; 8.6; H-2''' and H-6'''), 7.15 (d; 1.8; H-2''), 7.06 (dd; 1.8 and 8.3; H-6''), 6.97 (d; 15.4; H-2), 6.83 (d; 15.6; H-2'), 6.71 (d; 8.6; H-3''' and H-5'''), 6.54 (d; 8.3; H-5''), 3.77 (s; 3''-OCH_3).

^{13}C NMR (150 MHz, DMSO-*d*$_6$): 188.1 (C-1), 174.2 (C-4'''), 150.3 (C-3''), 149.0 (C-4''), 143.5 (C-3), 142.6 (C-3'), 130.9 (C-2''' and C-6'''), 128.9 (C-1''), 127.3 (C-1'''), 125.4 (C-6''), 124.6 (C-2), 122.6 (C-2'), 116.6 (C-3''' and C-5'''), 116.5 (C-5''), 111.5 (C-2''), 56.0 (3''-OCH_3).

1.21. Compound 20

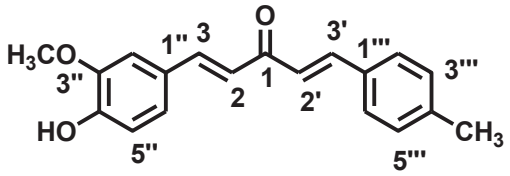

Yield: 87%

Purity: 98.1%

Melting point: 165–167 ºC

UV-Vis: λ_{max} 370 nm

^{1}H NMR (300 MHz, $CDCl_3$): 7.73 (d; 15.9; H-3'), 7.69 (d; 15.8; H-3), 7.53 (d; 8.1; H-2''' and H-6'''), 7.24 (d; 8.0; H-3''' and H-5'''), 7.20 (dd; 1.8 and 8.4; H-6''), 7.13 (d; 1.8; H-2''), 7.07 (d; 15.9; H-2'), 6.97 (d; 8.2; H-5''), 6.94 (d; 15.9; H-2), 3.98 (s; 3''-OCH_3).

^{13}C NMR (150 MHz, $CDCl_3$): 189.0 (C-1), 148.2 (C-3''), 146.8 (C-4''), 143.4 (C-3), 143.0 (C-3'), 140.9 (C-4'''), 132.1 (C-1'''), 129.7 (C-3''' and C-5'''), 128.4 (C-2''' and C-6'''), 127.4 (C-1''), 124.4 (C-6''), 123.5 (C-2'), 123.4 (C-2), 114.8 (C-5''), 109.7 (C-2''), 56.0 (3''-OCH_3), 22.6 (4'''-CH_3).

1.22. Compound 21

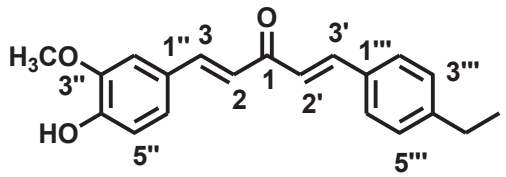

Yield: 50%

Purity: 97.3%

Melting point: 110–112 ºC

UV-Vis: λ_{max} 370 nm

^{1}H NMR (600 MHz, $CDCl_3$): 7.75 (d; 15.9; H-3), 7.70 (d; 15.8; H-3'), 7.57 (d; 8.1; H-2''' and H-6'''), 7.27 (d; 8.1; H-3''' and H-5'''), 7.21 (dd; 8.2 and 1.8; H-6''), 7.15 (d; 1.8; H-2''), 7.08 (d; 15.9; H-2), 6.98 (d; 8.2; H-5''), 6.96 (d; 15.8; H-2'), 5.94 (s; 4''-OH), 3.99 (s; 3''-OCH_3), 2.71 (q; 4'''-CH_2), 1.28 (t; CH_3).

^{13}C NMR (150 MHz, $CDCl_3$): 189.0 (C-1), 148.2 (C-3’’), 147.2 (C-4’’’), 146.8 (C-4’’), 143.4 (C-3), 143.0 (C-3’), 132.4 (C-1’’’), 128.5 (C-2’’’ and C-6’’’), 128.4 (C-3’’’ and C-5’’’), 127.4 (C-1’’), 124.5 (C-6’’), 123.5 (C-2’) 123.4 (C-2), 114.9 (C-5’’), 109.8 (C-2’’), 56.0 (3’’-OCH_3), 28.9 (4’’’-CH_2CH_3), 15.3 (4’’’-CH_2CH_3).

1.23. Compound 22

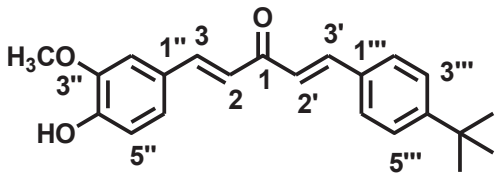

Yield: 83%

Purity: 98.3%

Melting point: 86–88 ºC

UV-Vis: λ_{max} 370 nm

^{1}H NMR (600 MHz, $CDCl_3$): 7.75 (d; 15.8; H-3’), 7.71 (d; 15.9; H-3), 7.59 (d; 8.3; H-2’’’ and H-6’’’), 7.46 (d; 8.3; H-3’’’ and H-5’’’), 7.21 (dd; 1.8 and 8.2; H-6’’), 7.15 (d; 1.8; H-2’’), 7.09 (d; 15.9; H-2), 6.98 (d; 8.2; H-5’’), 6.96 (d; 15.8; H-2’), 3.99 (s; 3’’-OCH_3), 1.37 (s; 4’’’- $C(CH_3)_3$).

^{13}C NMR (150 MHz, $CDCl_3$): 189.0 (C-1), 154.1 (C-4’’’), 148.2 (C-3’’), 146.8 (C-4’’), 143.4 (C-3), 142.9 (C-3’), 132.1 (C-1’’’), 128.2 (C-2’’’ and C-6’’’), 127.4 (C-1’’), 126.0 (C-3’’’ and C-5’’’), 124.7 (C-6’’), 123.5 (C-2 and C-2’), 114.8 (C-5’’), 109.7 (C-2’’), 56.0 (3’’-OCH_3), 34.9 (4’’’-$C(CH_3)_3$), 31.2 (4’’’-$C(CH_3)_3$).

1.24. Compound 23

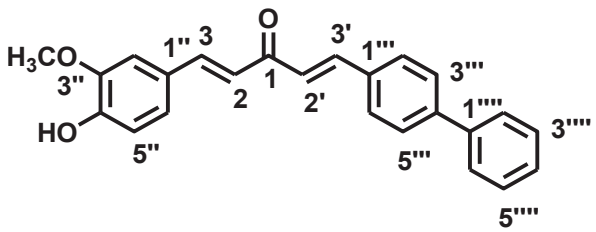

Yield: 84%

Purity: 99.5%

Melting point: 157–159 ºC

UV-Vis: λ_{max} 376 nm

^{1}H NMR (600 MHz, $CDCl_3$): 7.80 (d; 15.8; H-3'), 7.73 (d; 15.9; H-3), 7.73 (d; 8.3; H-3''' and H-5'''), 7.70 – 7.62 (m; H-2''', H-6''', H-2'''' and H-6''''), 7.49 (dd; 7.7 and 7.7; H-3'''' e H-5''''), 7.22 (dd; 1.8 and 8.1; H-6''), 7.16 (d; 15.9; H-2), 7.16 (d; 1.8; H-2''), 6.99 (d; 8.1; H-5''), 6.98 (d; 15.8; H-2'), 4.00 (s; 3''-OCH_3).

^{13}C NMR (150 MHz, $CDCl_3$): 188.8 (C-1), 148.3 (C-3''), 146.8 (C-4''), 143.6 (C-3), 143.2 (C-1''''), 142.5 (C-3'), 140.2 (C-4'''), 133.9 (C-1'''), 129.0 (C-3'''' and C-5''''), 128.9 (C-2'''' and C-6''''), 127.9 (C-4''''), 127.6 (C-3''' and C-5'''), 127.4 (C-1''), 127.1 (C-2''' and C-6'''), 125.2 (C-6''), 123.6 (C-2'), 123.5 (C-2), 114.9 (C-5''), 109.7 (C-2''), 56.0 (3''-OCH_3).

1.25. Compound 24

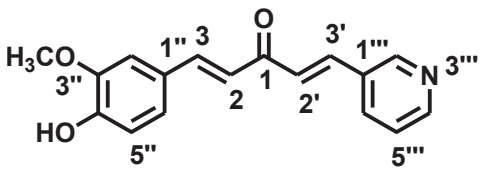

Yield: 70%

Purity: 98.8%

Melting point: 134–136 ºC

UV-Vis: λ_{max} 373 nm

^{1}H NMR (600 MHz, DMSO-*d*$_6$): 9.73 (s; 4’’-OH), 8.95 (d; 1.2; H-2’’’), 8.61 (d; 4.8; H-4’’’), 8.24 (d; 7.8; H-6’’’), 7.79 (d; 16.2; H-3’), 7.74 (d; 16.2; H-3), 7.53 (d; 16.2; H-2’), 7.50 (dd; 4.8 and 7.8; H-5’’’), 7.39 (d; 1.8; H-2’’), 7.24 (dd; 1.8 and 8.4; H-6’’), 7.14 (d; 16.2; H-2), 6.86 (d; 8.4; H-5’’), 3.86 (s; 3’’-OCH_3).

^{13}C NMR (150 MHz, DMSO-*d*$_6$): 188.5 (C-1), 151.3 (C-2’’’), 150.4 (C-4’’’), 150.2 (C-3’’), 148.4 (C-4’’), 144.7 (C-3), 138.9 (C-3’), 135.2 (C-6’’’), 131.2 (C-1’’’), 127.6 (C-2’), 126.6 (C-1’’), 124.4 (C-5’’’), 124.1 (C-2), 123.4 (C-6’’), 116.2 (C-5’’), 111.9 (C-2’’), 56.1 (3’’-OCH_3).

1.26. Compound 25

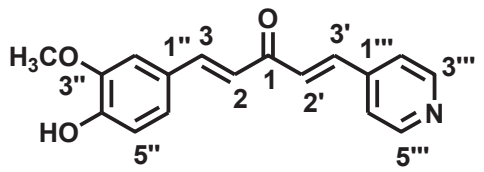

Yield: 74%

Purity: 93.7%

Melting point: 219–221 ºC

UV-Vis: λ_{max} 378 nm

^{1}H NMR (600 MHz, DMSO-*d*$_6$): 9.77 (s; 4’’-OH), 8.67 (d; 6.0; H-3’’’ and H-5’’’), 7.80 (d; 15.6; H-3’), 7.74 (d; 6.0; H-2’’’ and H-6’’’), 7.66 (d; 15.6; H-3), 7.60 (d; 15.6; H-2’), 7.40 (d; 1.8; H-2’’), 7.24 (dd; 1.8 and 7.8; H-6’’), 7.15 (d; 15.6; H-2), 6.86 (d; 7.8; H-5’’), 3.86 (s; 3’’-OCH_3).

^{13}C NMR (150 MHz, DMSO-*d*$_6$): 188.6 (C-1), 150.8 (C-3’’’ and C-5’’’), 150.3 (C-3’’), 148.5 (C-4’’), 145.2 (C-3), 142.5 (C-1’’’), 139.4 (C-3’), 129.9 (C-2’), 126.5 (C-1’’), 124.2 (C-2), 123.3 (C-6’’), 122.7 (C-2’’’ and C-6’’’), 116.2 (C-5’’), 112.0 (C-2’’), 56.1 (3’’-OCH_3).

1.27. Compound 26

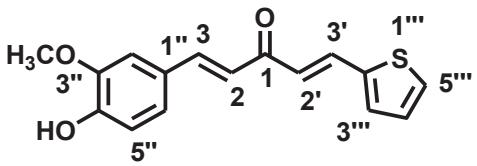

Yield: 78%

Purity: 97.4%

Melting point: 94–96 ºC

UV-Vis: λ_{max} 381 nm

^{1}H NMR (600 MHz, DMSO-*d*$_6$): 9.68 (s; 4’’-OH), 7.90 (d; 15.6; H-3’), 7.76 (d; 5.4; H-3’’’), 7.65 (d; 16.2; H-3), 7.59 (d; 3.6; H-5’’’), 7.40 (d; 1.8; H-2’’), 7.22 (dd; 1.8 and 8.4; H-6’’), 7.19 (d; 15.6; H-2’), 7.19 (dd; 3.6 and 5.4; H-4’’’), 6.98 (d; 16.2; H-2), 6.84 (d; 8.4; H-5’’), 3.86 (s; 3’’-OCH_3).

^{13}C NMR (150 MHz, DMSO-*d*$_6$): 188.0 (C-1), 150.0 (C-3’’), 148.4 (C-4’’), 143.8 (C-3), 140.4 (C-2’’’), 135.3 (C-5’’’), 132.8 (C-3’), 130.4 (C-4’’’), 129.2 (C-2’), 126.7 (C-1’’), 125.2 (C-3’’’), 124.1 (C-2), 123.2 (C-6’’), 116.1 (C-5’’), 111.9 (C-2’’), 56.2 (3’’-OCH_3).

1.28. Compound 27

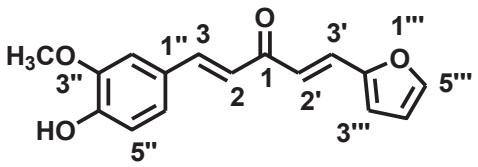

Yield: 79%

Purity: 99.4%

UV-Vis: λ_{max} 381 nm

^{1}H NMR (600 MHz, DMSO-*d*$_6$): 9.68 (s; 4’’-OH), 7.89 (d; 1.8; H-5’’’), 7.64 (d; 16.2; H-3’), 7.56 (d; 15.6; H-3), 7.41 (d; 1.8; H-2’’), 7.22 (dd; 1.8 and 7.8; H-6’’), 7.18 (d; 16.2; H-2’), 7.00 (d; 3.0; H-3’’’), 6.99 (d; 15.6; H-2), 6.84 (d; 7.8; H-5’’), 6.68 (dd; 1.8 and 3.0; H-4’’’), 3.86 (s; 3’’-OCH_3).

^{13}C NMR (150 MHz, DMSO-*d*$_6$): 188.0 (C-1), 151.5 (C-2’’’), 150.0 (C-3’’), 148.4 (C-4’’), 146.4 (C-5’’’), 143.8 (C-3), 129.1 (C-3’), 126.7 (C-1’’), 124.1 (C-2’), 123.5 (C-2), 123.2 (C-6’’), 116.8 (C-4’’’), 116.1 (C-5’’), 113.5 (C-3’’’), 111.9 (C-2’’), 56.1 (3’’-OCH_3).

1.29. Compound 28

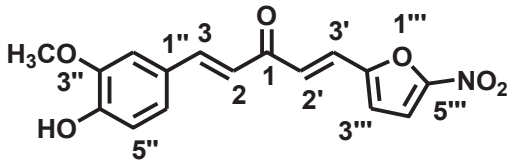

Yield: 77%

Purity: 99.1%

Melting point: 78–80 ºC

UV-Vis: λ_{max} 386 nm

^{1}H NMR (600 MHz, DMSO-*d*$_6$): 9.77 (s; 4’’-OH), 7.81 (d; 3.6; H-4’’’), 7.71 (d; 16.2; H-3’), 7.59 (d; 16.2; H-3), 7.44 (d; 1.8; H-2’’), 7.34 (d; 3.6; H-3’’’), 7.32 (d; 16.2; H-2’), 7.26 (d; 16.2; H-2), 7.25 (dd; 1.8 and 8.4; H-6’’), 6.85 (d; 8.4; H-5’’), 3.86 (s; 3’’-OCH_3).

^{13}C NMR (150 MHz, DMSO-*d*$_6$): 187.6 (C-1), 153.9 (C-5’’’), 152.4 (C-2’’’), 150.4 (C-3’’), 148.5 (C-4’’), 145.1 (C-3), 129.4 (C-3’), 127.2 (C-2’), 126.5 (C-1’’), 124.6 (C-2), 123.0 (C-6’’), 117.9 (C-4’’’), 116.1 (C-5’’), 115.3 (C-3’’’), 111.9 (C-2’’), 56.2 (3’’-OCH_3).

Figure S1. i) ^{1}H NMR spectrum of dehydrozingerone (DZG)

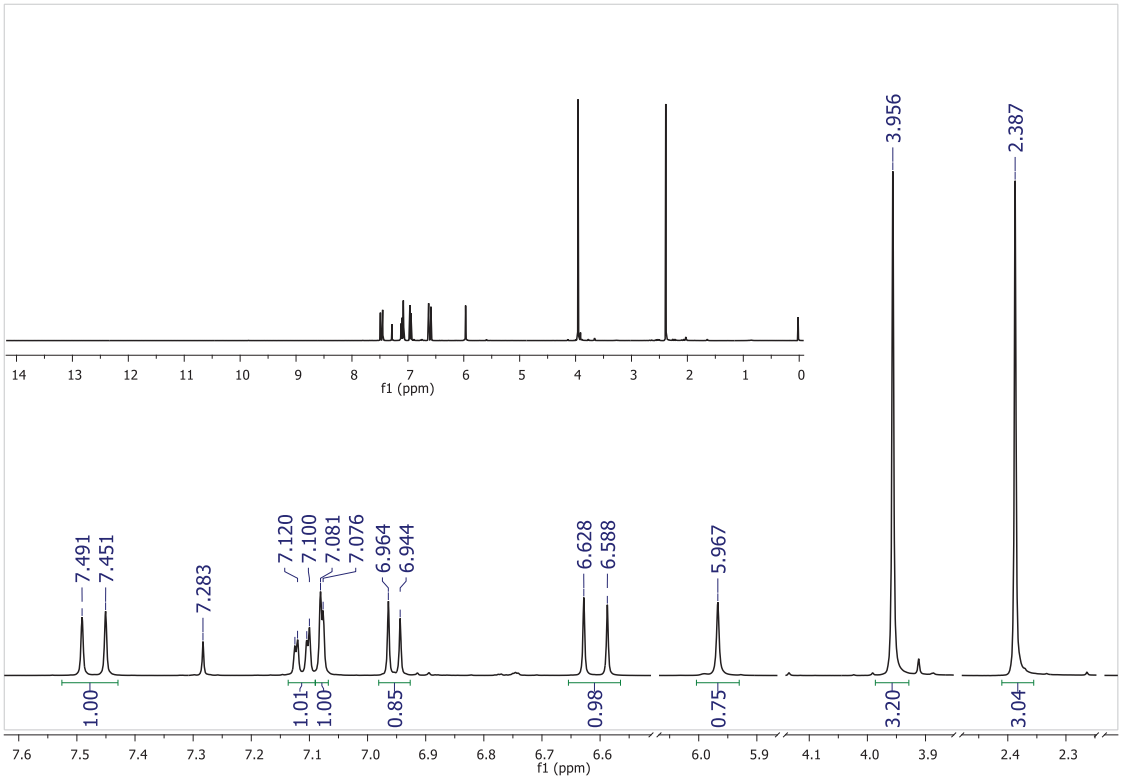

Figure S1. ii) ^{13}C NMR spectrum of dehydrozingerone (DZG)

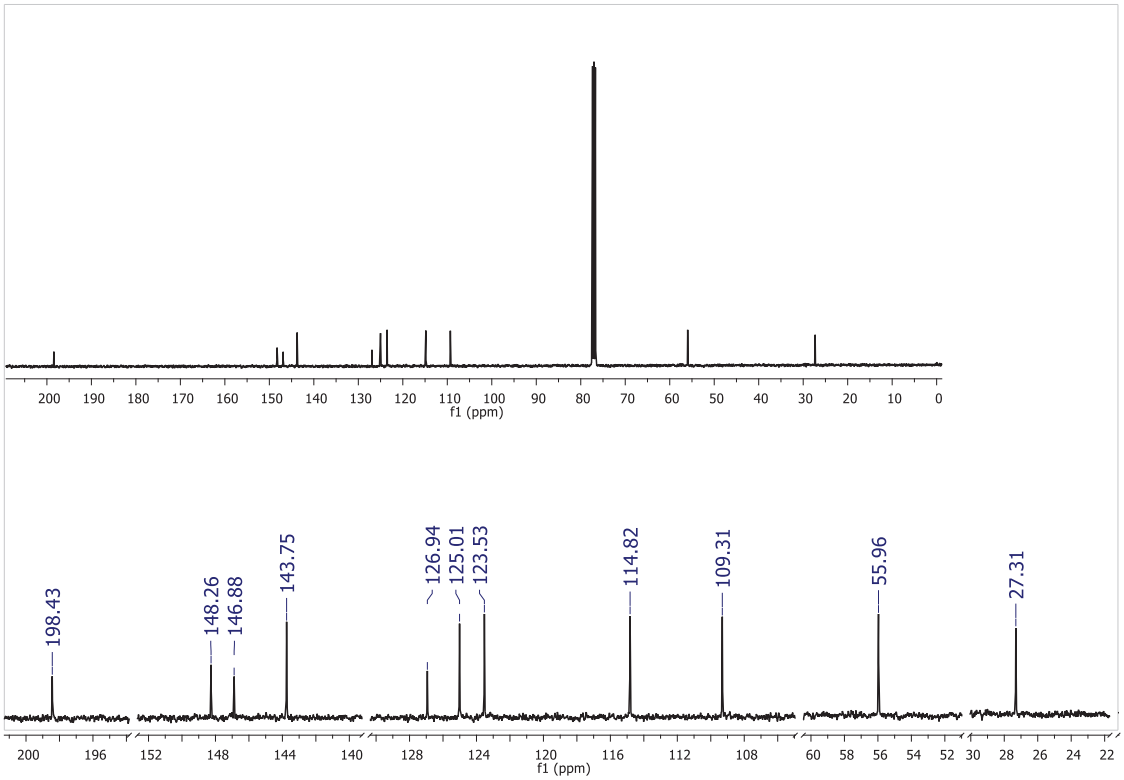

Figure S1. iii) UV-Vis spectrum of dehydrozingerone (DZG)

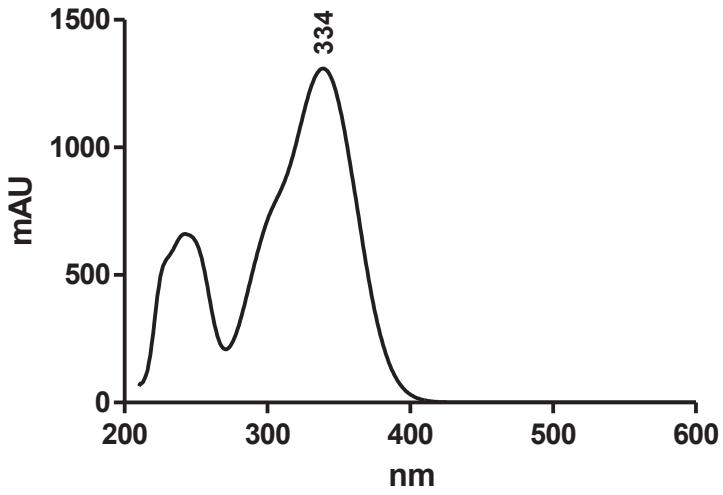

Figure S1. iv) HPLC chromatogram of dehydrozingerone (DZG)

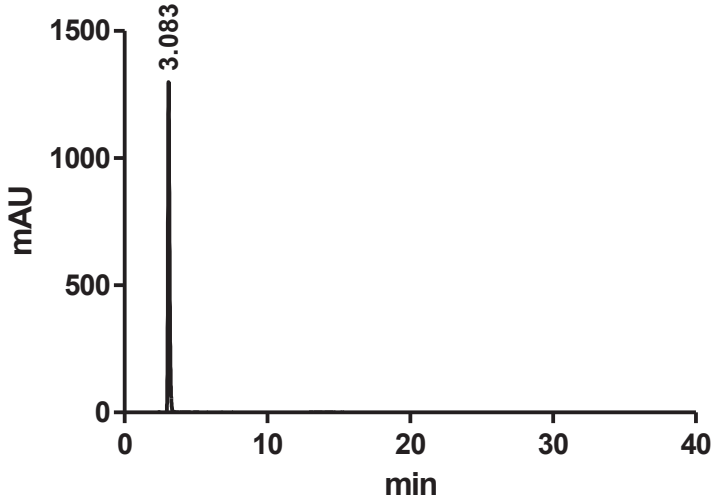

Figure S2. i) ^{1}H NMR spectrum of compound **1**

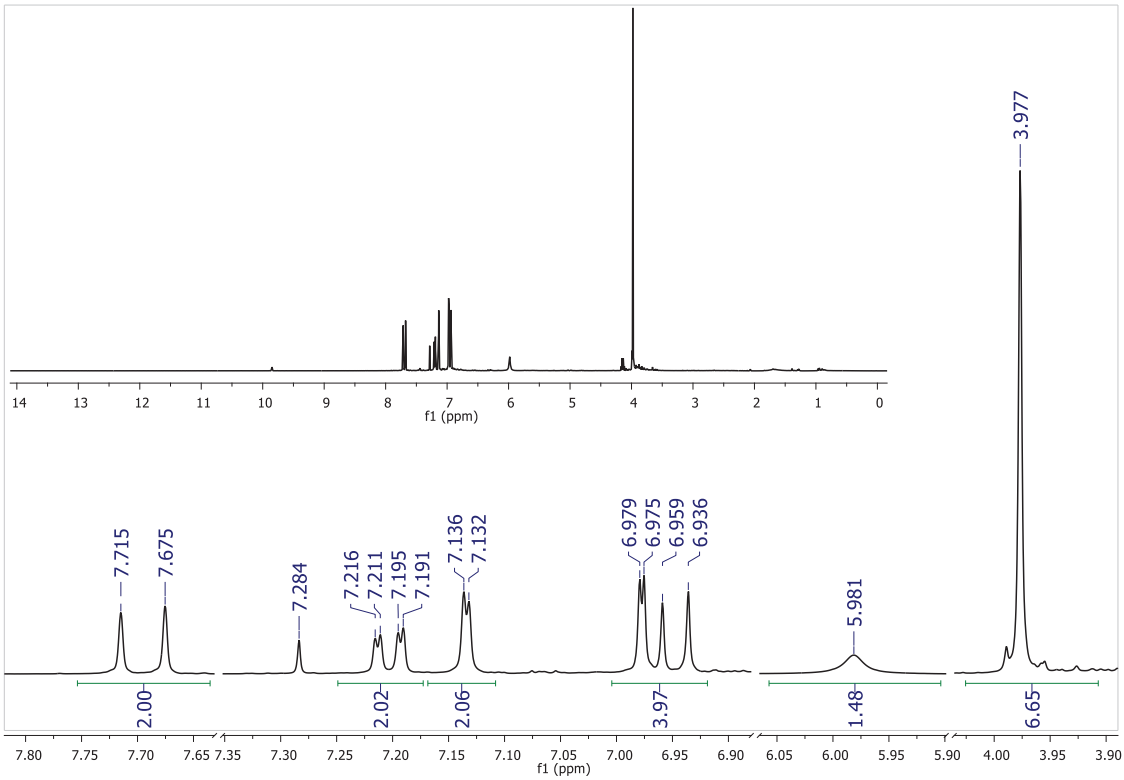

Figure S2. ii) ^{13}C NMR spectrum of compound **1**

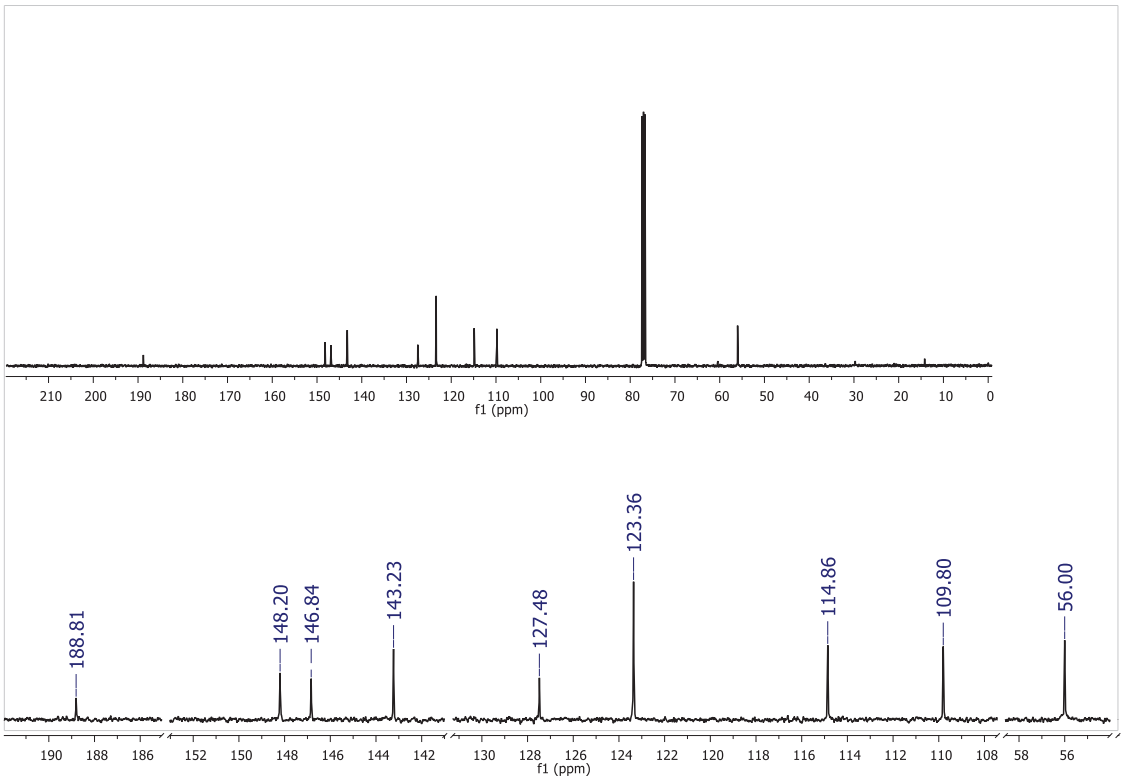

Figure S2. iii) UV-Vis spectrum of compound **1**

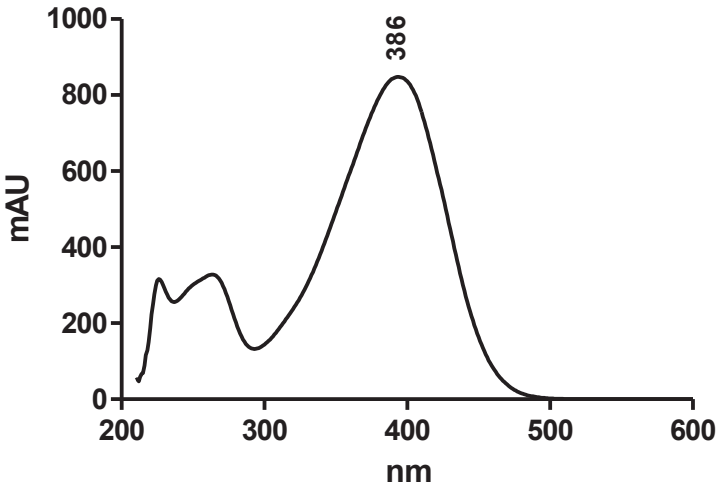

Figure S2. iv) HPLC chromatogram of compound **1**

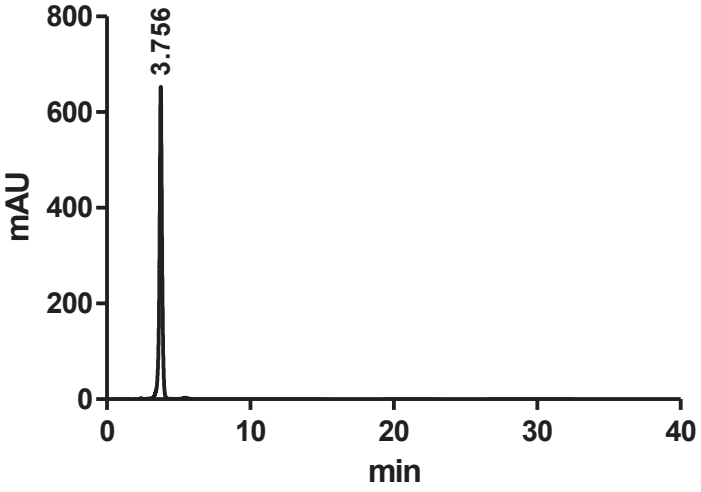

Figure S3. i) ^{1}H NMR spectrum of compound **2**

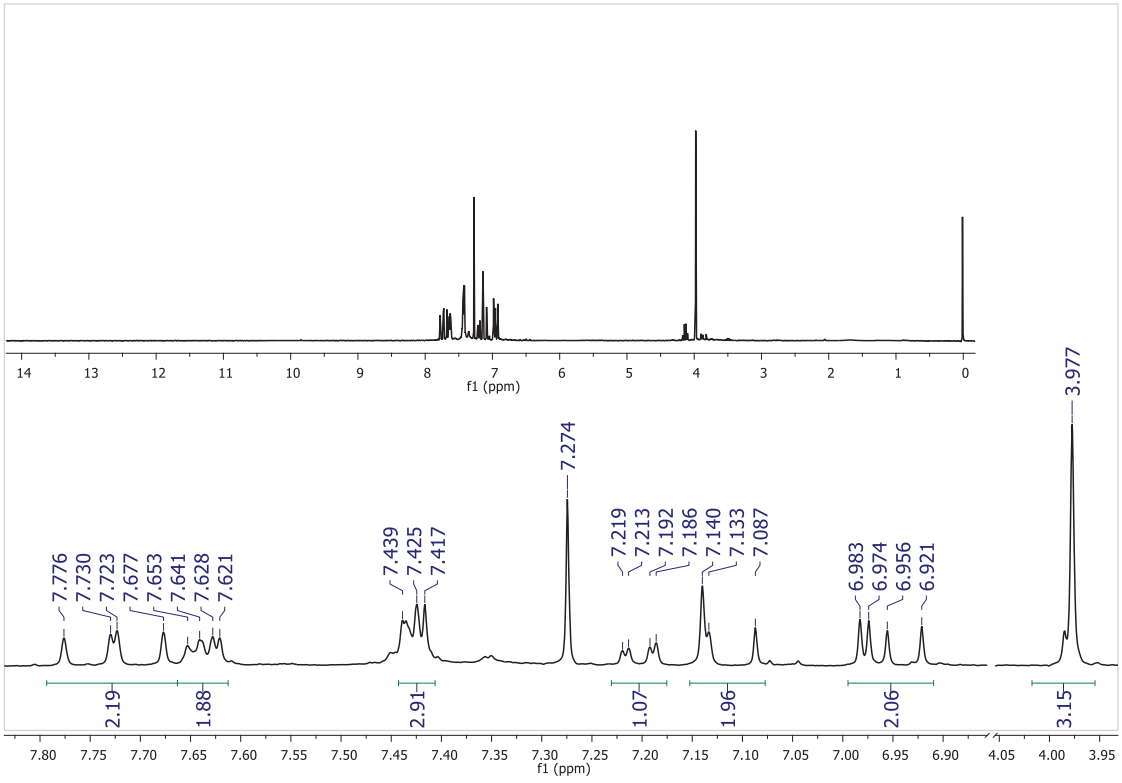

Figure S3. ii) ^{13}C NMR spectrum of compound **2**

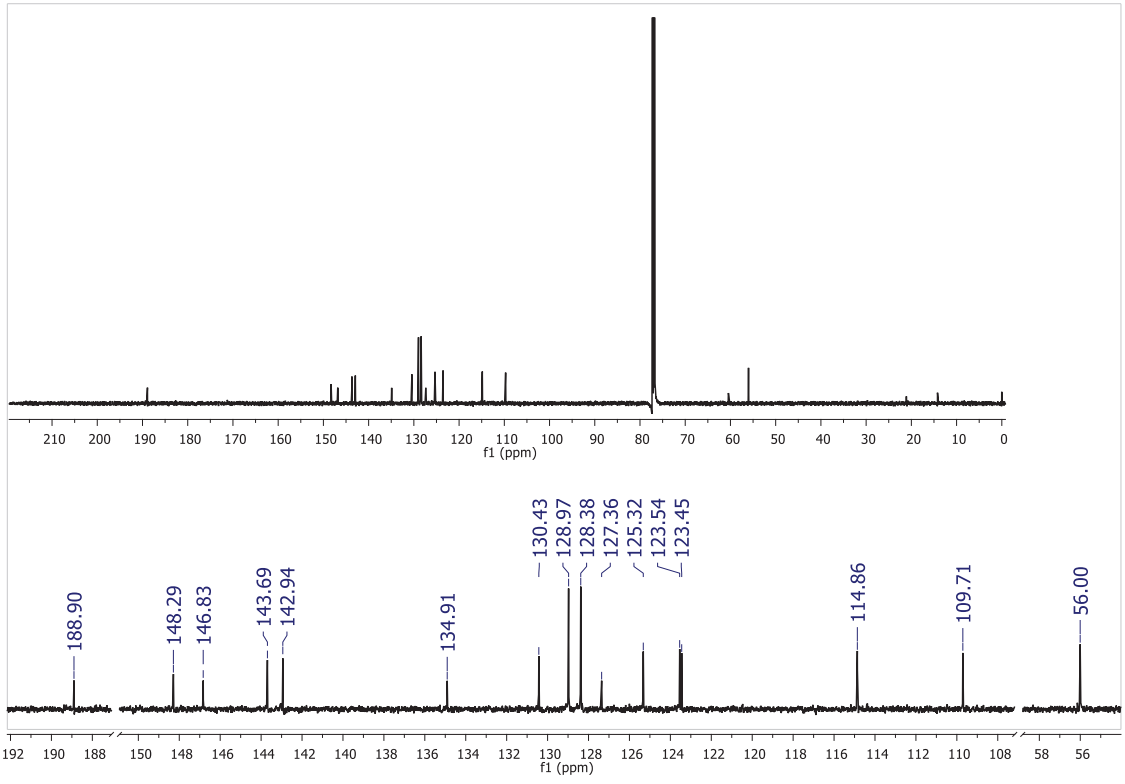

Figure S3. iii) UV-Vis spectrum of compound **2**

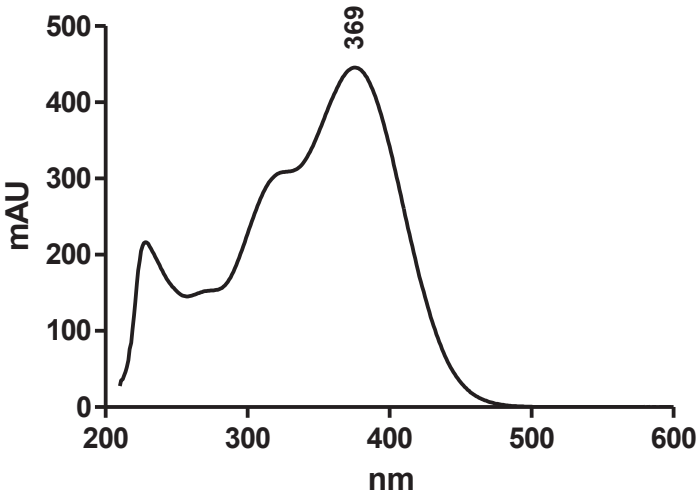

Figure S3. iv) HPLC chromatogram of compound **2**

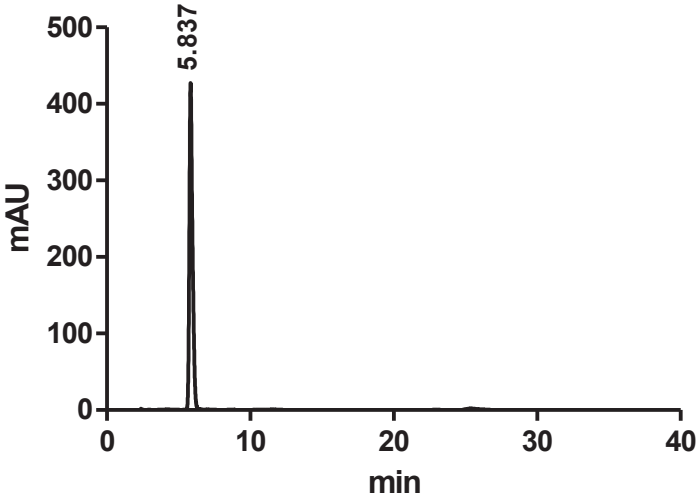

Figure S4. i) ^{1}H NMR spectrum of compound **3**

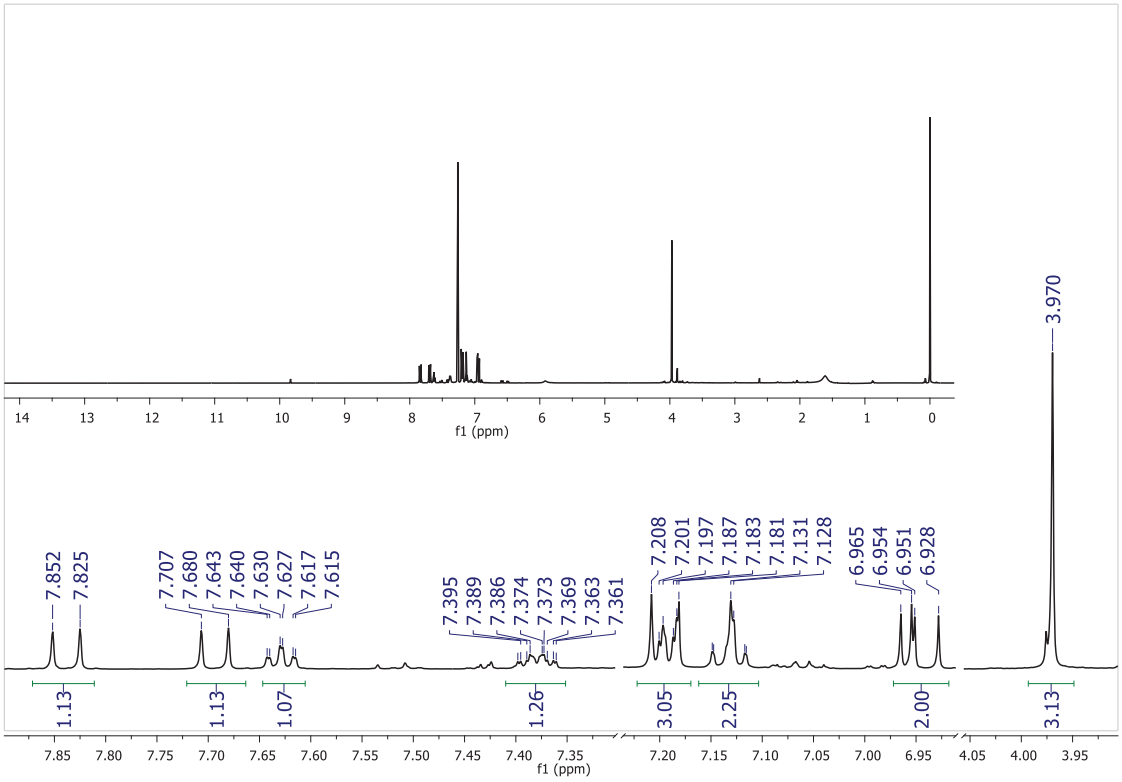

Figure S4. ii) ^{13}C NMR spectrum of compound **3**

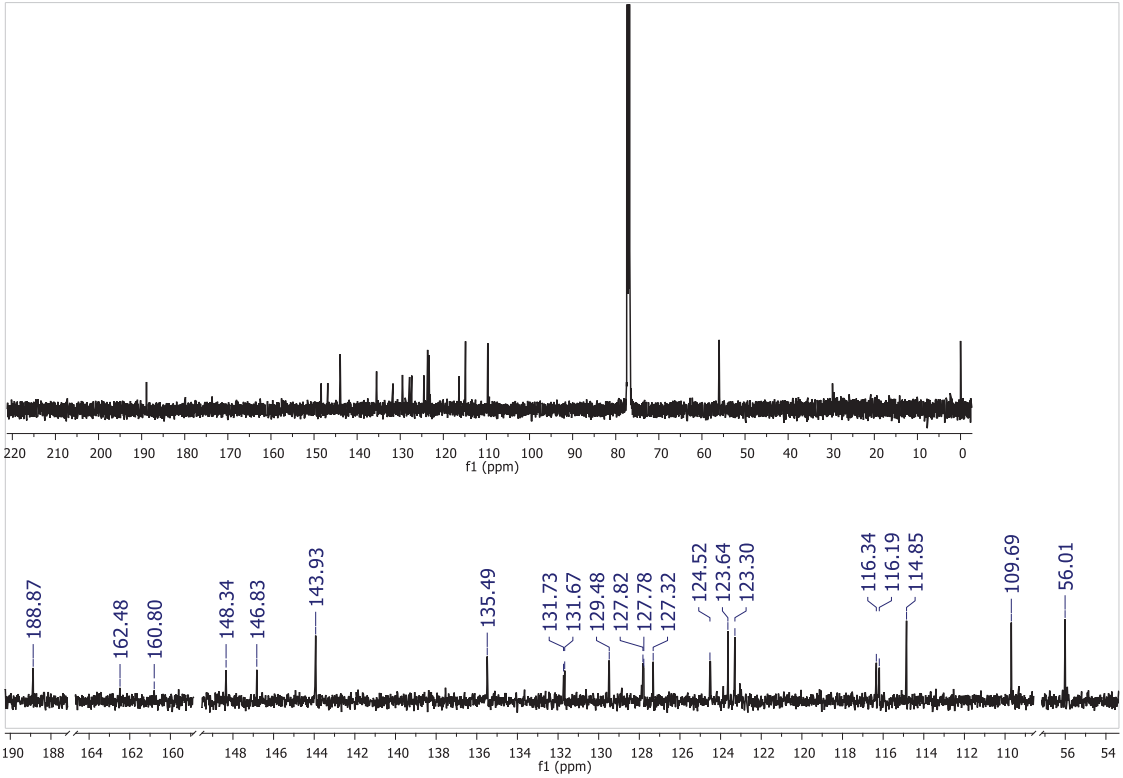

Figure S4. iii) UV-Vis spectrum of compound **3**

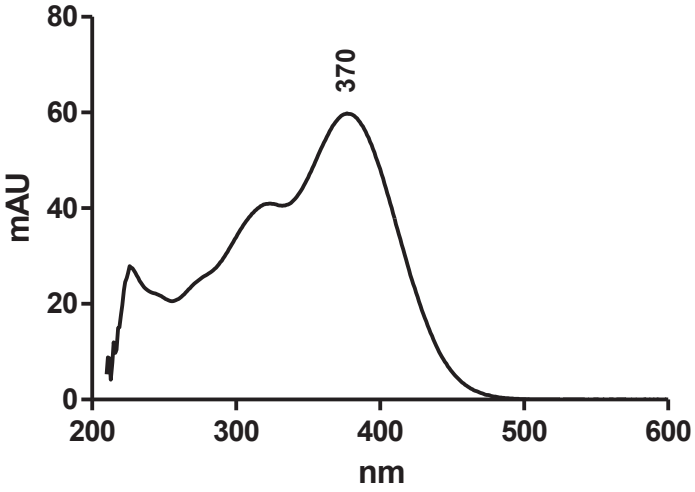

Figure S4. iv) HPLC chromatogram of compound **3**

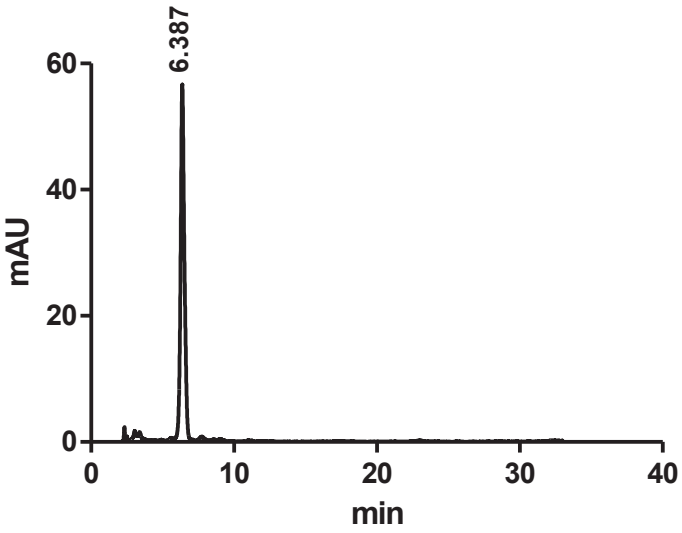

Figure S5. i) ^{1}H NMR spectrum of compound **4**

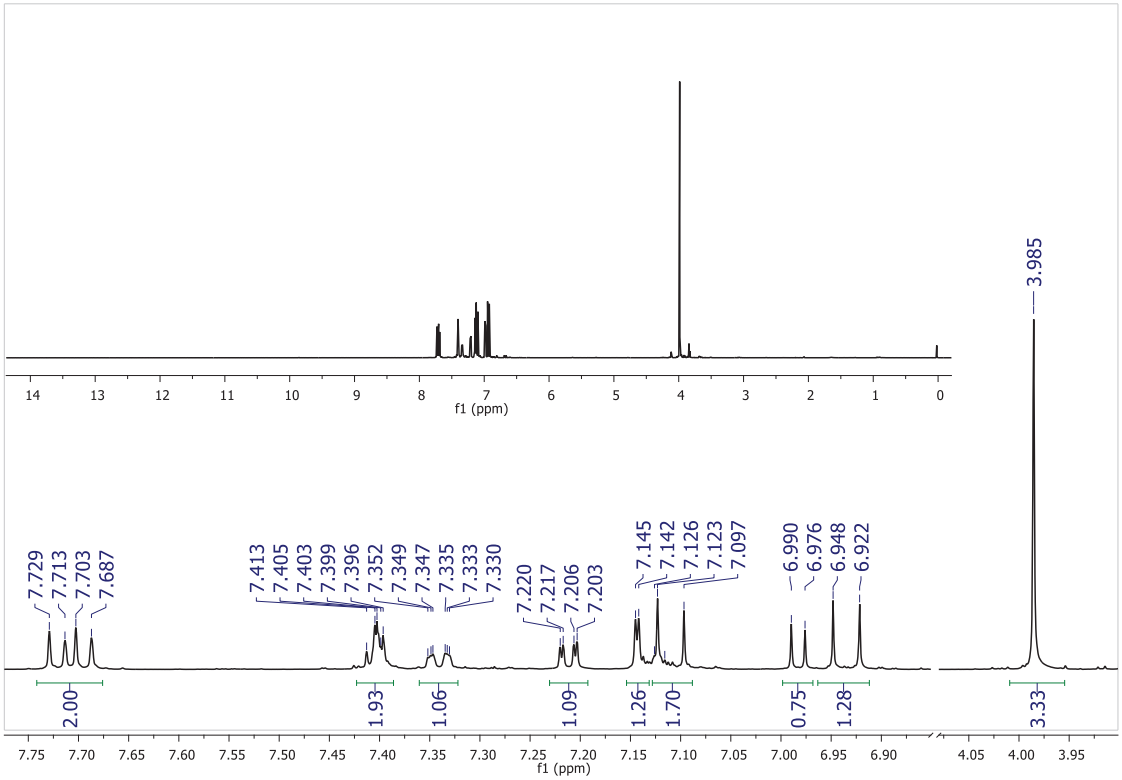

Figure S5. ii) ^{13}C NMR spectrum of compound **4**

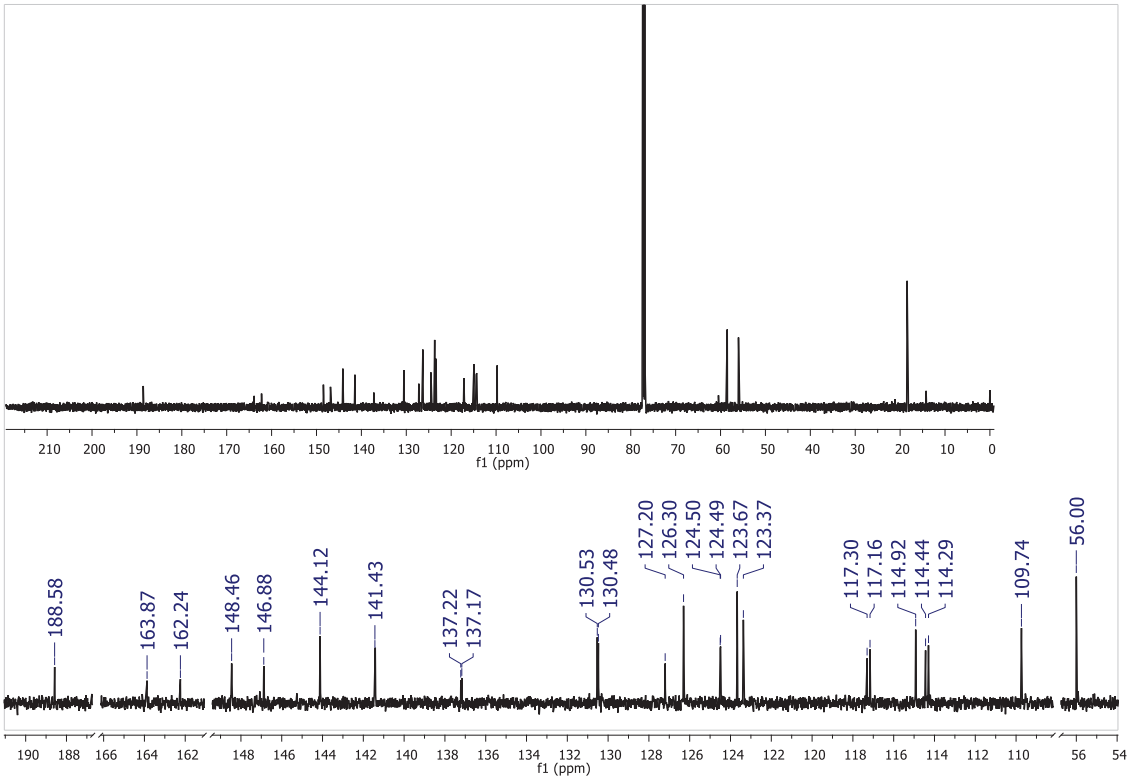

Figure S5. iii) UV-Vis spectrum of compound **4**

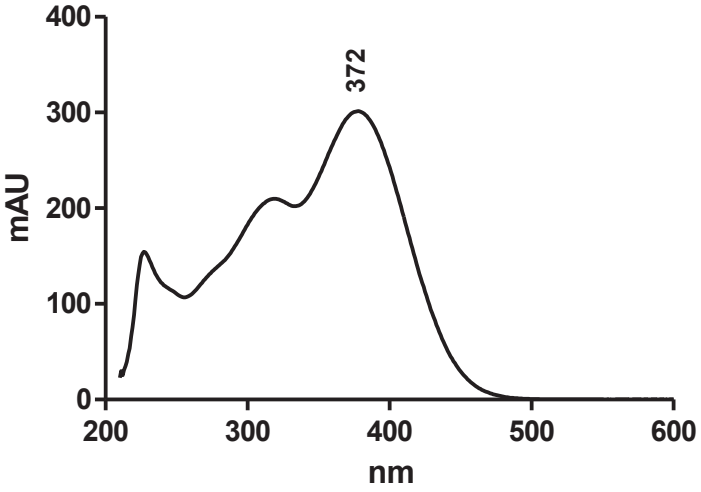

Figure S5. iv) HPLC chromatogram of compound **4**

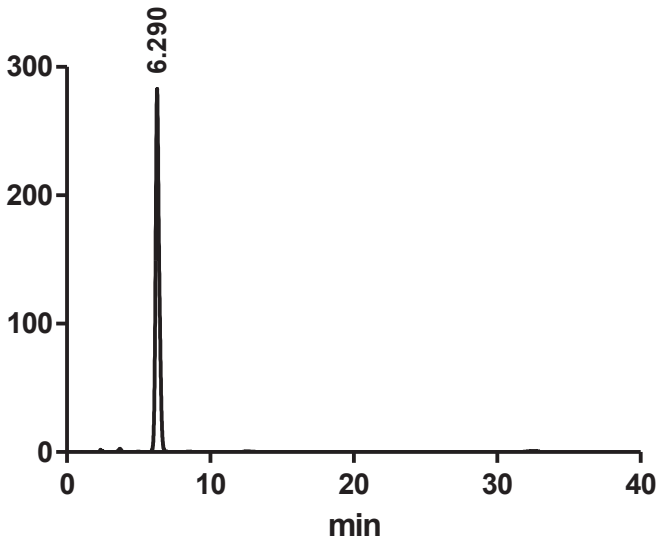

Figure S6. i) ^{1}H NMR spectrum of compound **5**

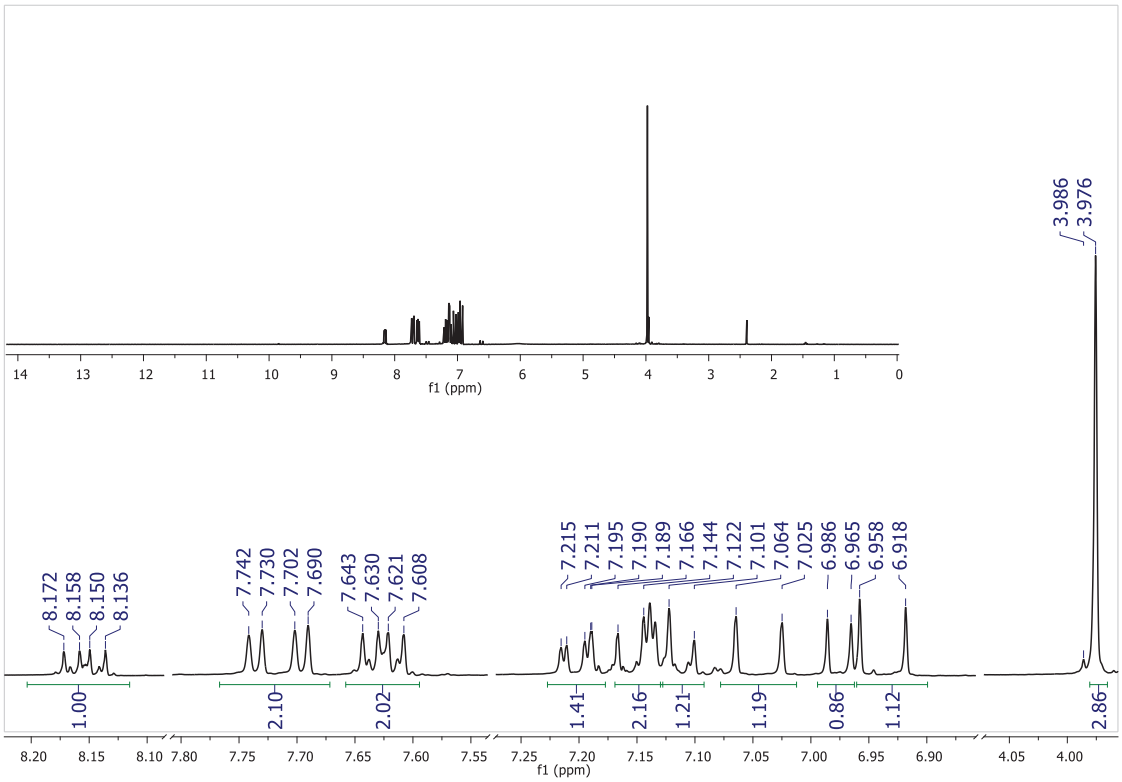

Figure S6. ii) ^{13}C NMR spectrum of compound **5**

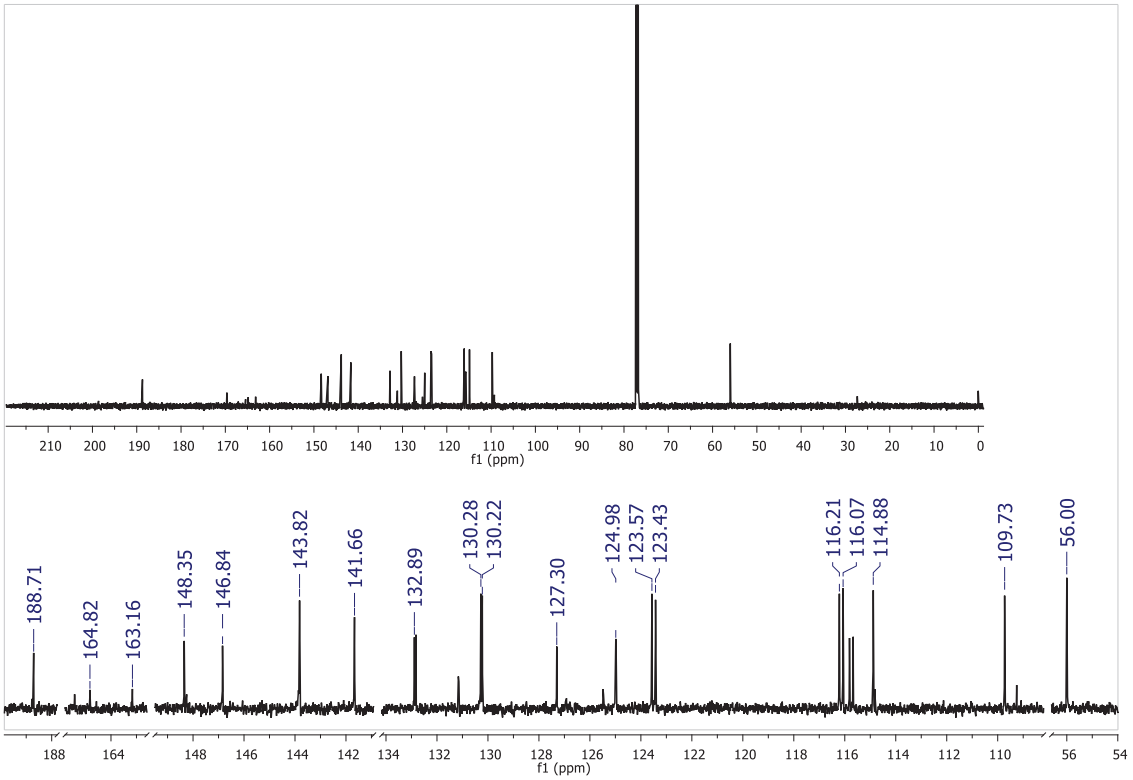

Figure S6. iii) UV-Vis spectrum of compound **5**

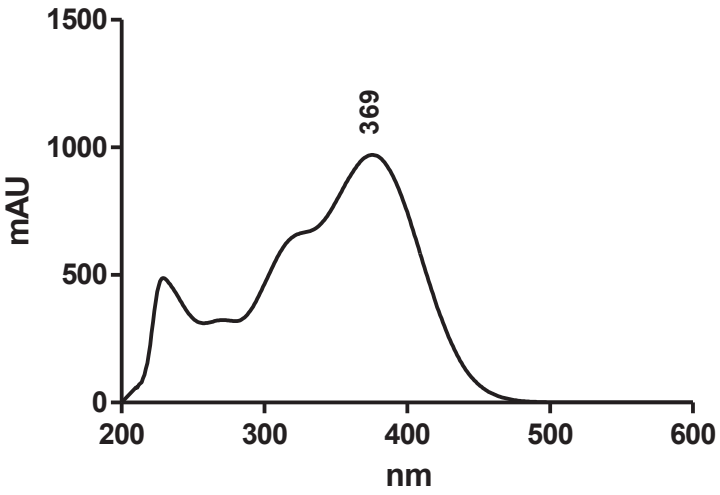

Figure S6. iv) HPLC chromatogram of compound **5**

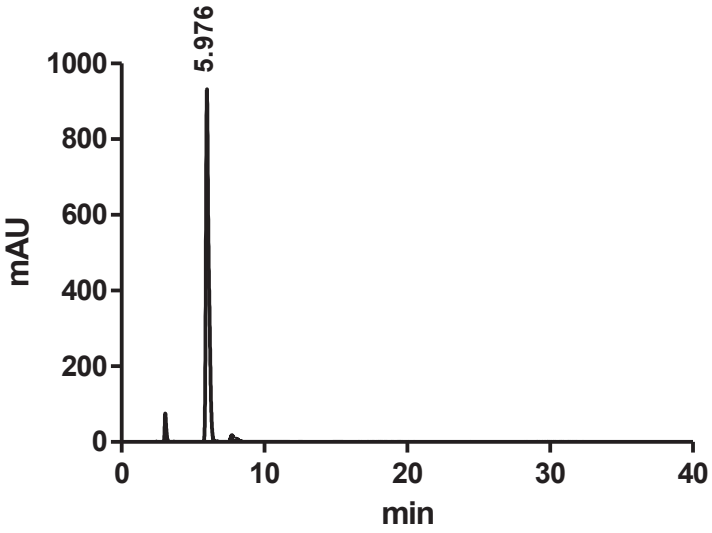

Figure S7. i) ^{1}H NMR spectrum of compound **6**

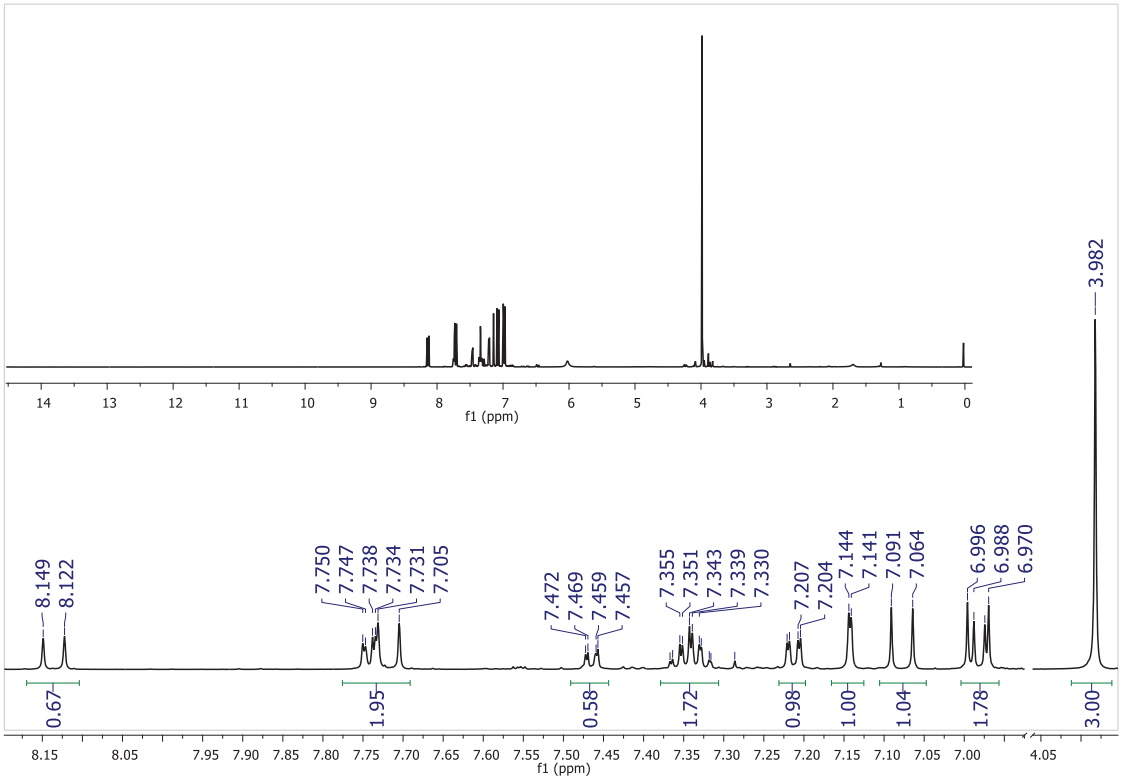

Figure S7. ii) ^{13}C NMR spectrum of compound **6**

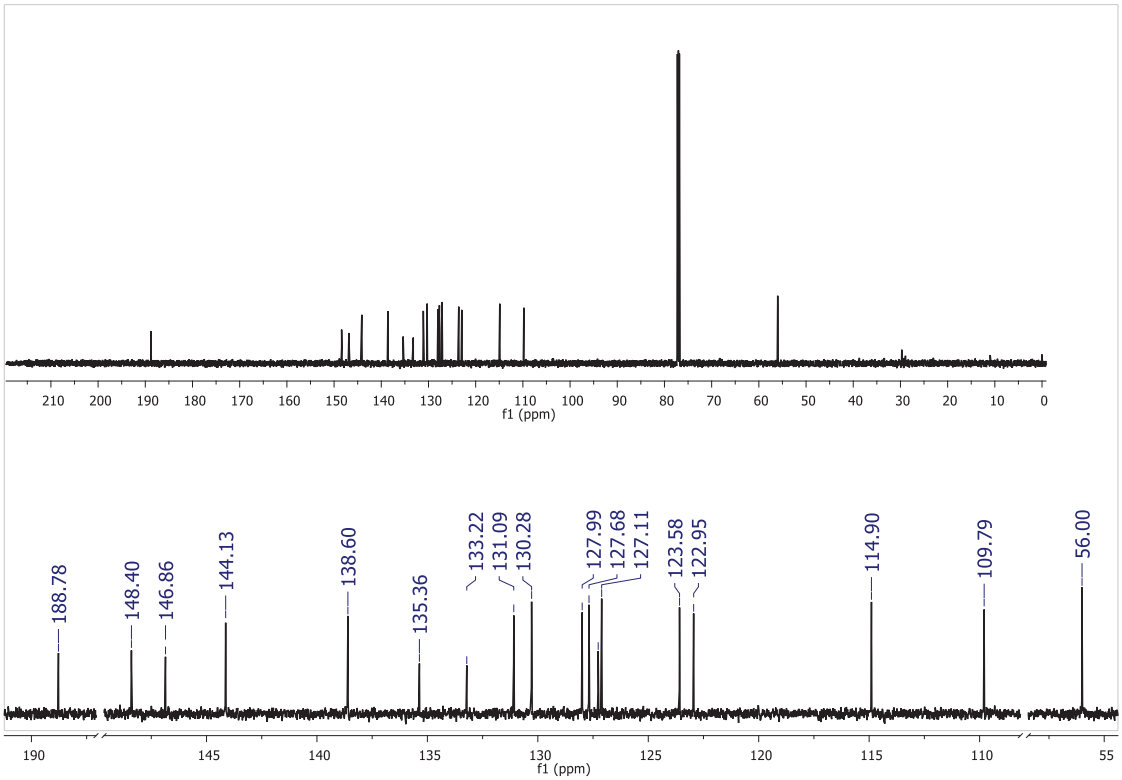

Figure S7. iii) UV-Vis spectrum of compound **6**

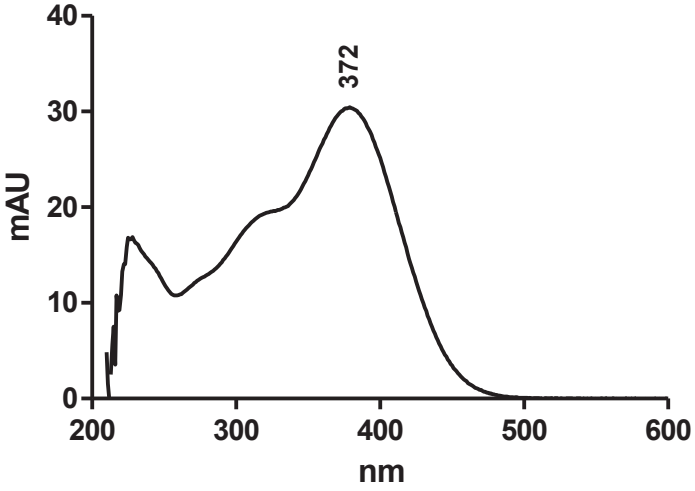

Figure S7. iv) HPLC chromatogram of compound **6**

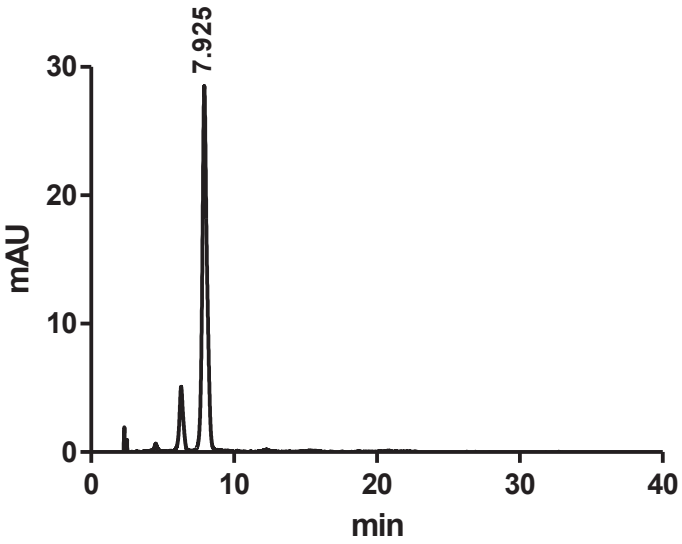

Figure S8. i) ^{1}H NMR spectrum of compound **7**

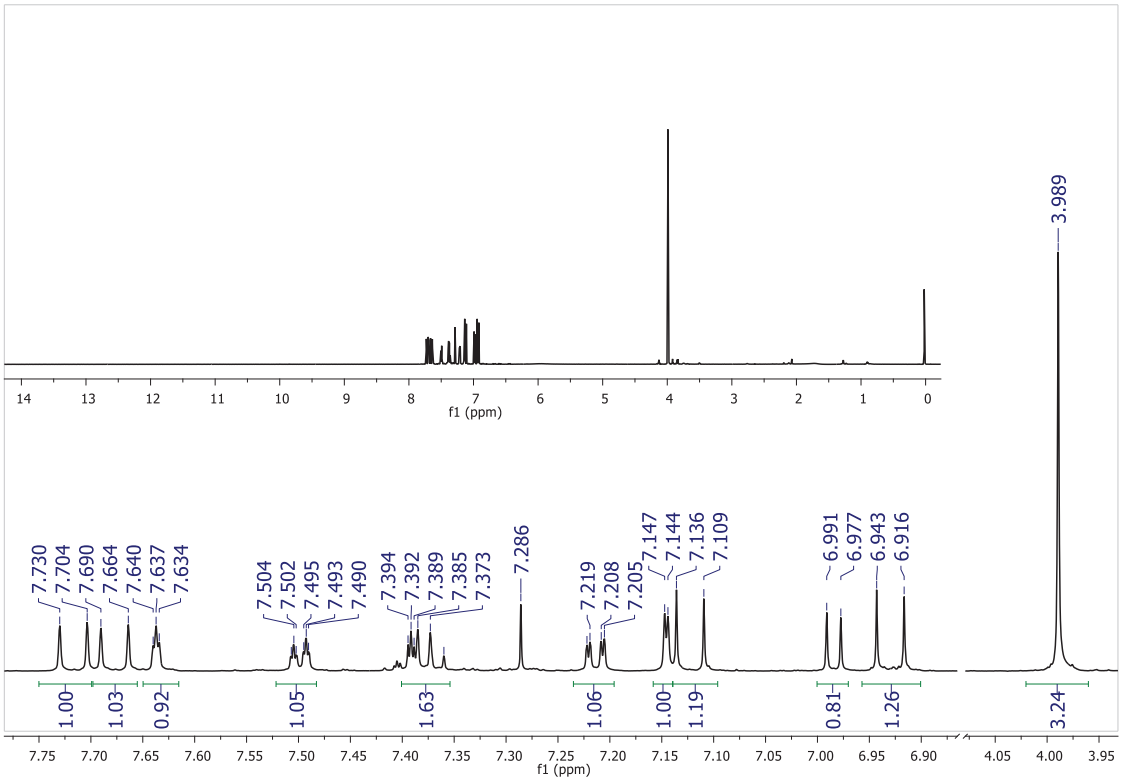

Figure S8. ii) ^{13}C NMR spectrum of compound **7**

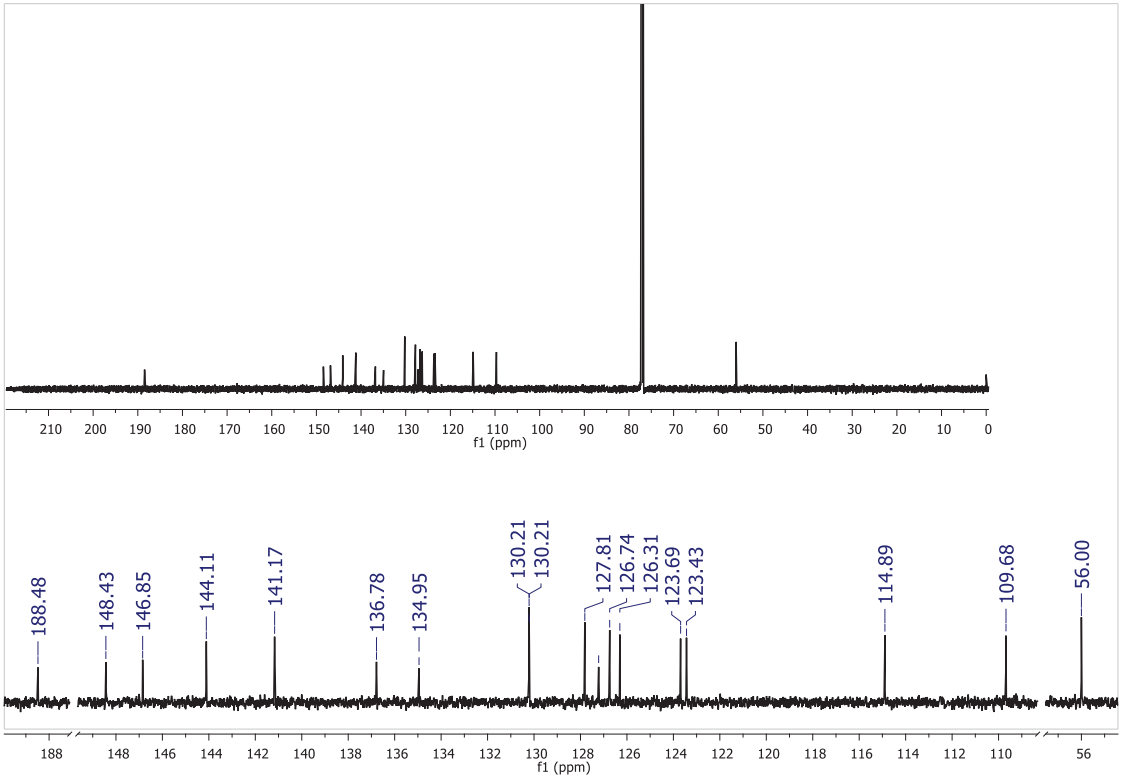

Figure S8. iii) UV-Vis spectrum of compound **7**

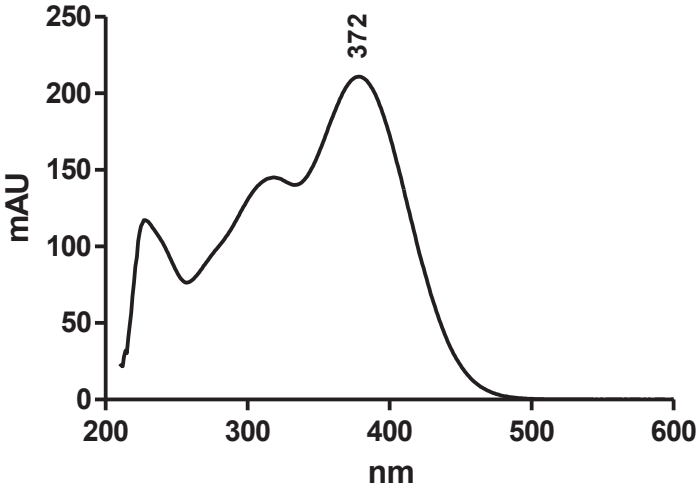

Figure S8. iv) HPLC chromatogram of compound **7**

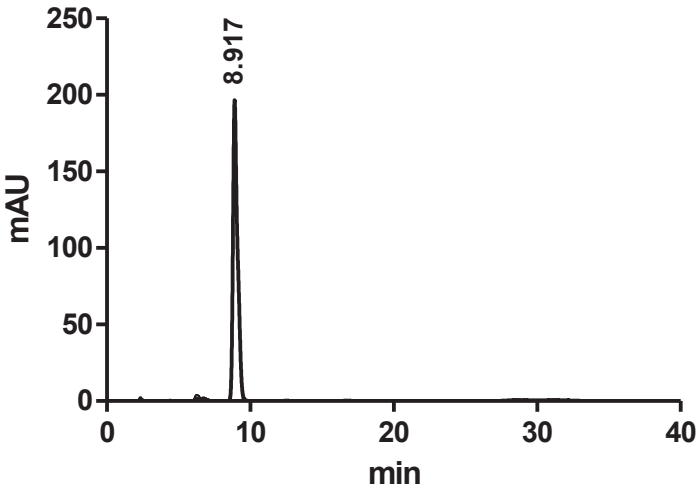

Figure S9. i) ^{1}H NMR spectrum of compound **8**

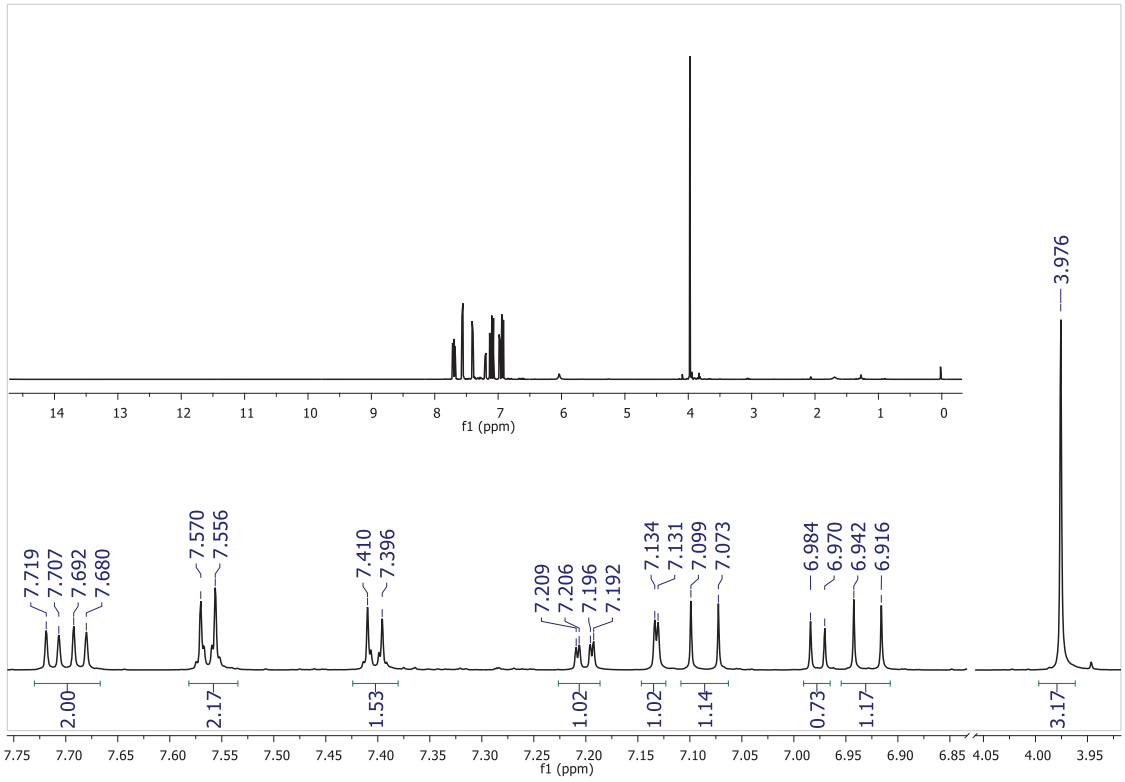

Figure S9. ii) ^{13}C NMR spectrum of compound **8**

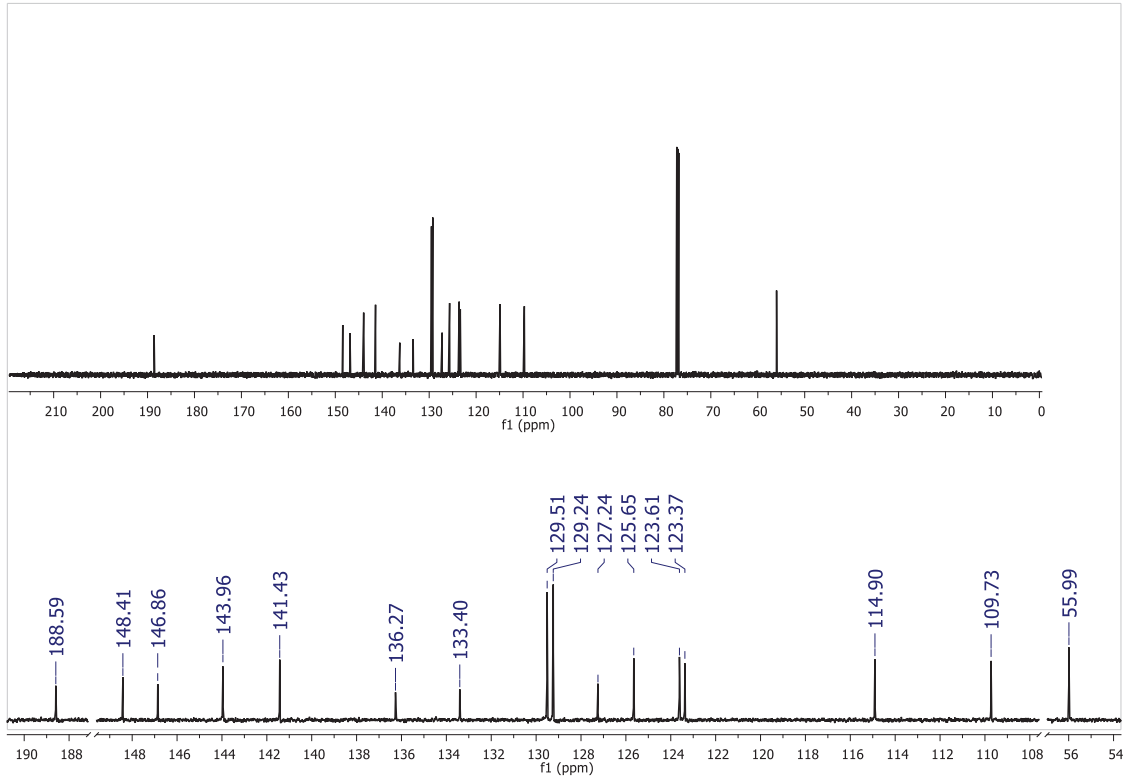

Figure S9. iii) UV-Vis spectrum of compound **8**

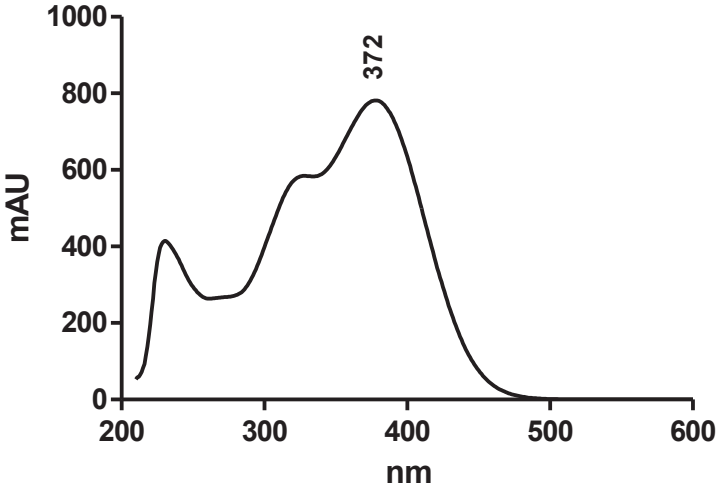

Figure S9. iv) HPLC chromatogram of compound **8**

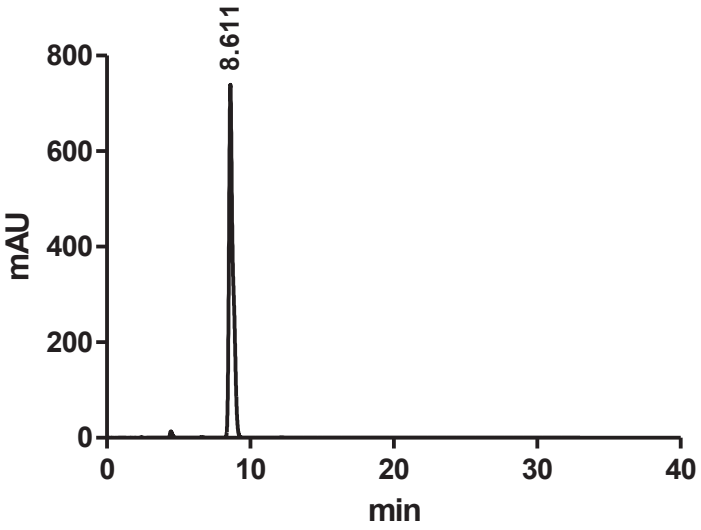

Figure S10. i) ^{1}H NMR spectrum of compound **9**

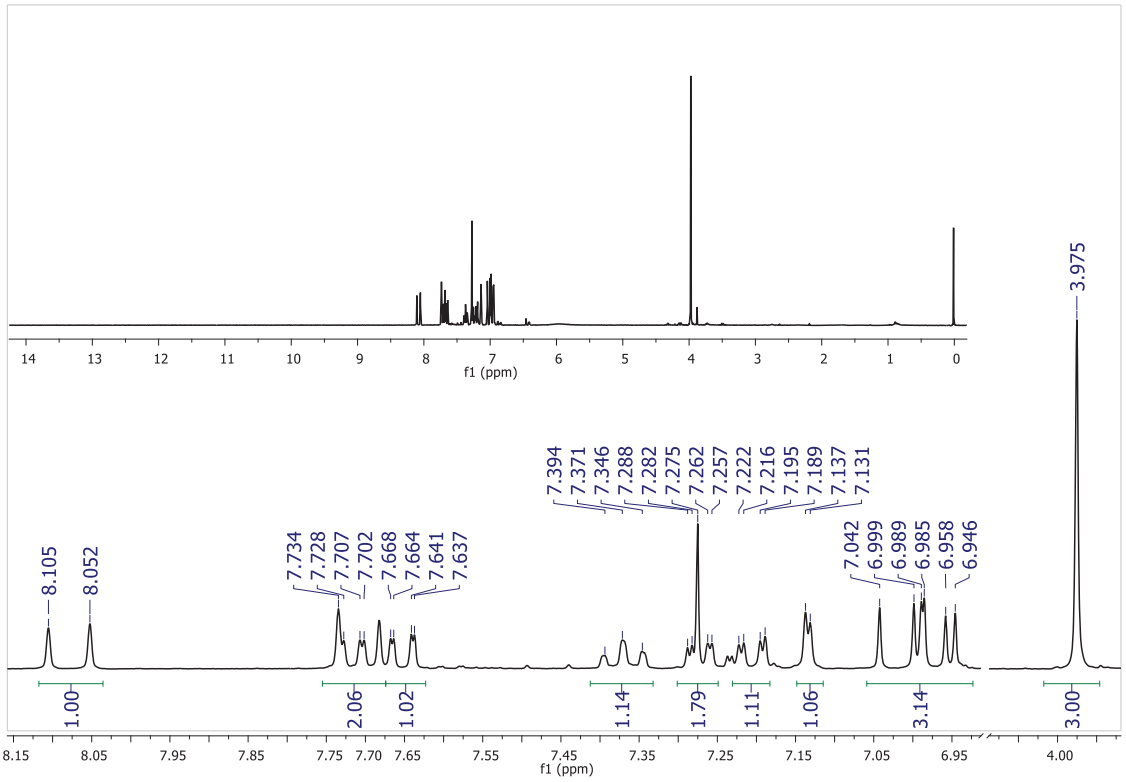

Figure S10. ii) ^{13}C NMR spectrum of compound **9**

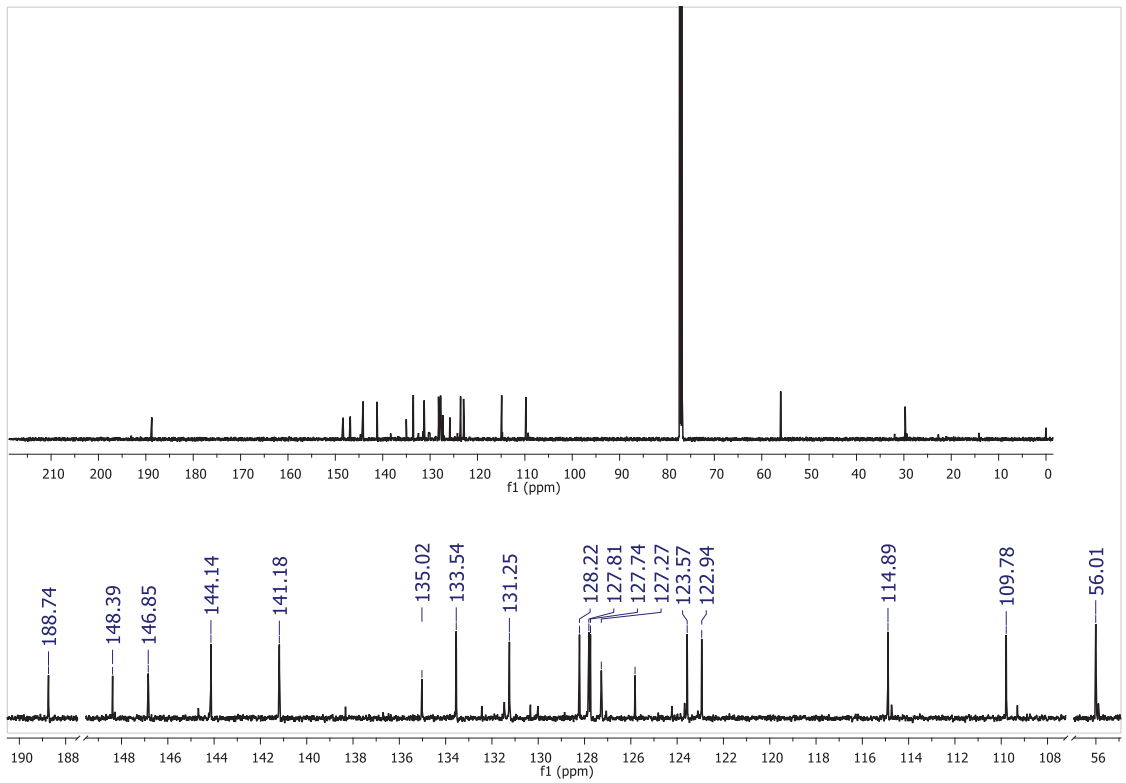

Figure S10. iii) UV-Vis spectrum of compound **9**

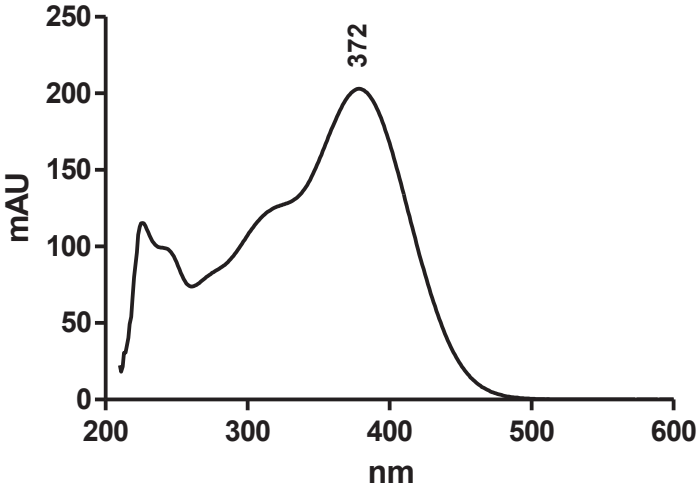

Figure S10. iv) HPLC chromatogram of compound **9**

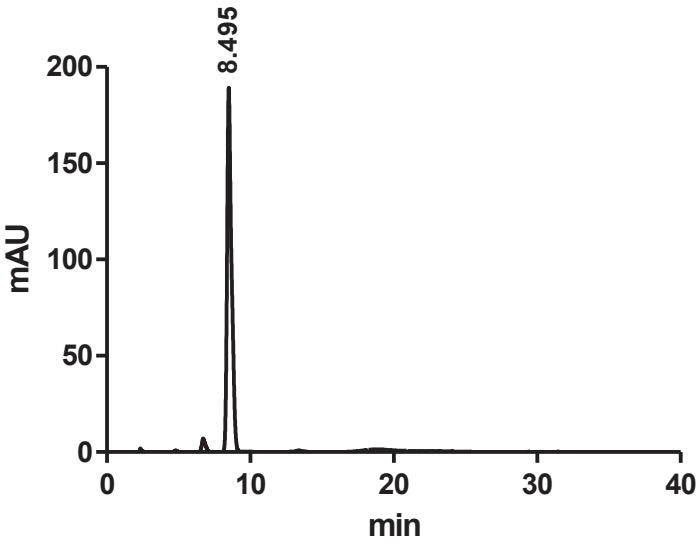

Figure S11. i) ^{1}H NMR spectrum of compound **10**

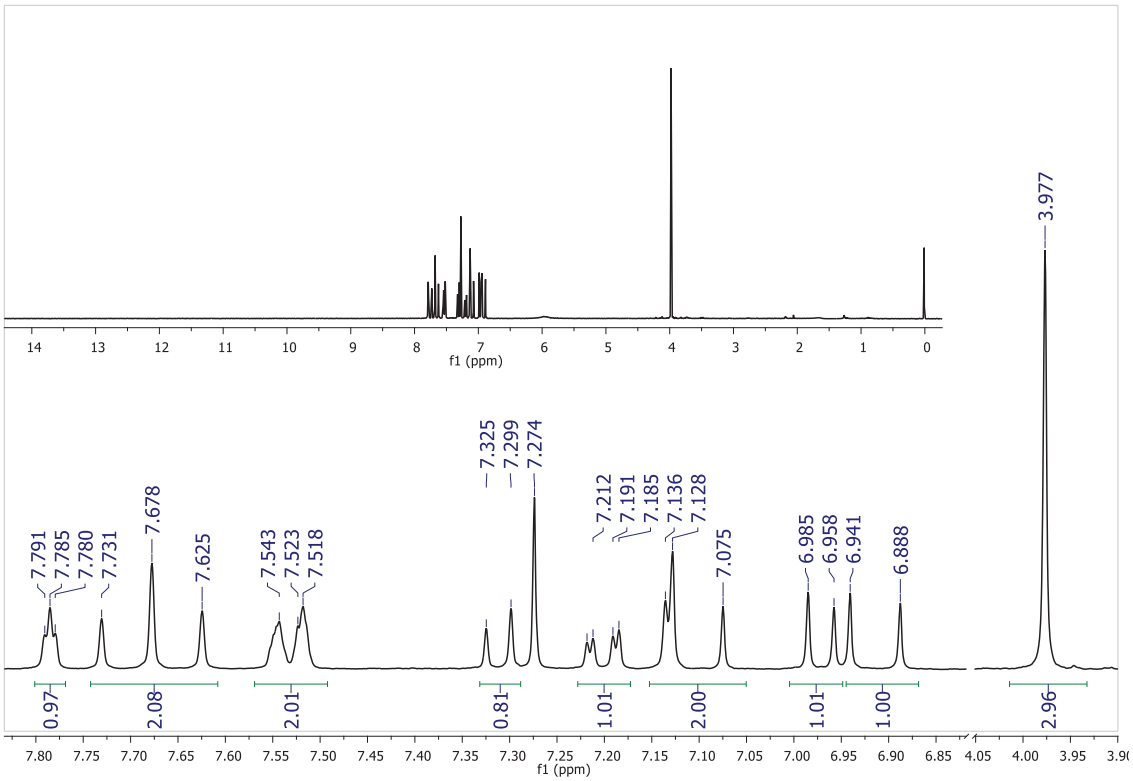

Figure S11. ii) ^{13}C NMR spectrum of compound **10**

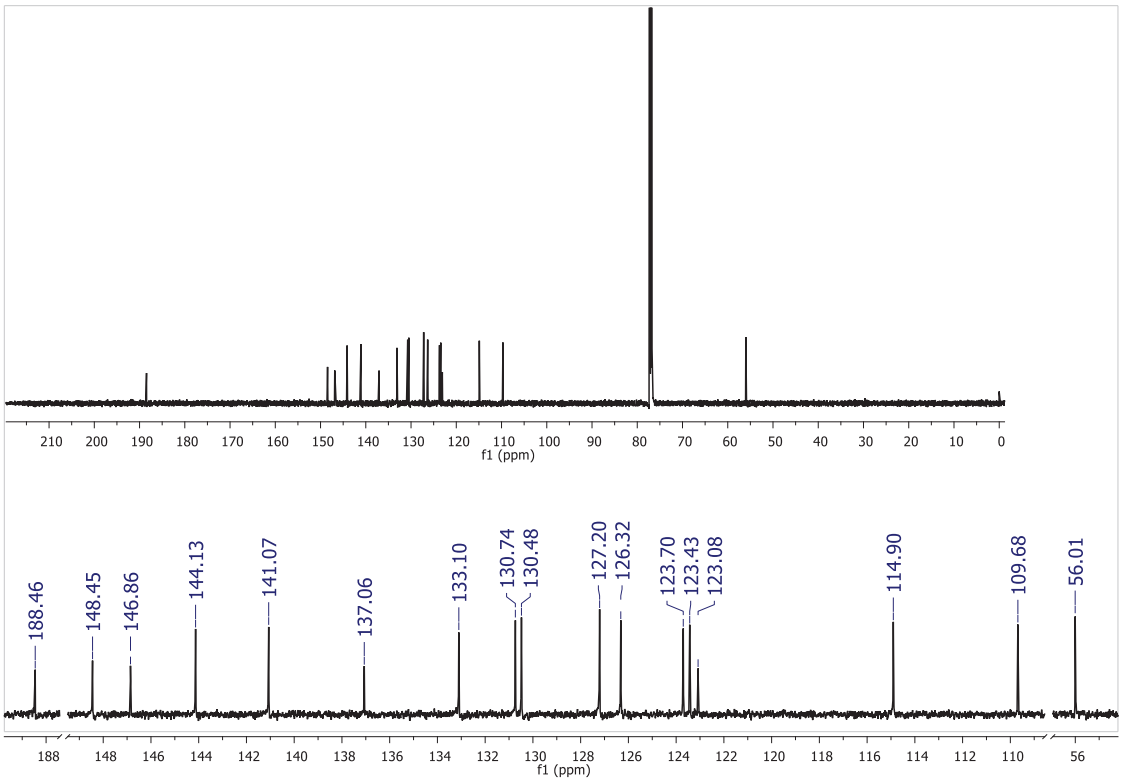

Figure S11. iii) UV-Vis spectrum of compound **10**

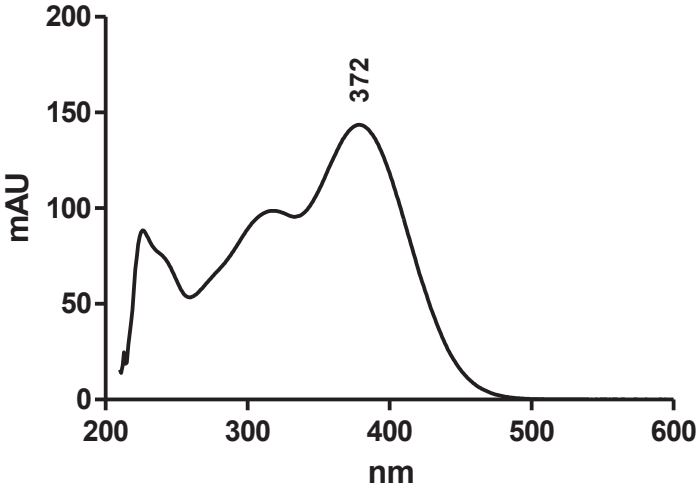

Figure S11. iv) HPLC chromatogram of compound **10**

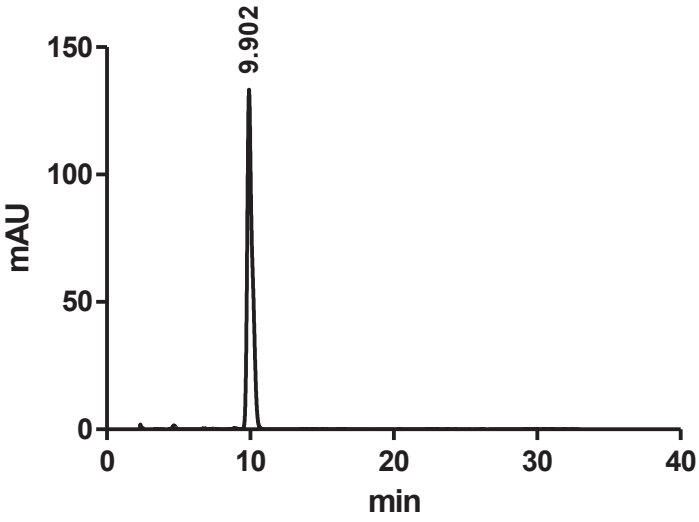

Figure S12. i) ^{1}H NMR spectrum of compound **11**

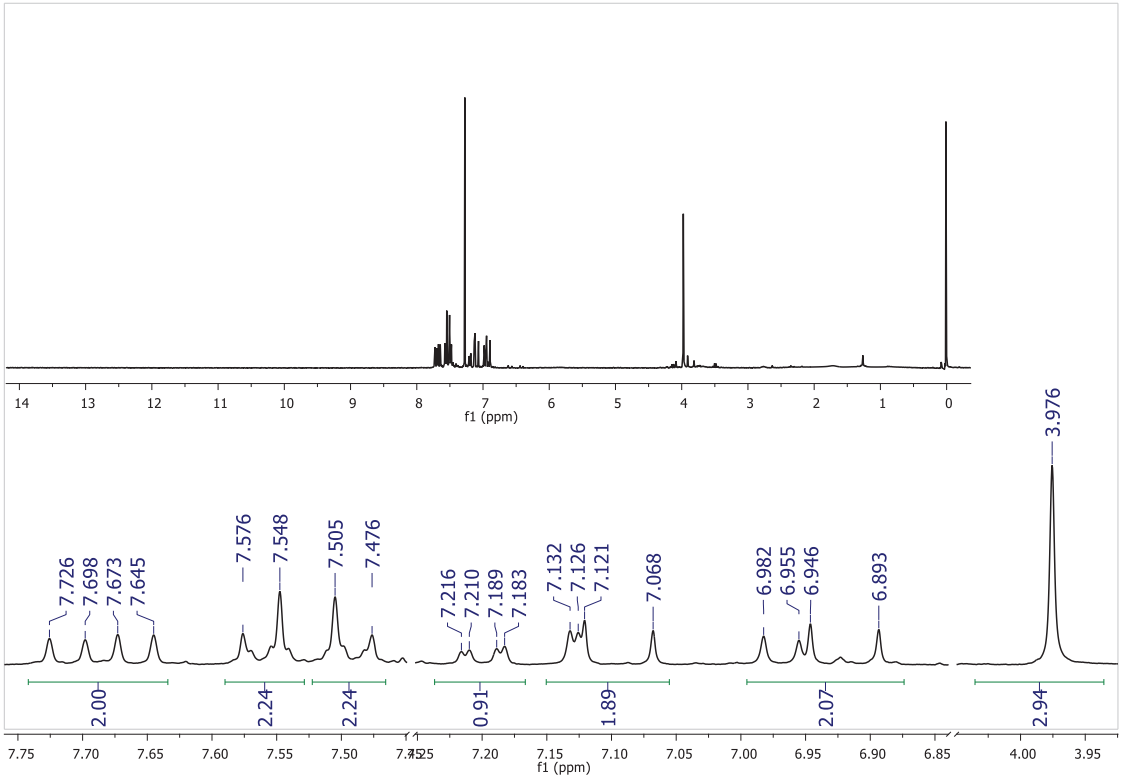

Figure S12. ii) ^{13}C NMR spectrum of compound **11**

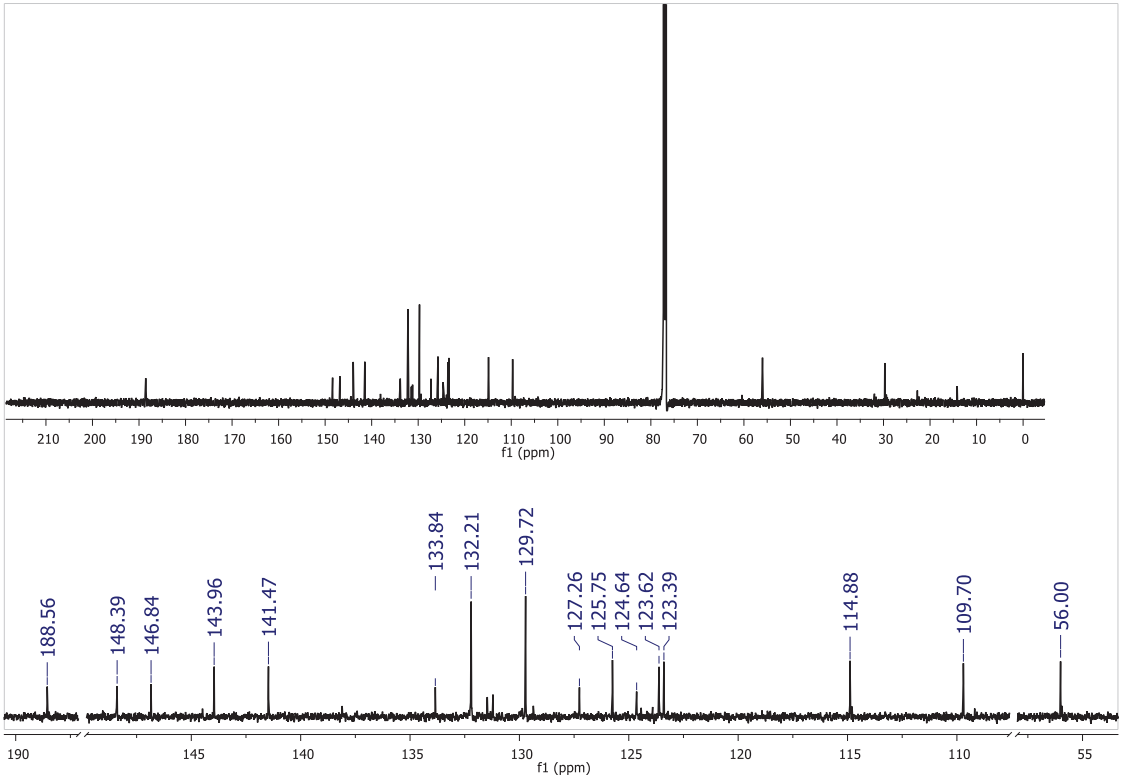

Figure S12. iii) UV-Vis spectrum of compound **11**

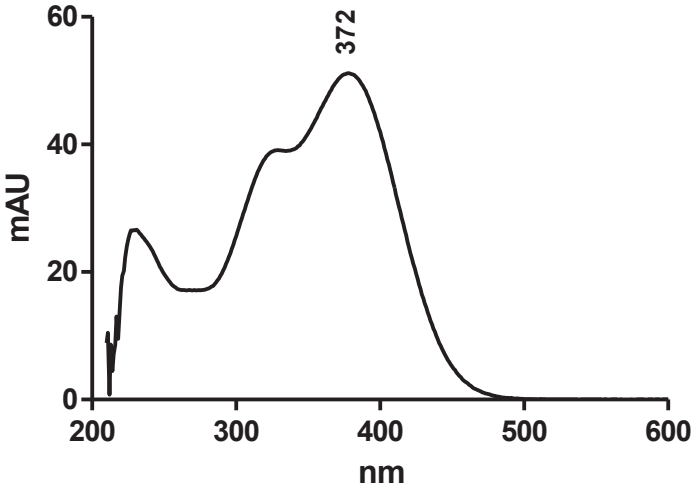

Figure S12. iv) HPLC chromatogram of compound **11**

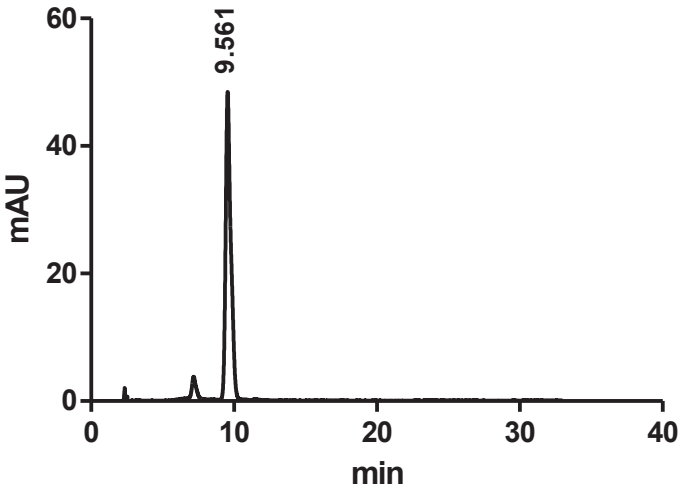

Figure S13. i) ^{1}H NMR spectrum of compound **12**

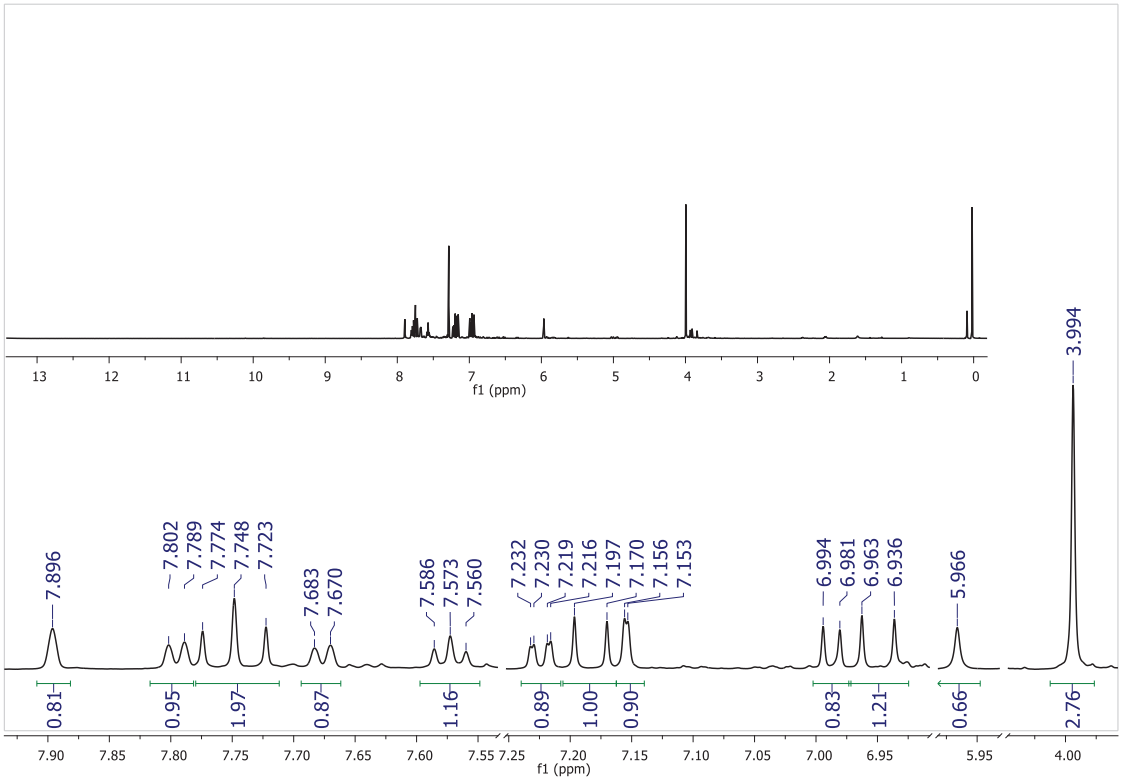

Figure S13. ii) ^{13}C NMR spectrum of compound **12**

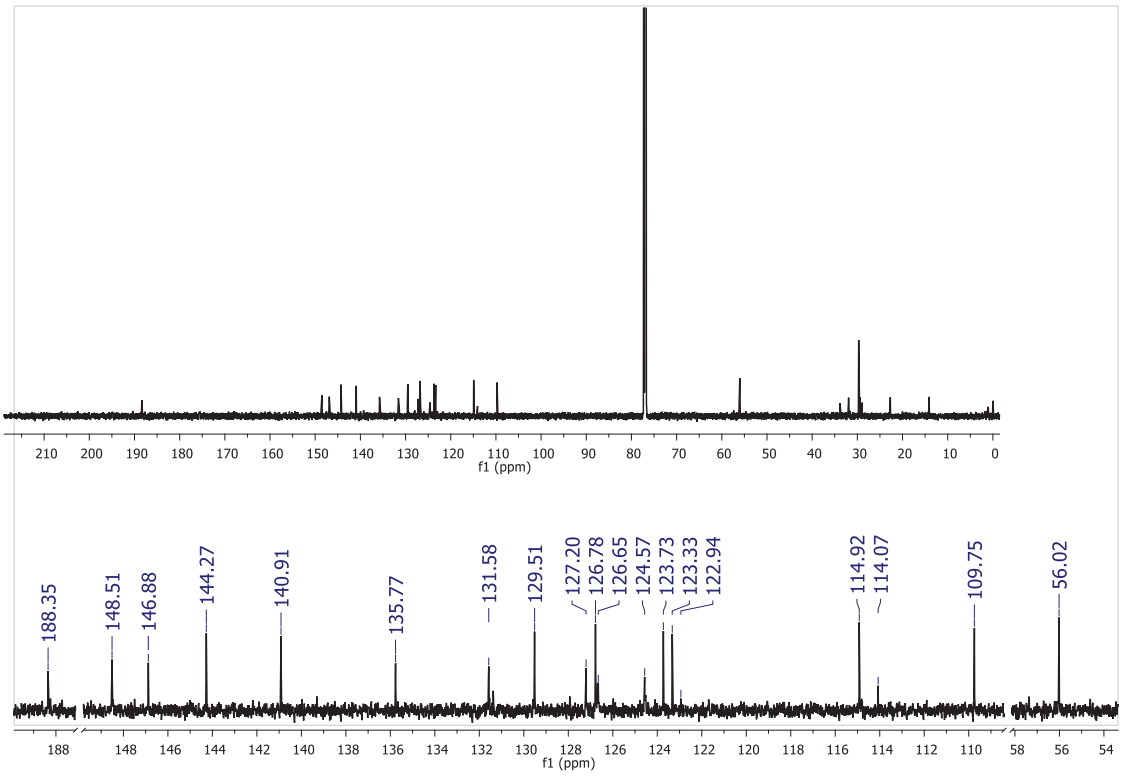

Figure S13. iii) UV-Vis spectrum of compound **12**

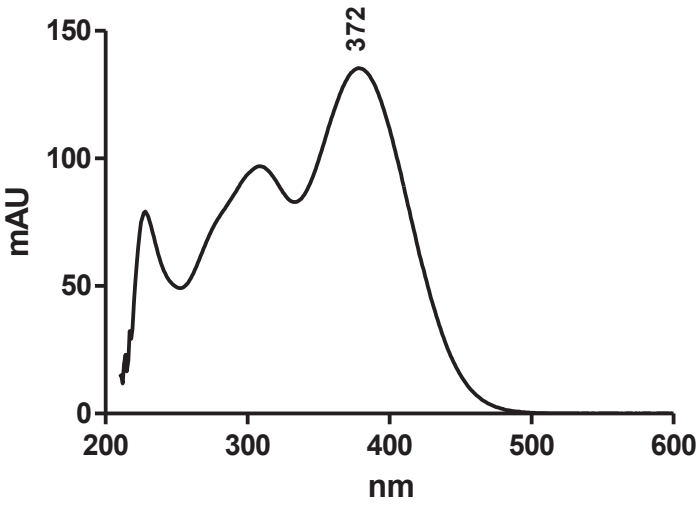

Figure S13. iv) HPLC chromatogram of compound **12**

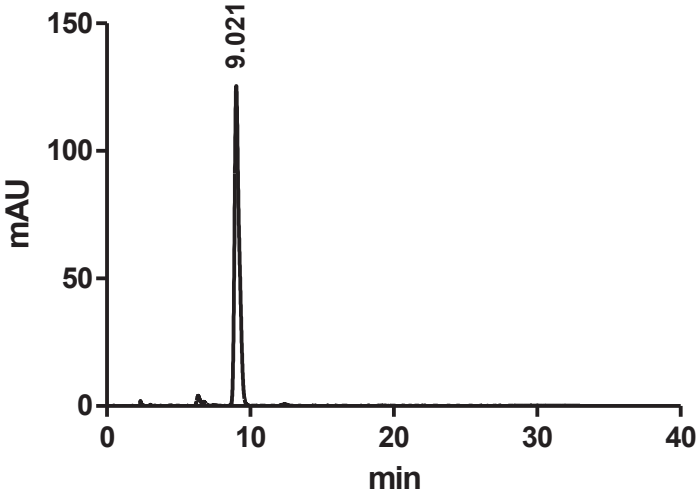

Figure S14. i) ^{1}H NMR spectrum of compound **13**

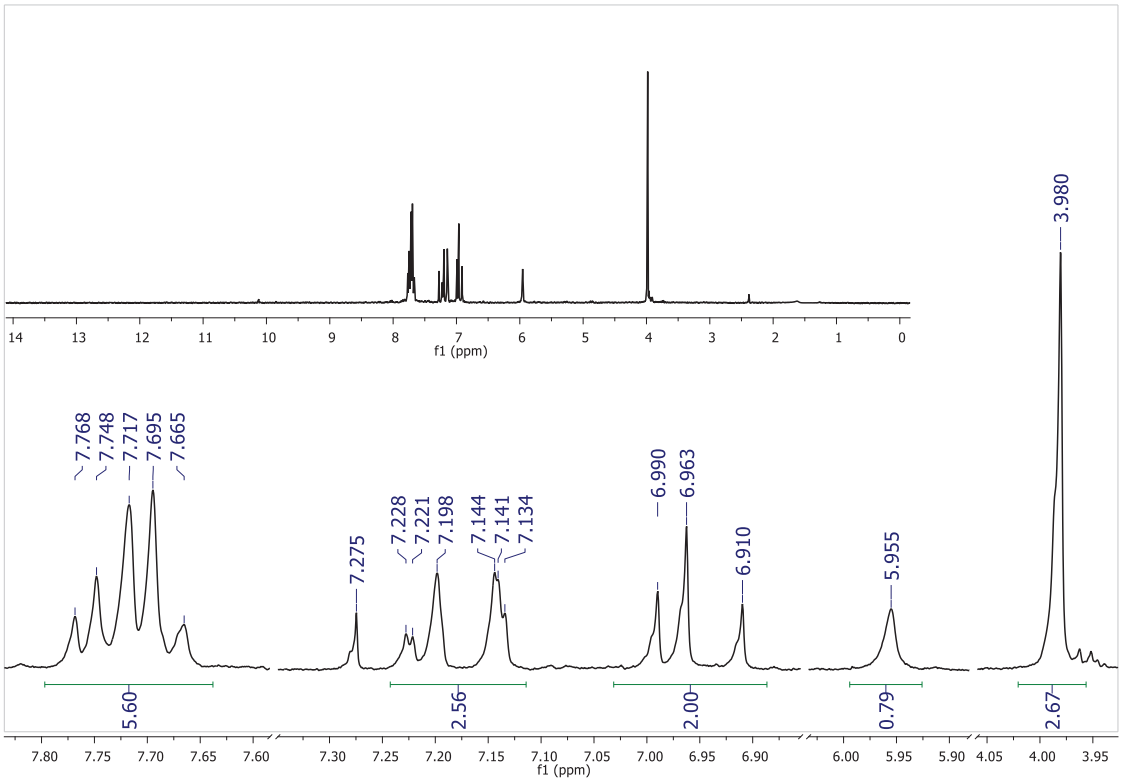

Figure S14. ii) ^{13}C NMR spectrum of compound **13**

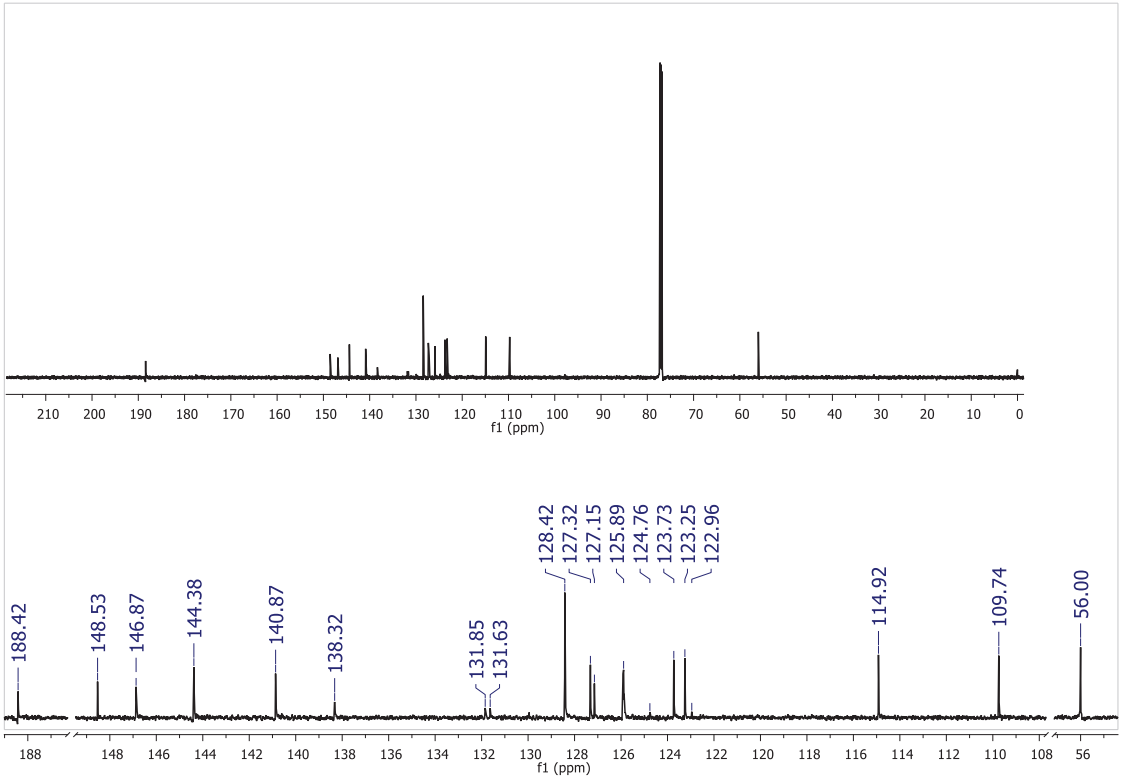

Figure S14. iii) UV-Vis spectrum of compound **13**

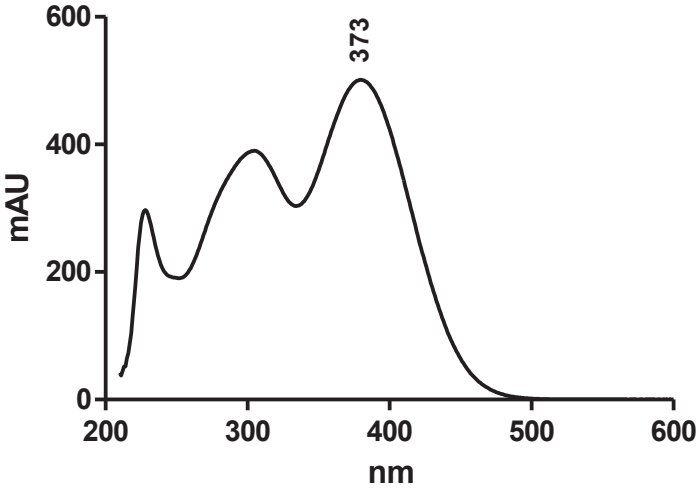

Figure S14. iv) HPLC chromatogram of compound **13**

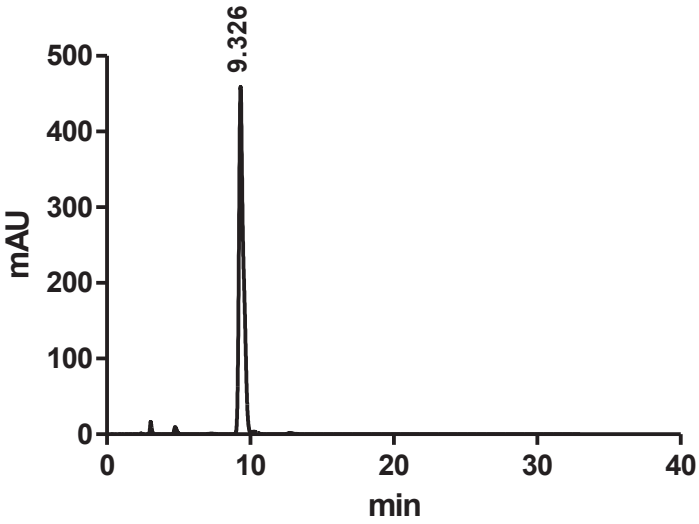

Figure S15. i) ^{1}H NMR spectrum of compound **14**

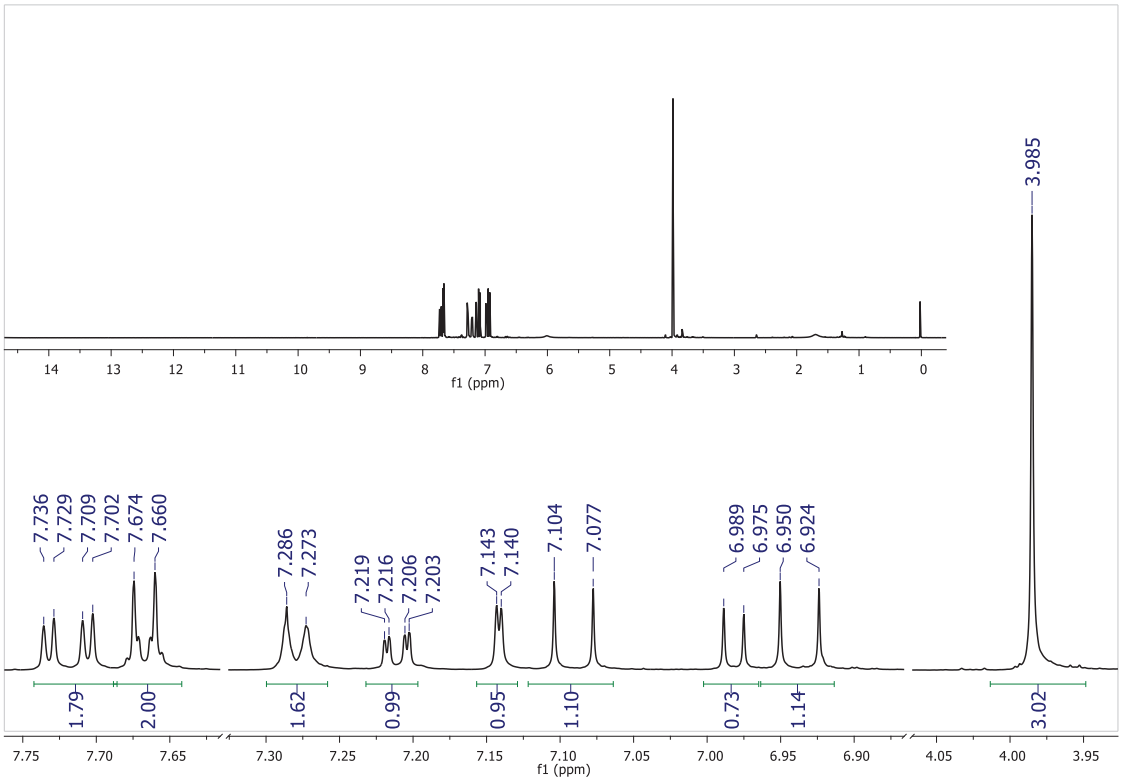

Figure S15. ii) ^{13}C NMR spectrum of compound **14**

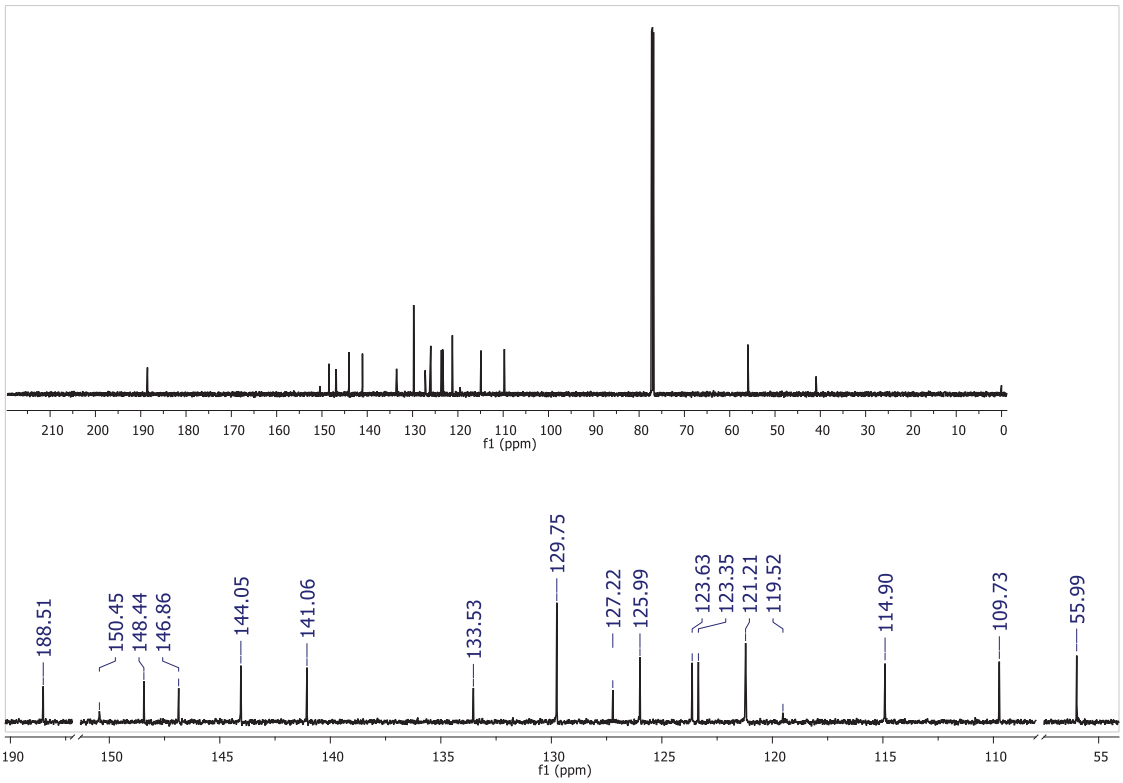

Figure S15. iii) UV-Vis spectrum of compound **14**

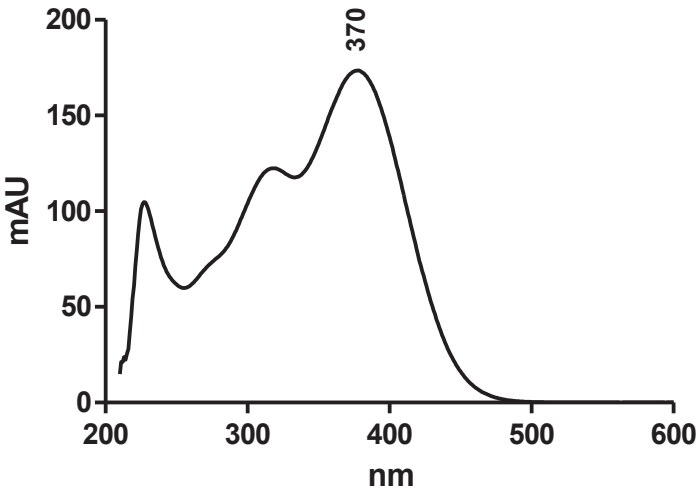

Figure S15. iv) HPLC chromatogram of compound **14**

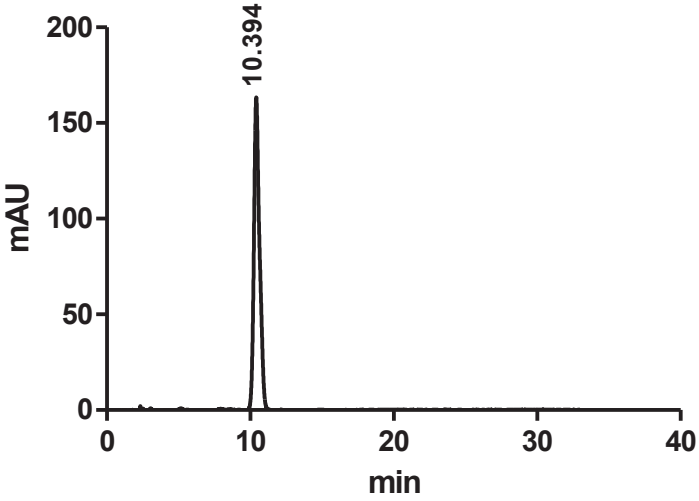

Figure S16. i) ^{1}H NMR spectrum of compound **15**

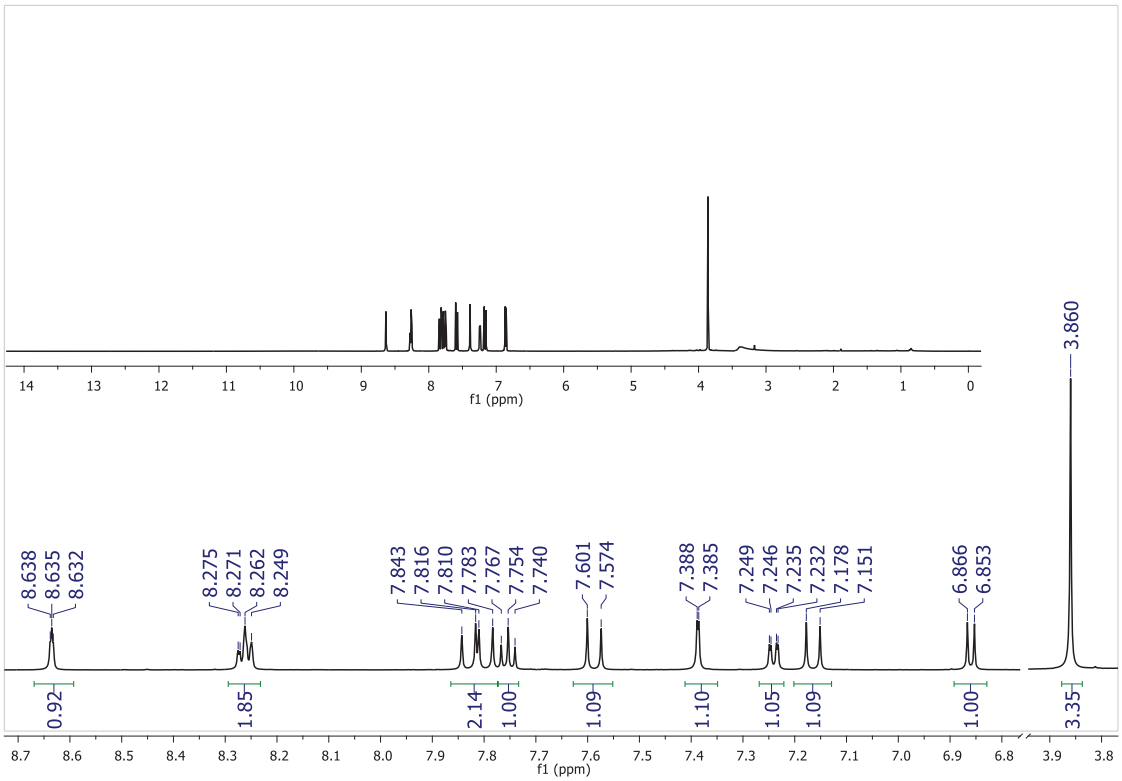

Figure S16. ii) ^{13}C NMR spectrum of compound **15**

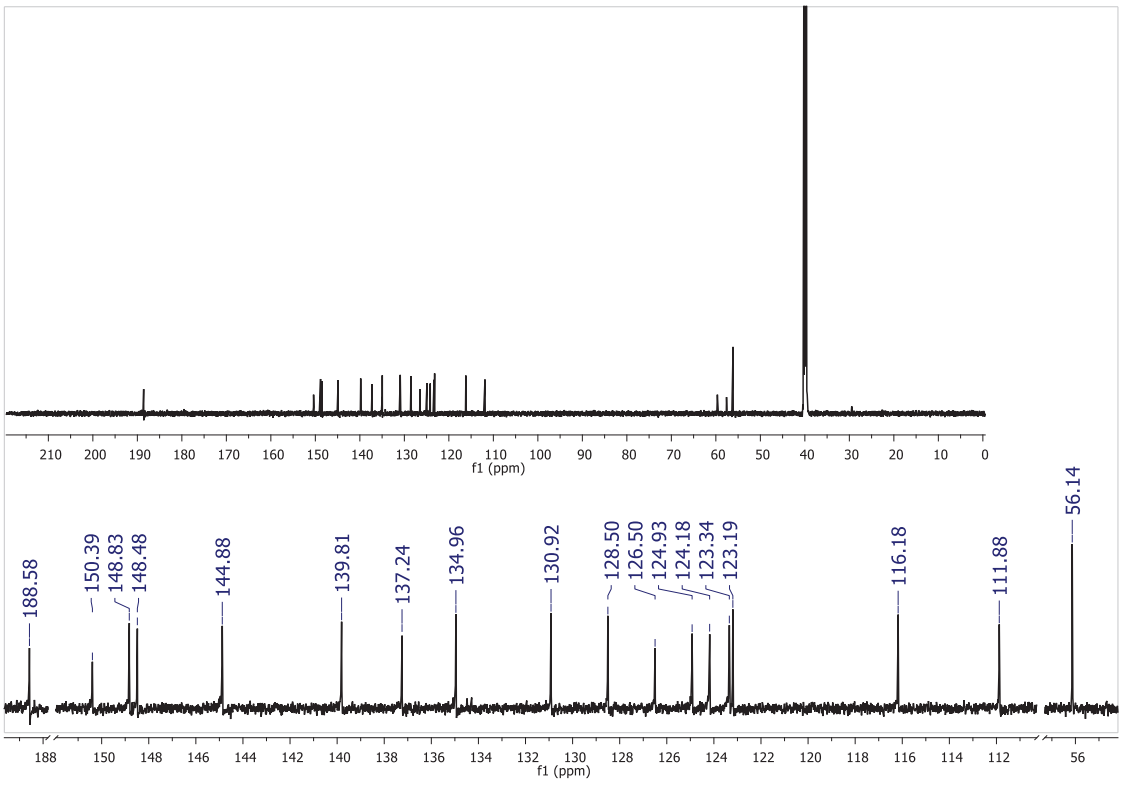

Figure S16. iii) UV-Vis spectrum of compound **15**

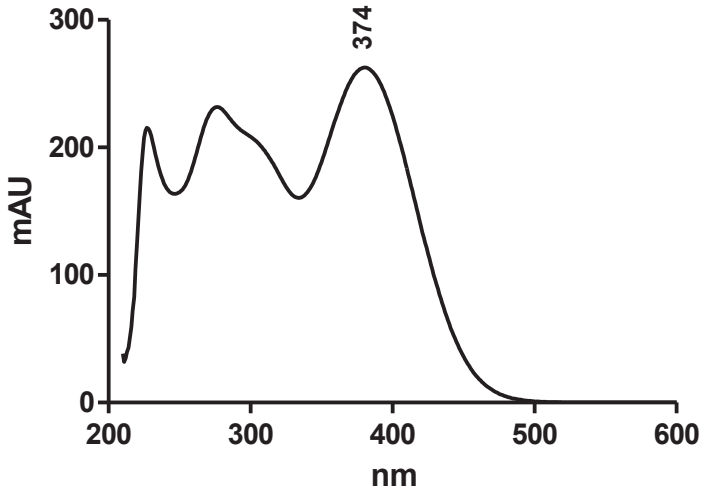

Figure S16. iv) HPLC chromatogram of compound **15**

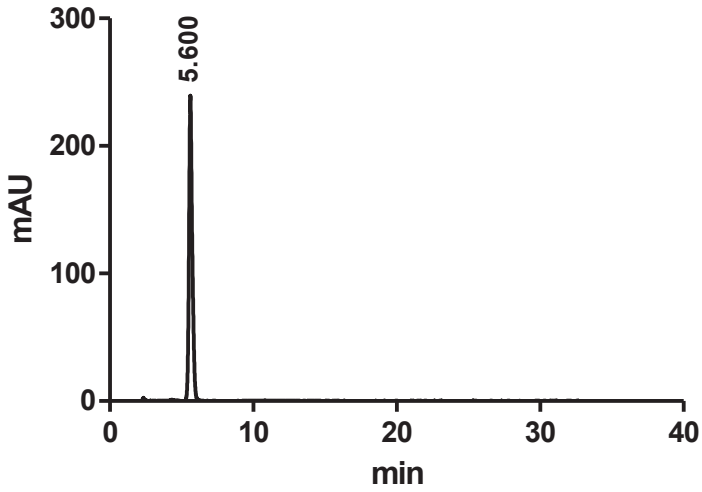

Figure S17. i) ^{1}H NMR spectrum of compound **16**

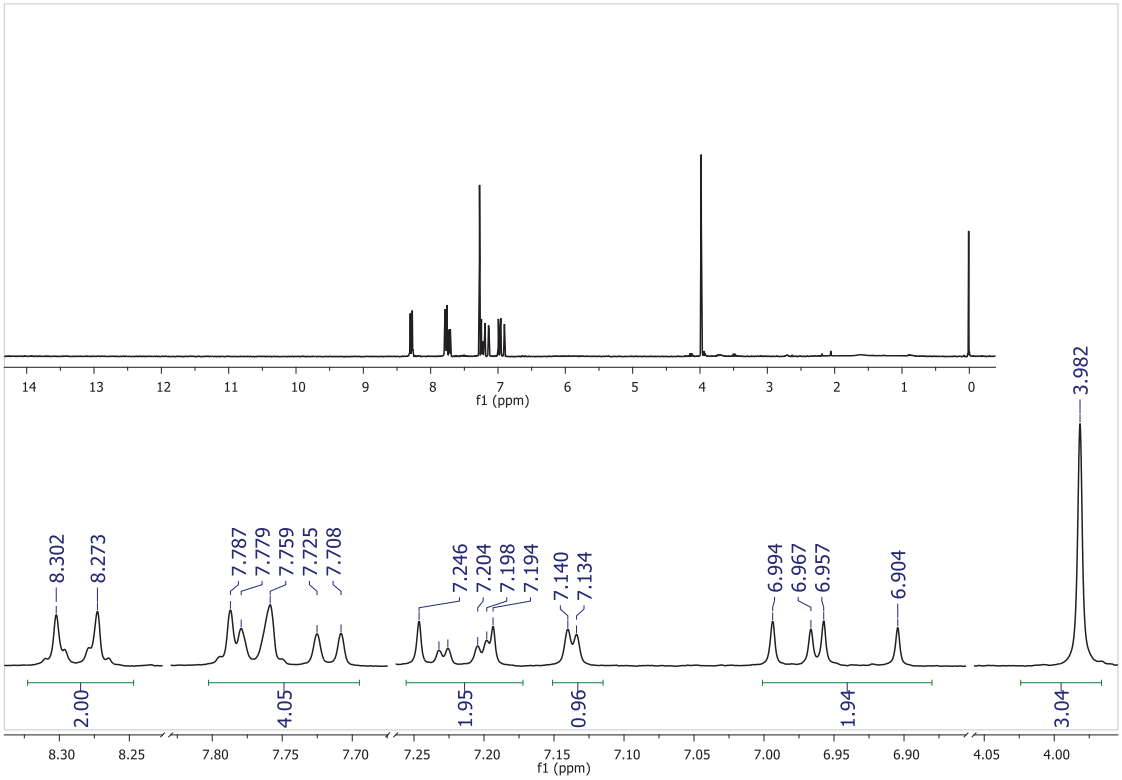

Figure S17. ii) ^{13}C NMR spectrum of compound **16**

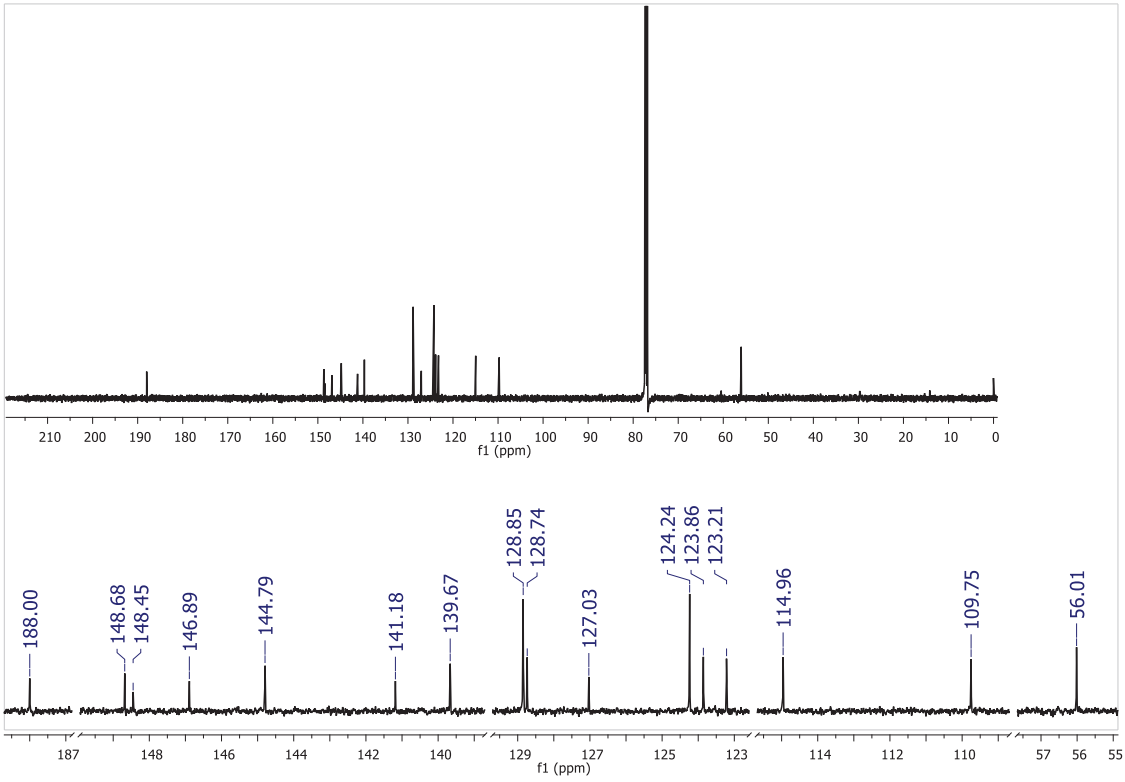

Figure S17. iii) UV-Vis spectrum of compound **16**

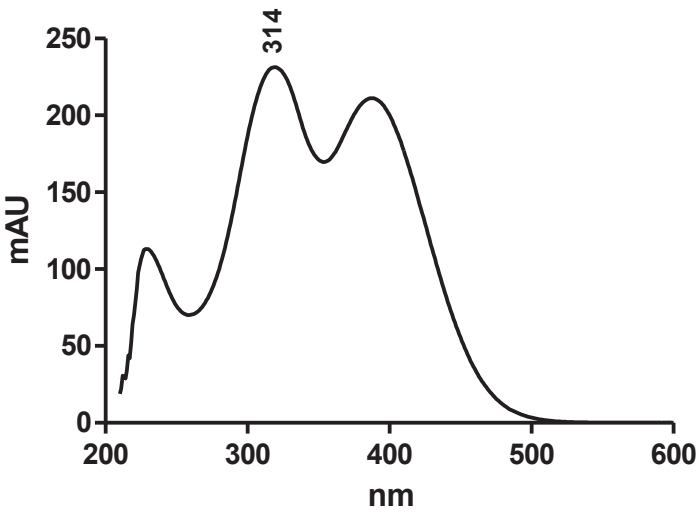

Figure S17. iv) HPLC chromatogram of compound **16**

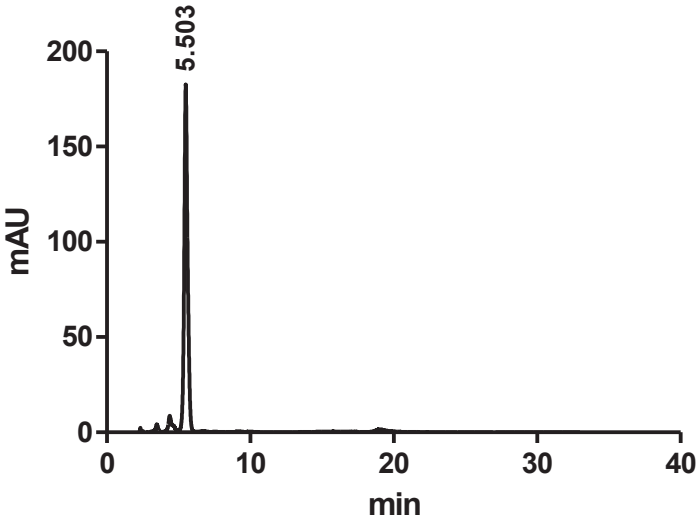

Figure S18. i) ^{1}H NMR spectrum of compound **17**

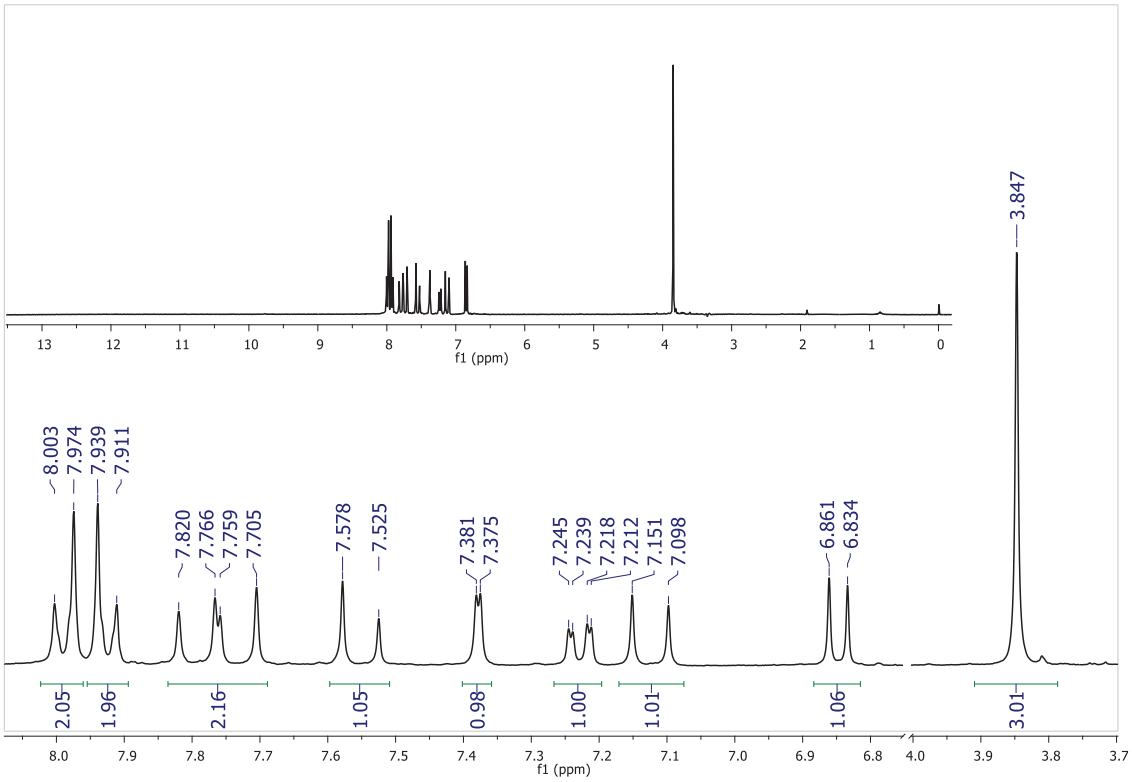

Figure S18. ii) ^{13}C NMR spectrum of compound **17**

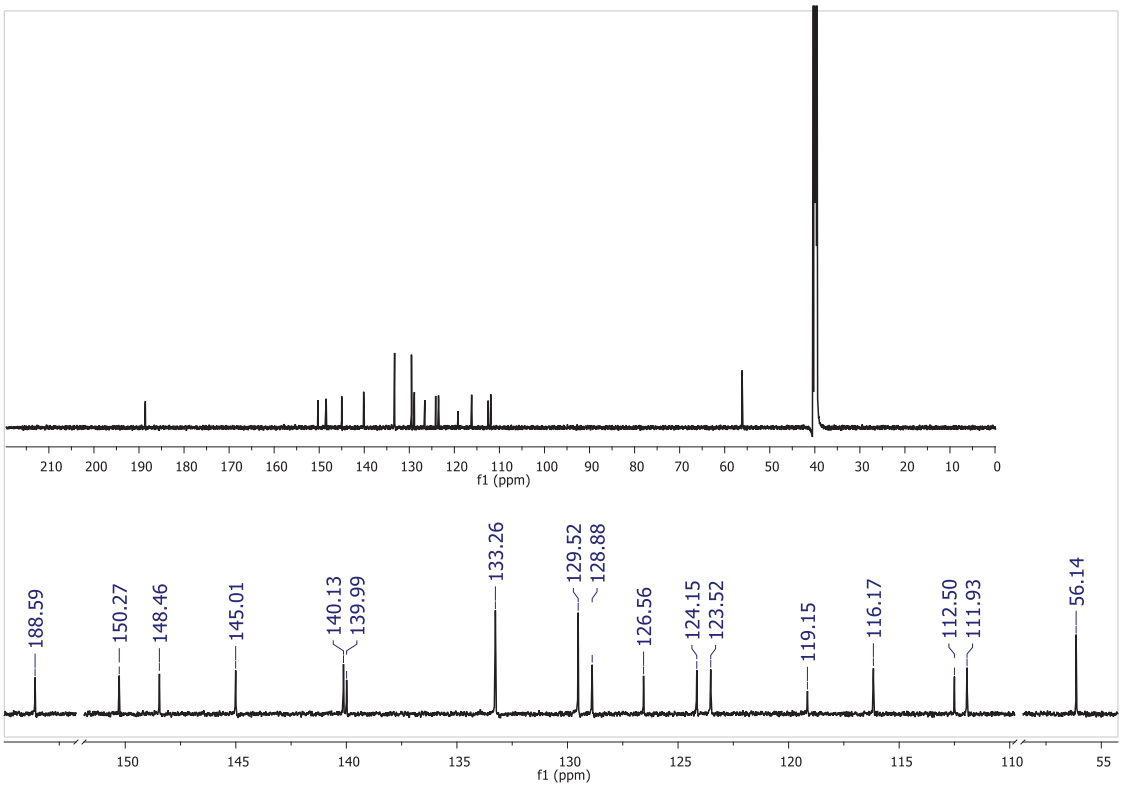

Figure S18. iii) UV-Vis spectrum of compound **17**

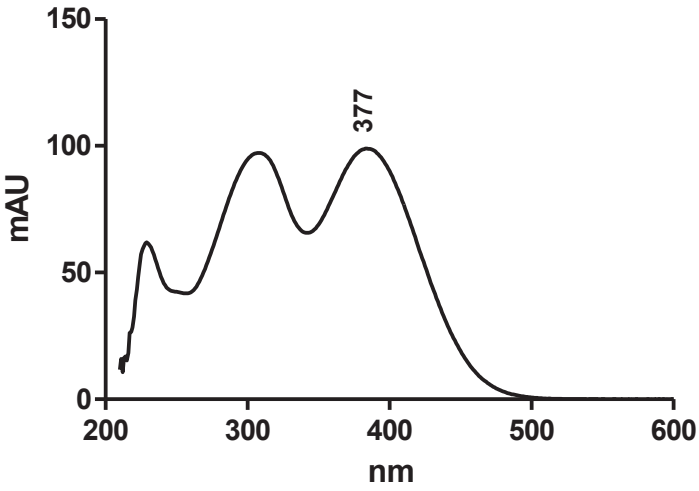

Figure S18. iv) HPLC chromatogram of compound **17**

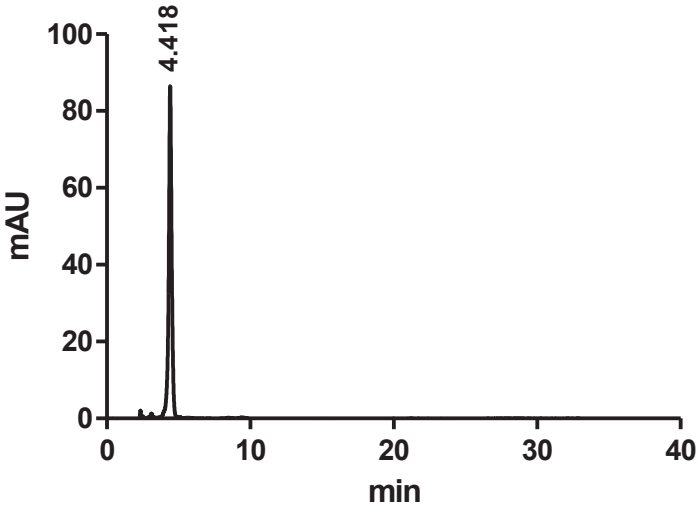

Figure S19. i) ^{1}H NMR spectrum of compound **18**

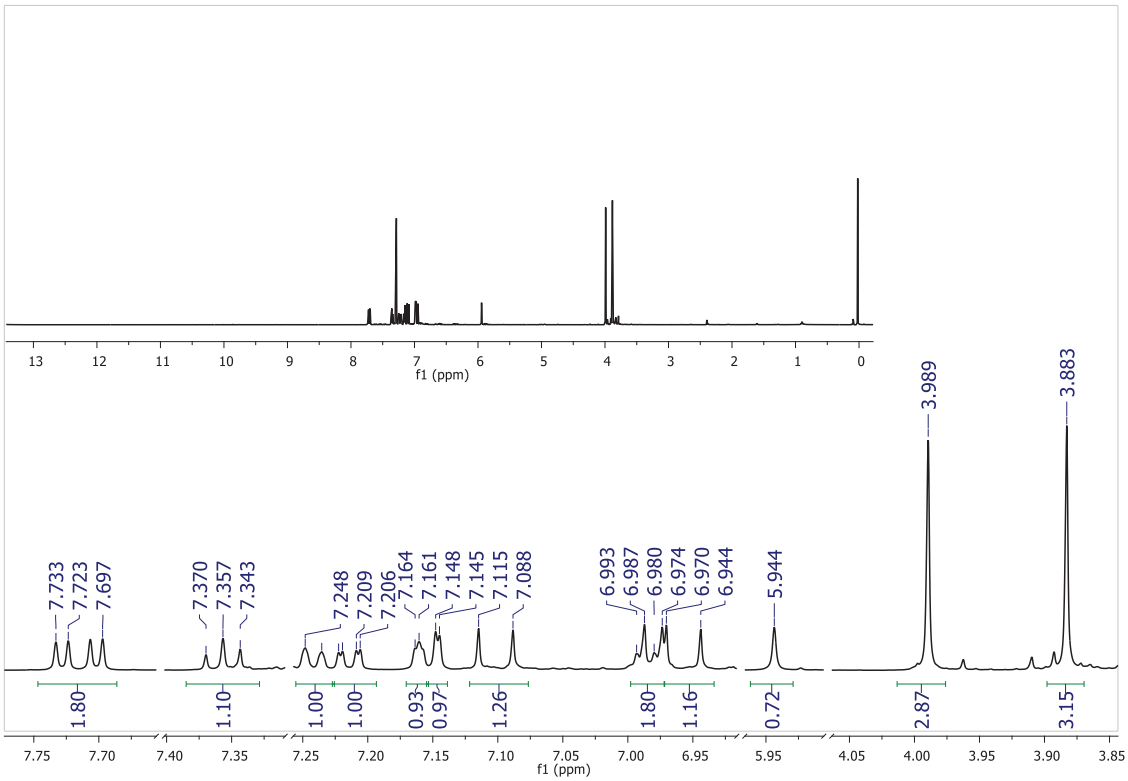

Figure S19. ii) ^{13}C NMR spectrum of compound **18**

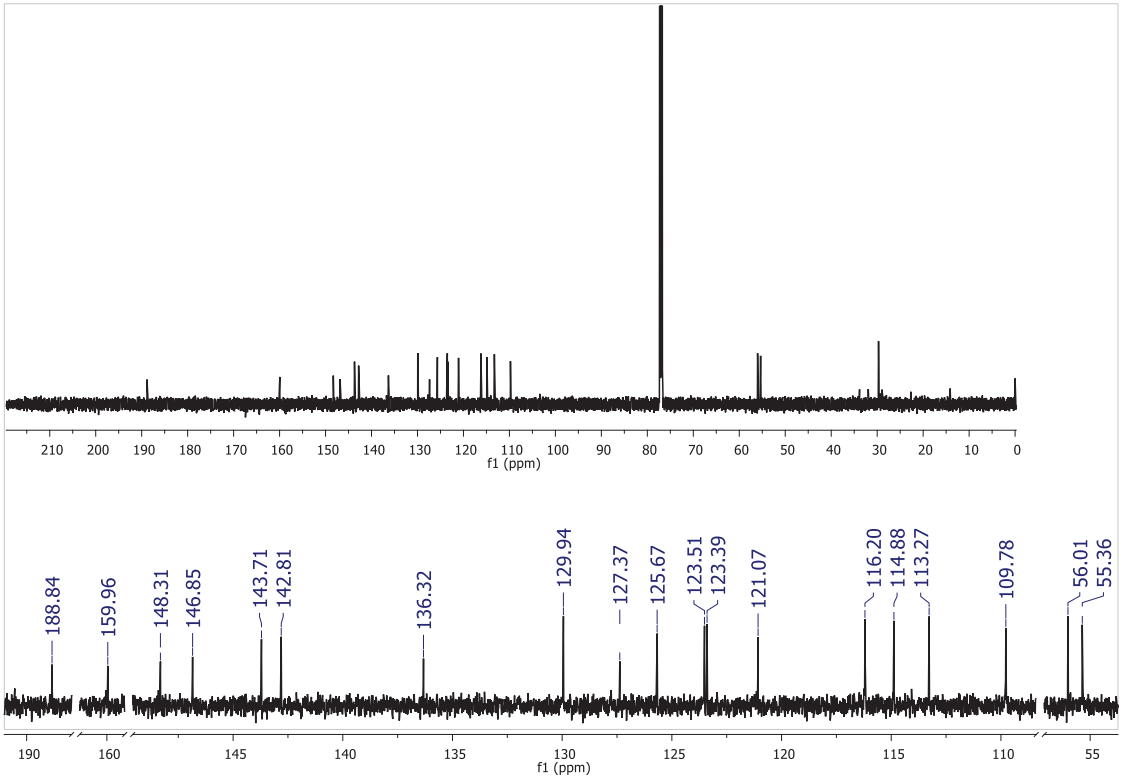

Figure S19. iii) UV-Vis spectrum of compound **18**

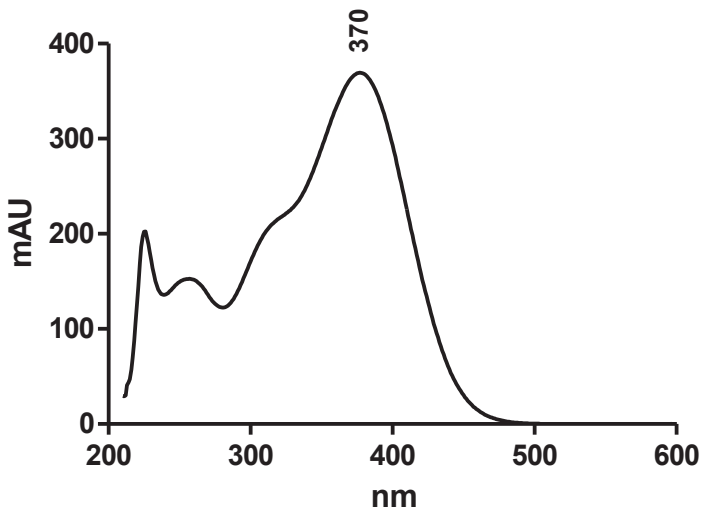

Figure S19. iv) HPLC chromatogram of compound **18**

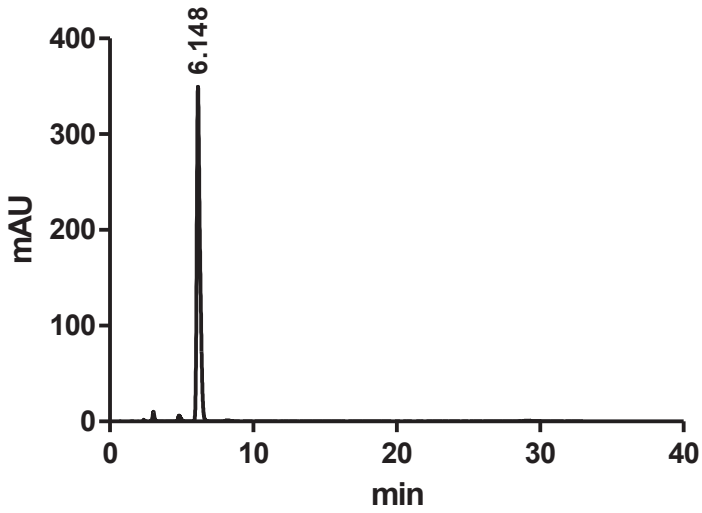

Figure S20. i) ^{1}H NMR spectrum of compound **19**

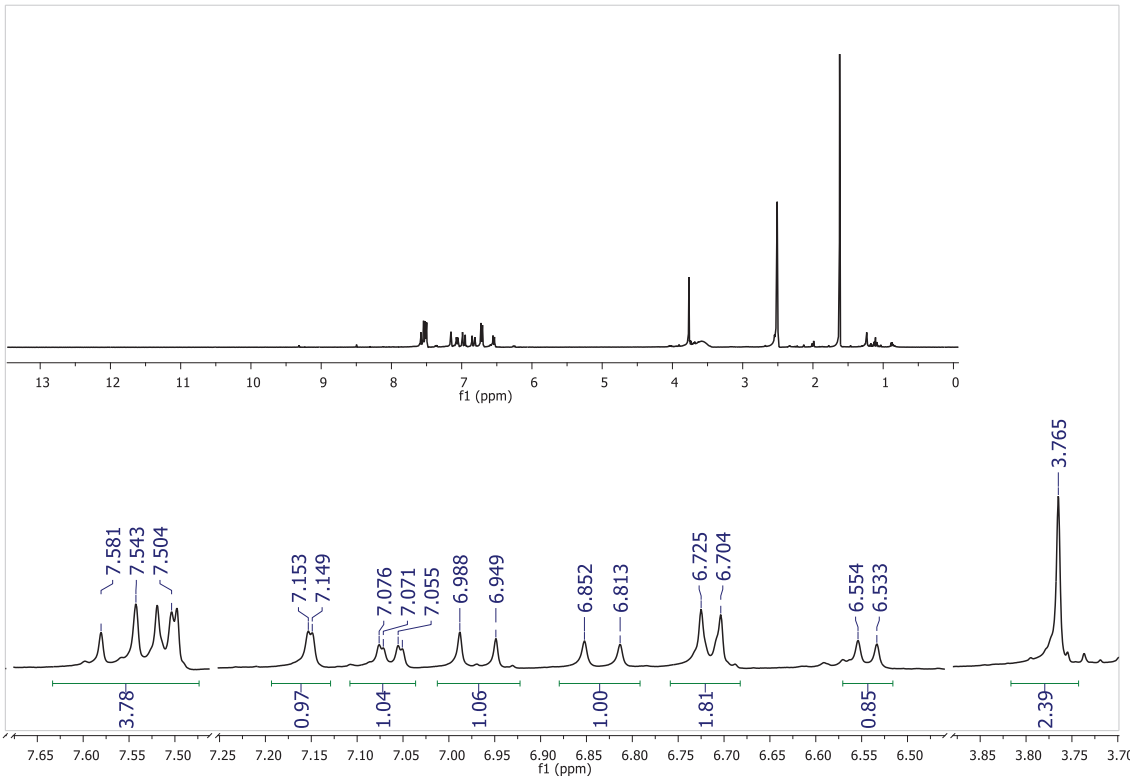

Figure S20. ii) ^{13}C NMR spectrum of compound **19**

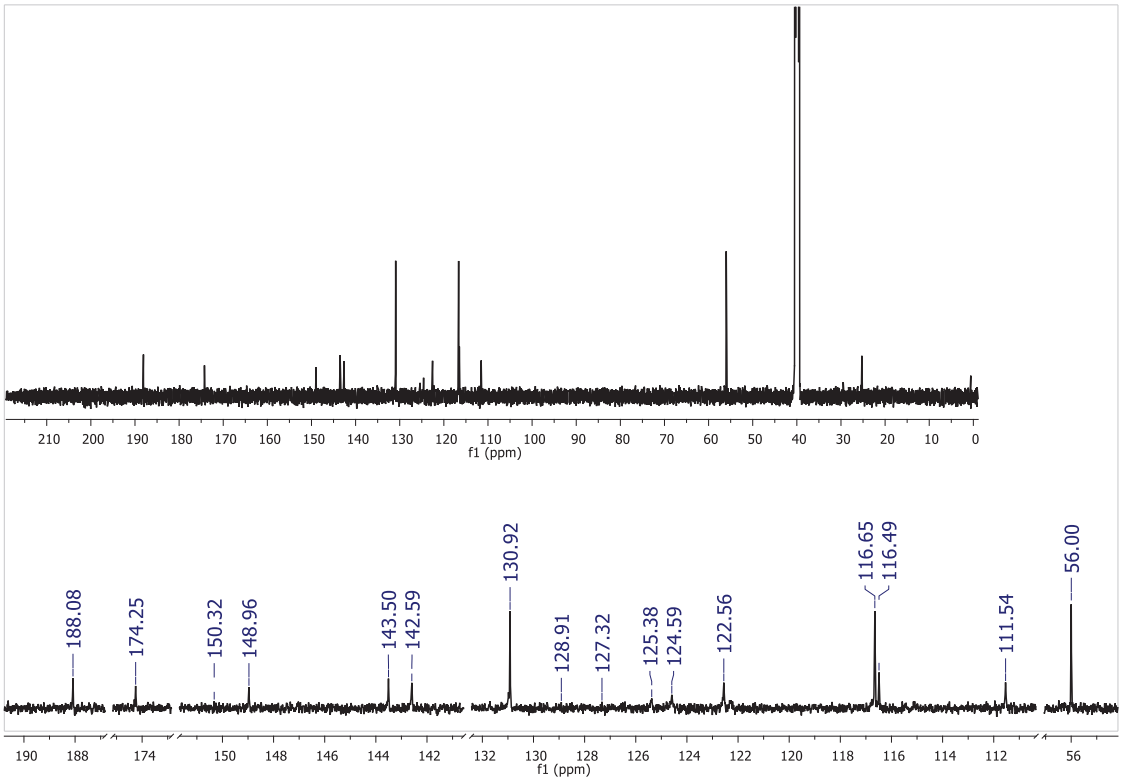

Figure S20. iii) UV-Vis spectrum of compound **19**

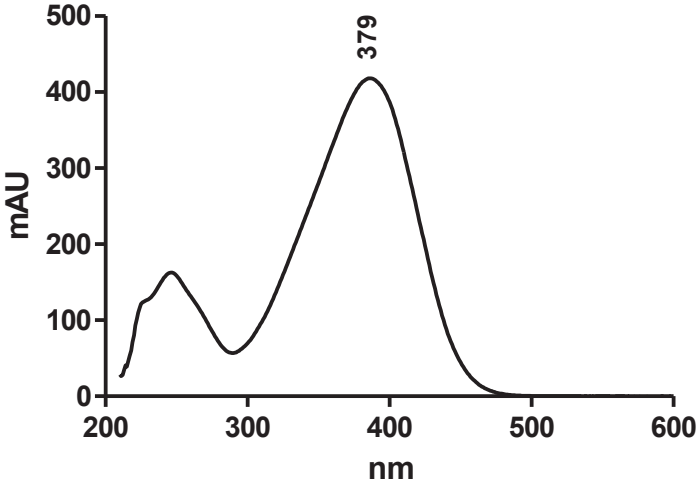

Figure S20. iv) HPLC chromatogram of compound **19**

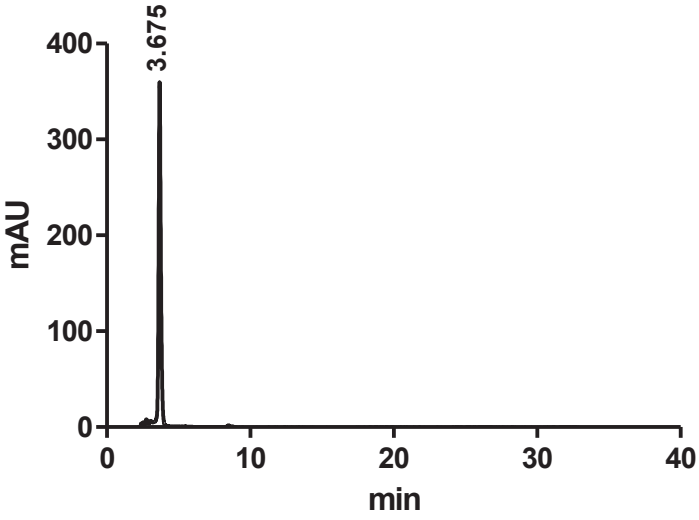

Figure S21. i) ^{1}H NMR spectrum of compound **20**

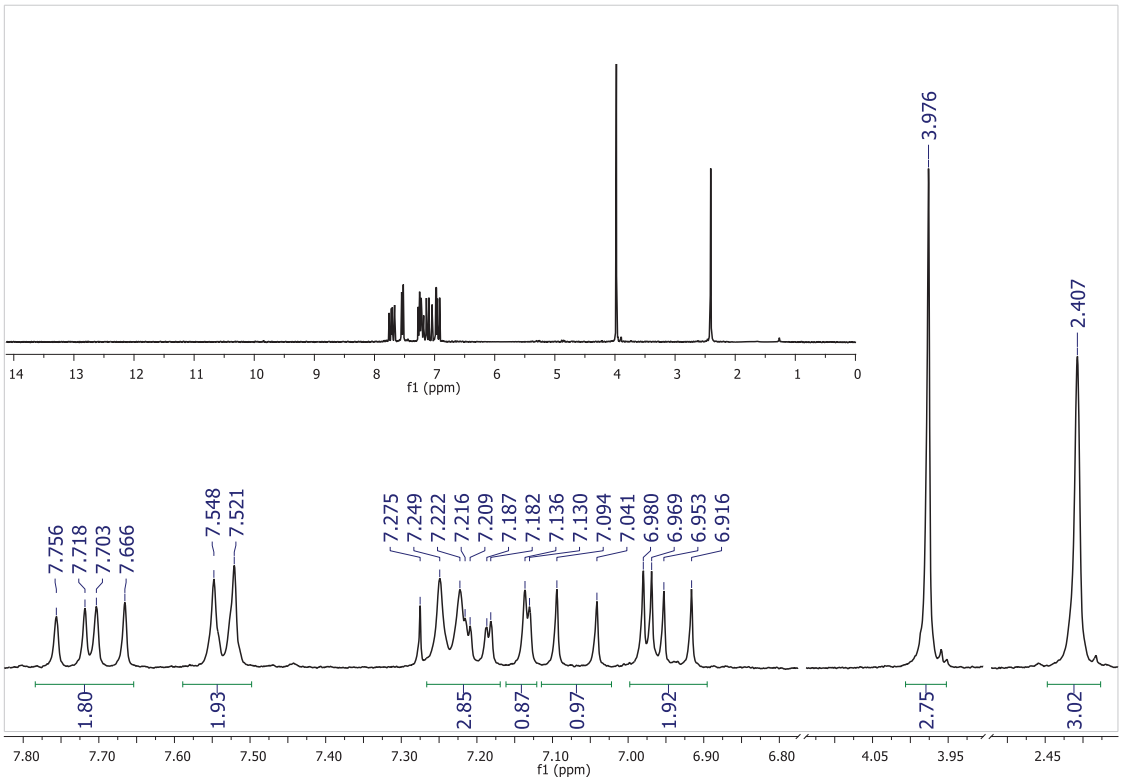

Figure S21. ii) ^{13}C NMR spectrum of compound **20**

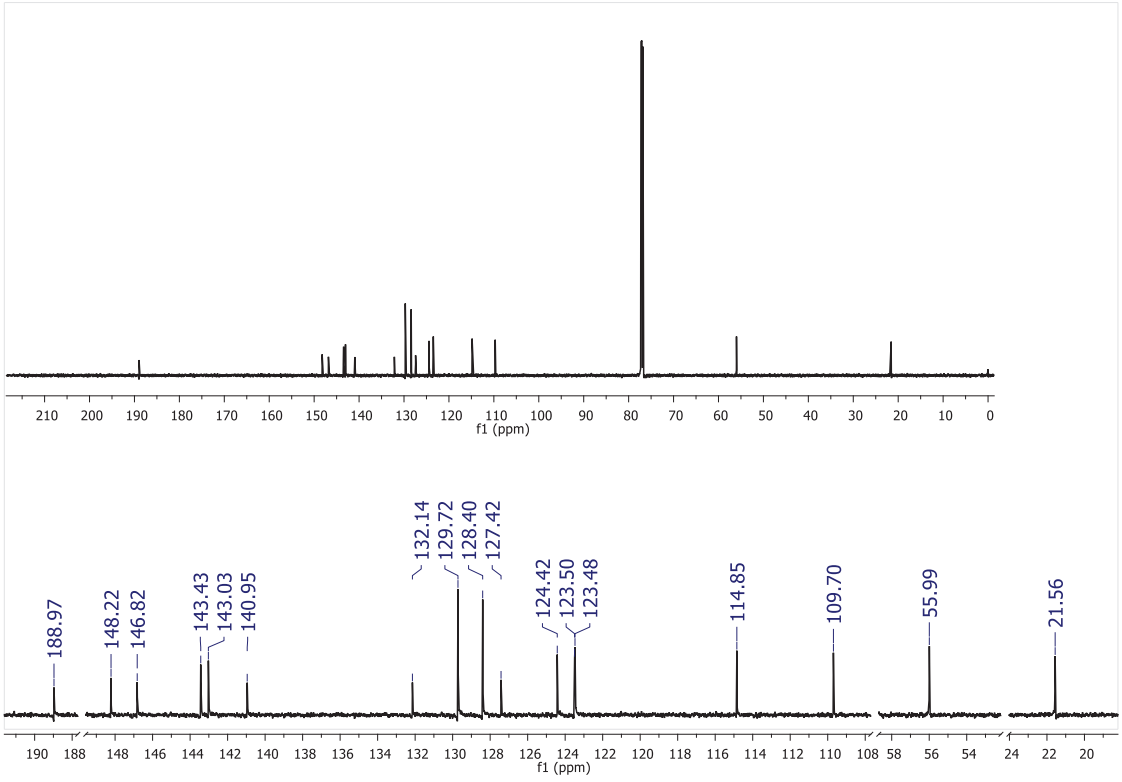

Figure S21. iii) UV-Vis spectrum of compound **20**

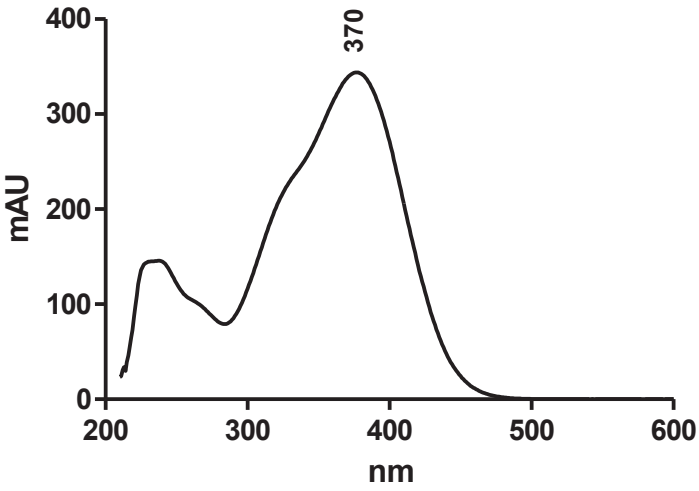

Figure S21. iv) HPLC chromatogram of compound **20**

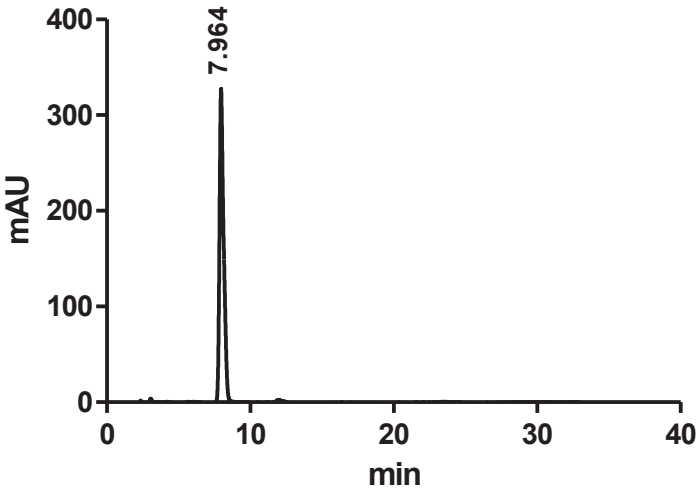

Figure S22. i) ^{1}H NMR spectrum of compound **21**

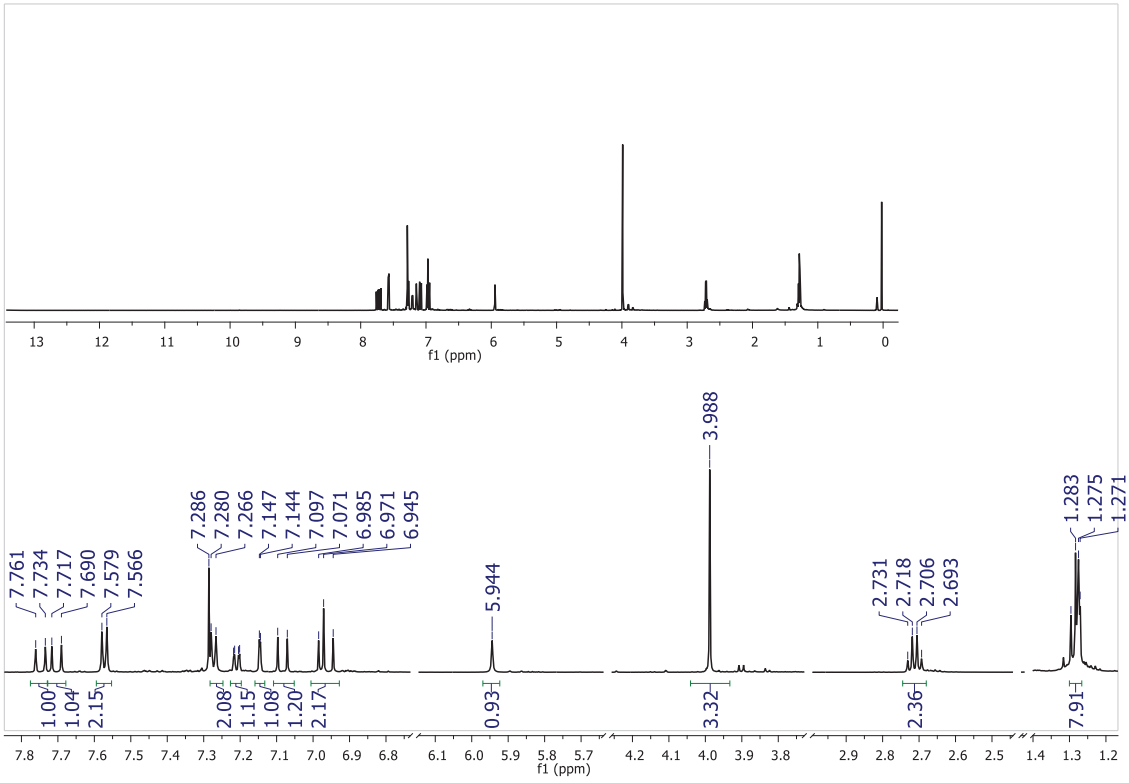

Figure S22. ii) ^{13}C NMR spectrum of compound **21**

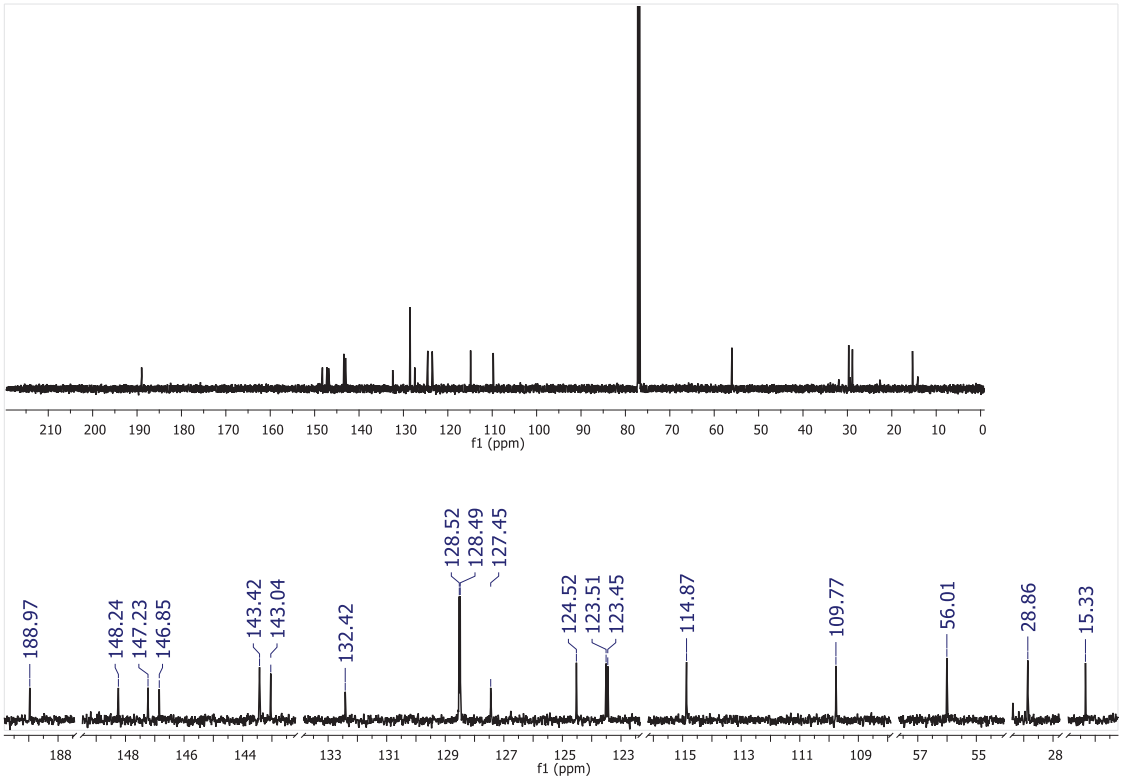

Figure S22. iii) UV-Vis spectrum of compound **21**

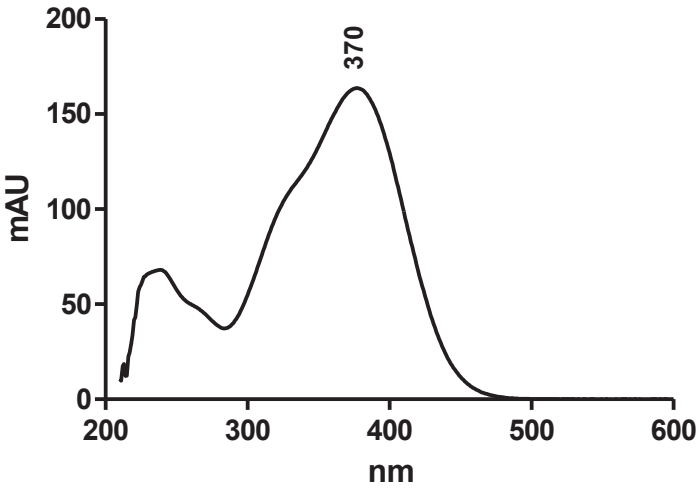

Figure S22. iv) HPLC chromatogram of compound **21**

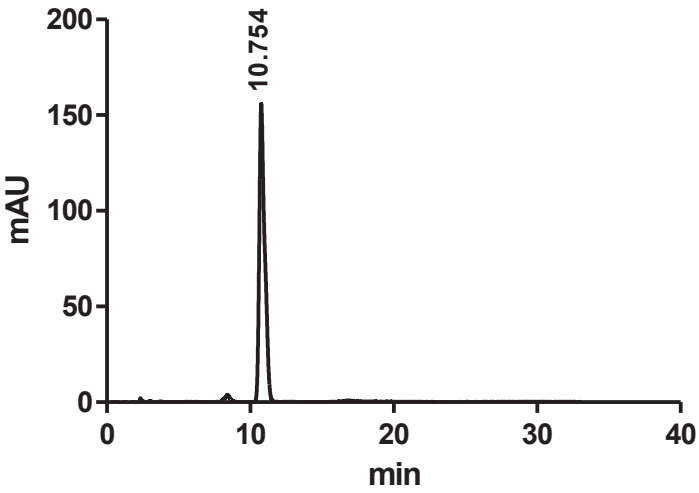

Figure S23. i) ^{1}H NMR spectrum of compound **22**

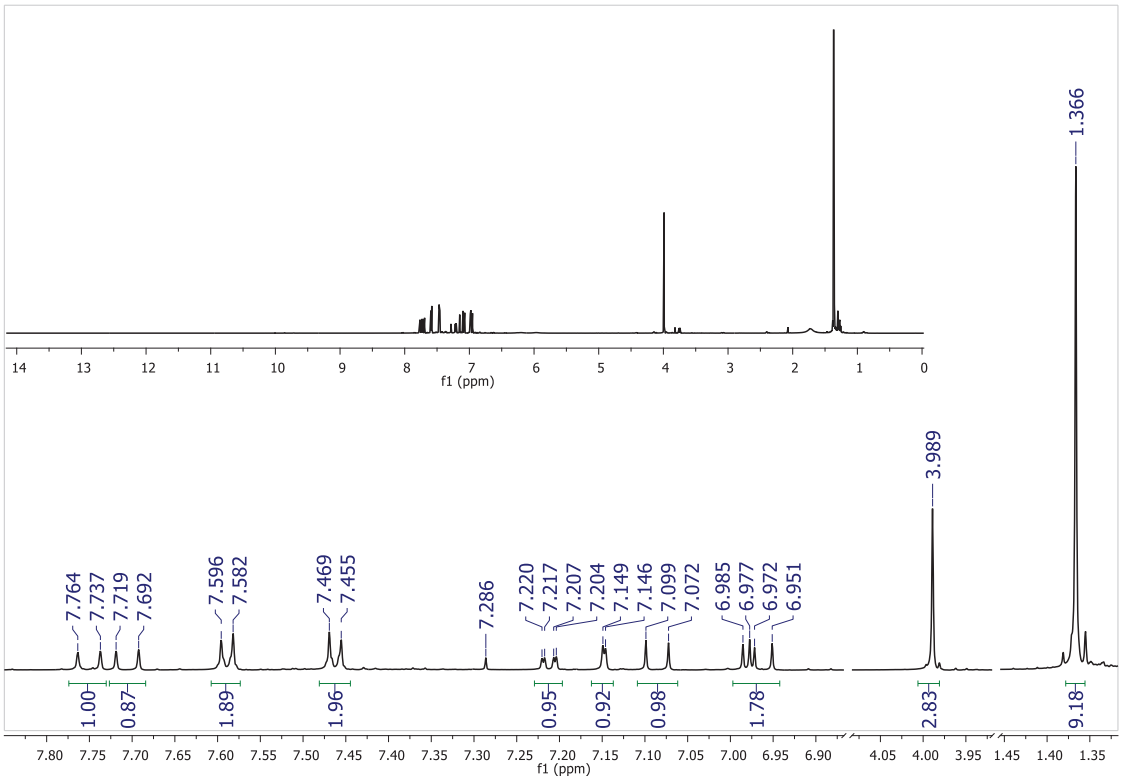

Figure S23. ii) ^{13}C NMR spectrum of compound **22**

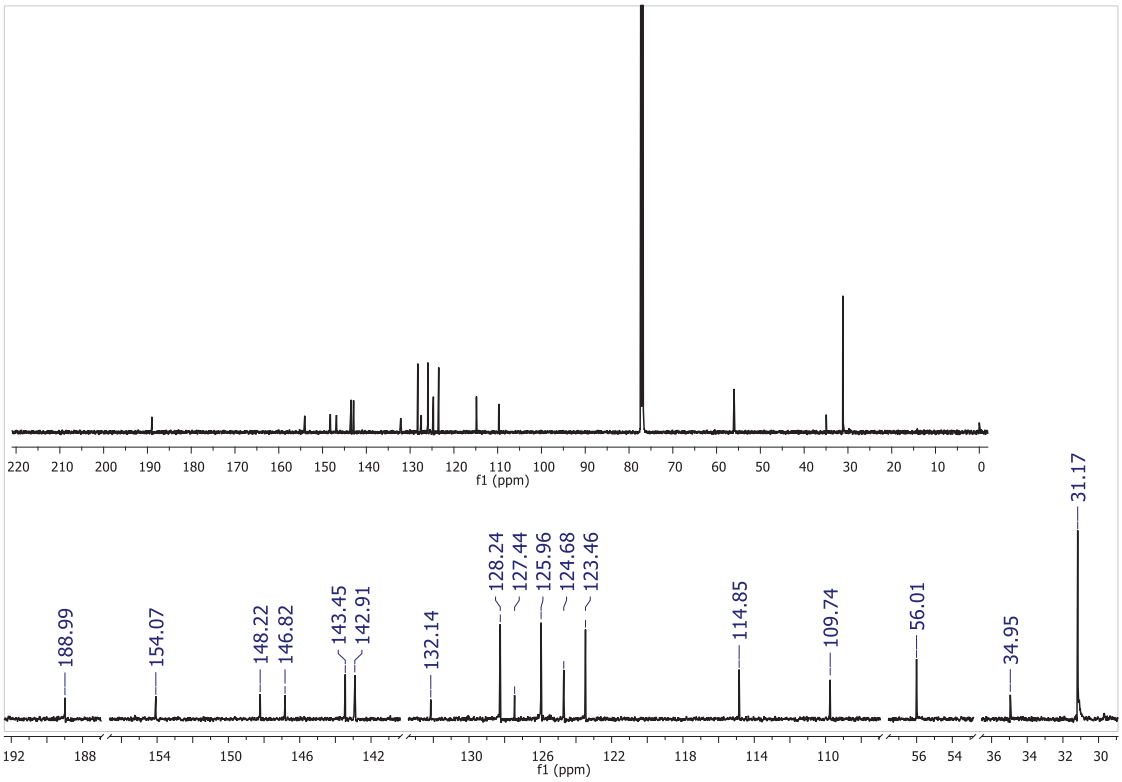

Figure S23. iii) UV-Vis spectrum of compound **22**

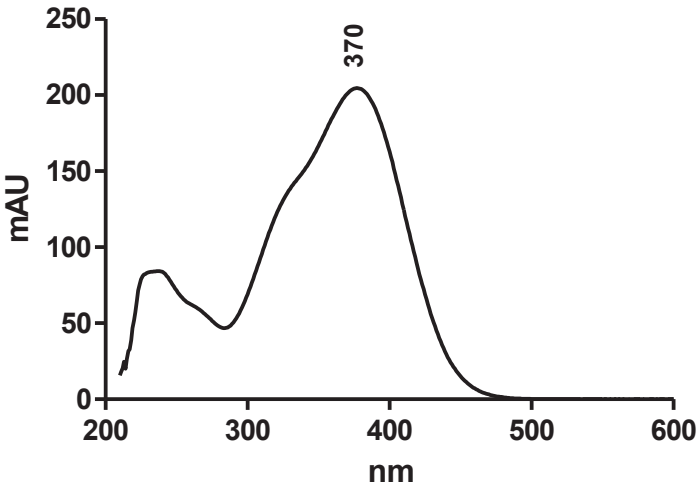

Figure S23. iv) HPLC chromatogram of compound **22**

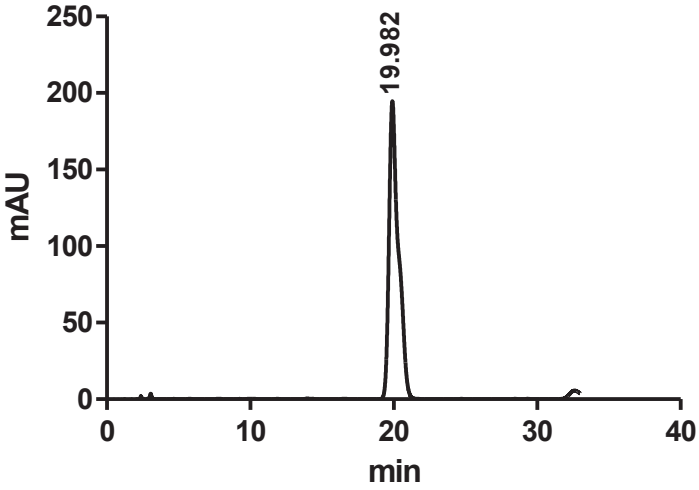

Figure S24. i) ^{1}H NMR spectrum of compound **23**

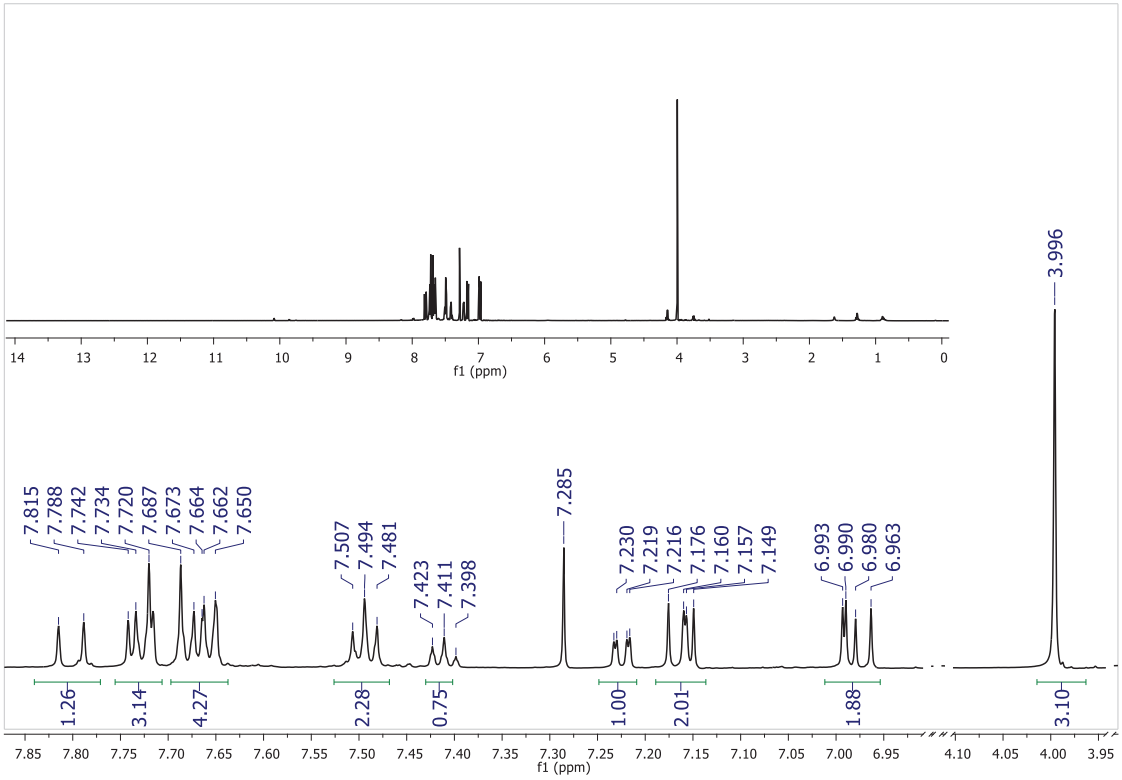

Figure S24. ii) ^{13}C NMR spectrum of compound **23**

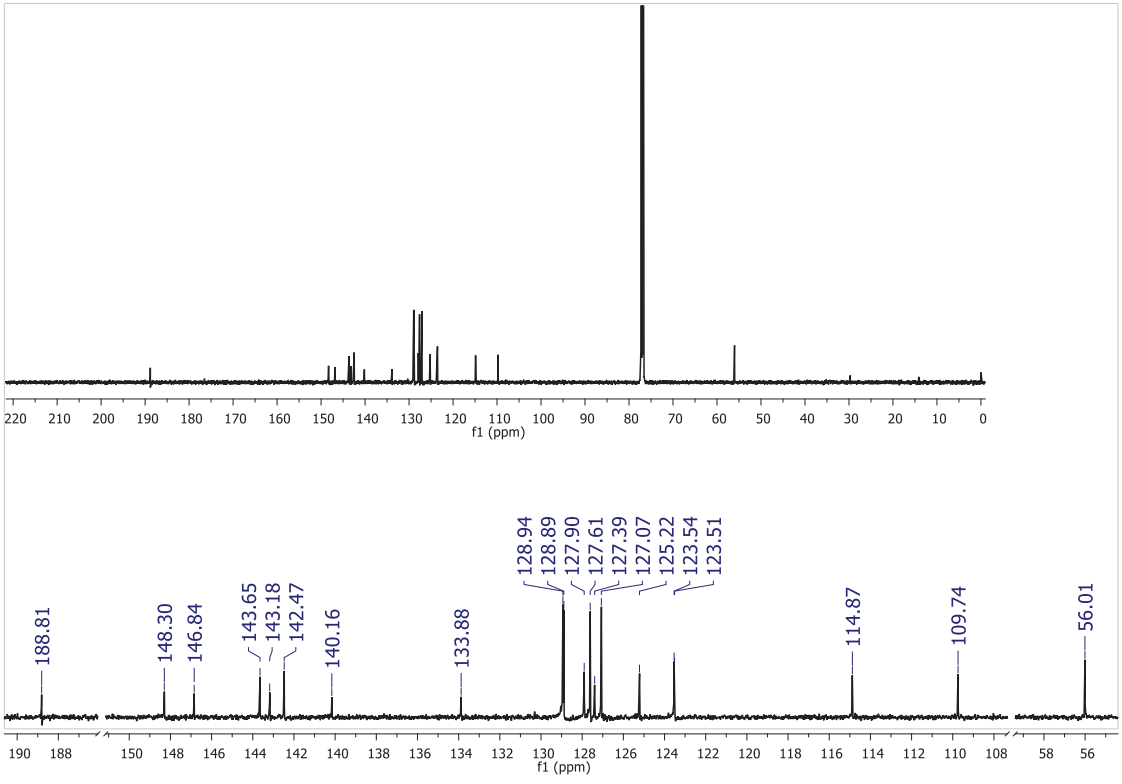

Figure S24. iii) UV-Vis spectrum of compound **23**

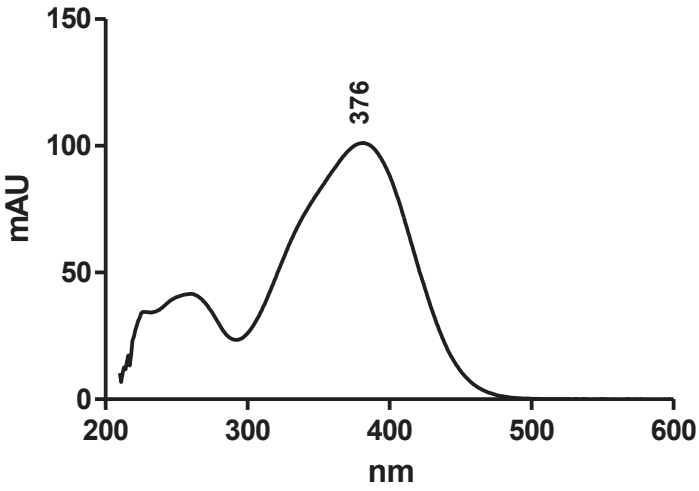

Figure S24. iv) HPLC chromatogram of compound **23**

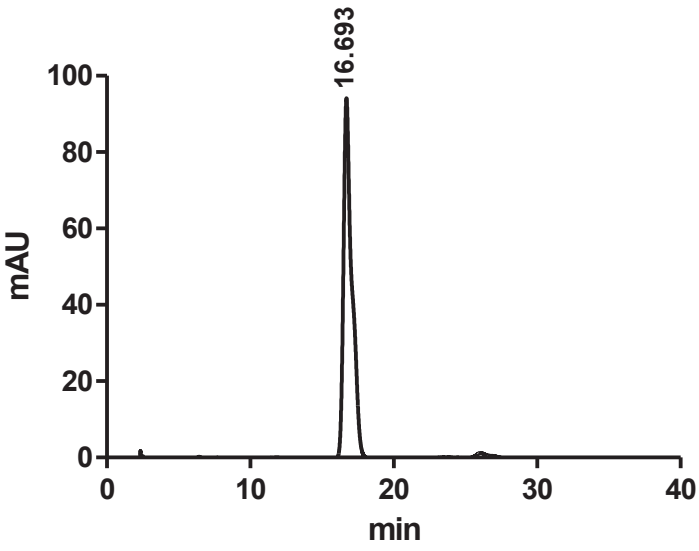

Figure S25. i) ^{1}H NMR spectrum of compound **24**

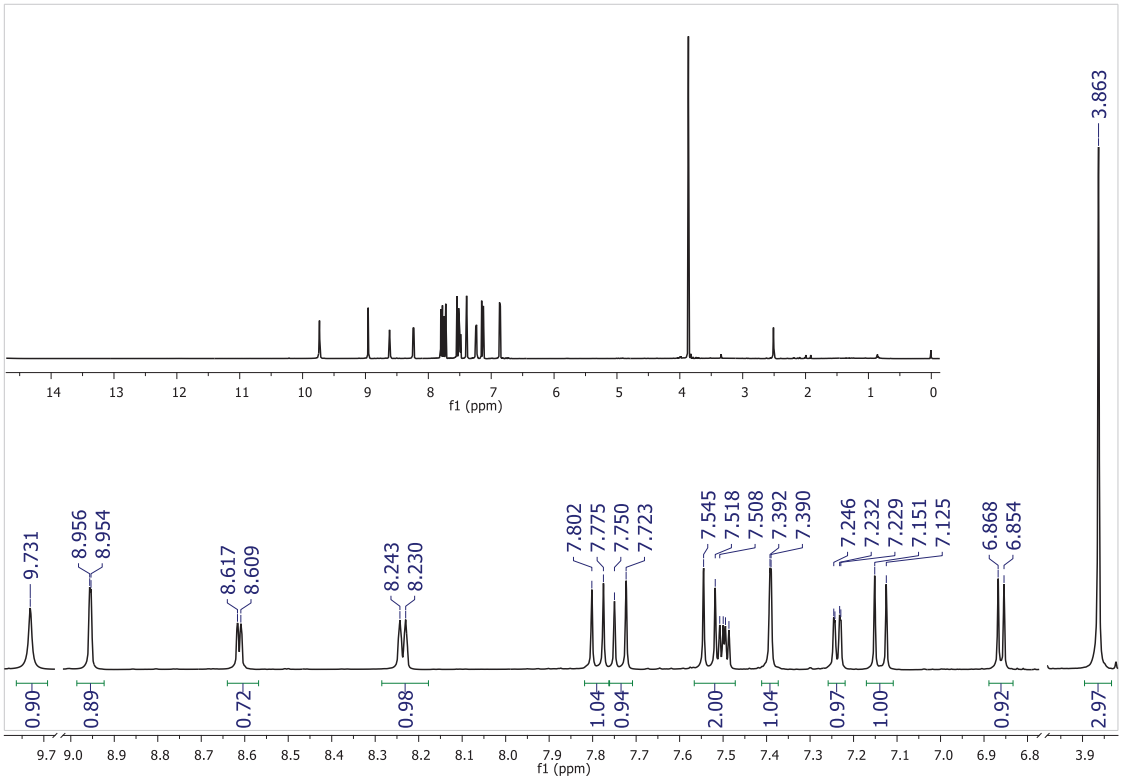

Figure S25. ii) ^{13}C NMR spectrum of compound **24**

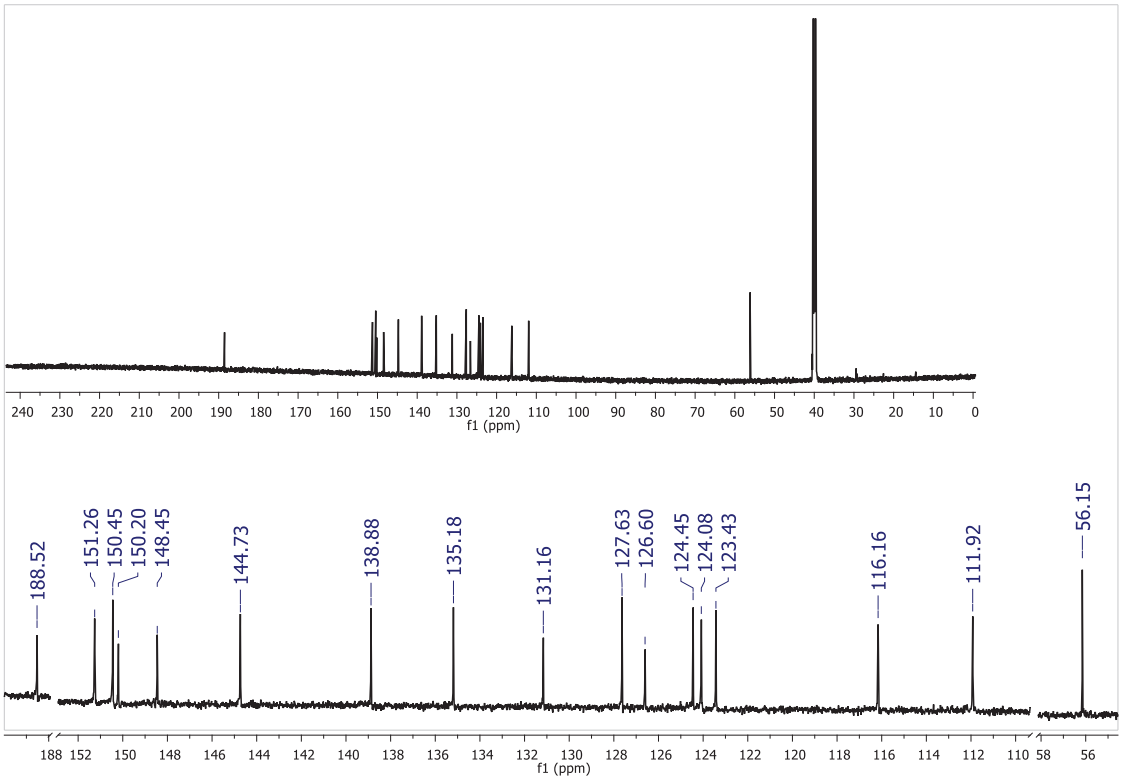

Figure S25. iii) UV-Vis spectrum of compound **24**

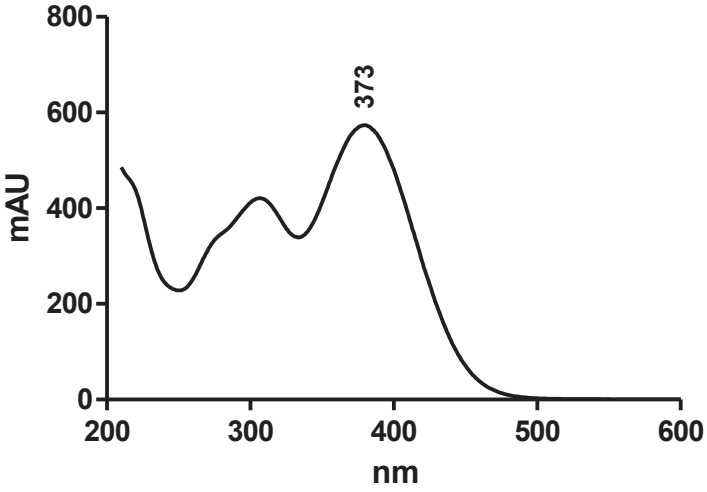

Figure S25. iv) HPLC chromatogram of compound **24**

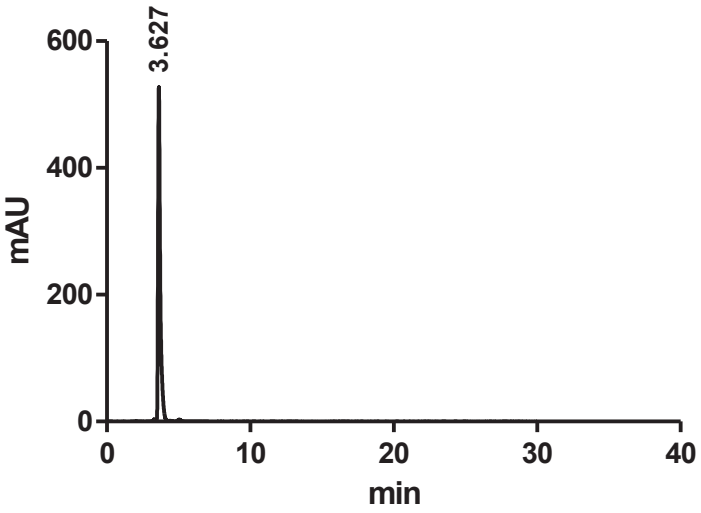

Figure S26. i) ^{1}H NMR spectrum of compound **25**

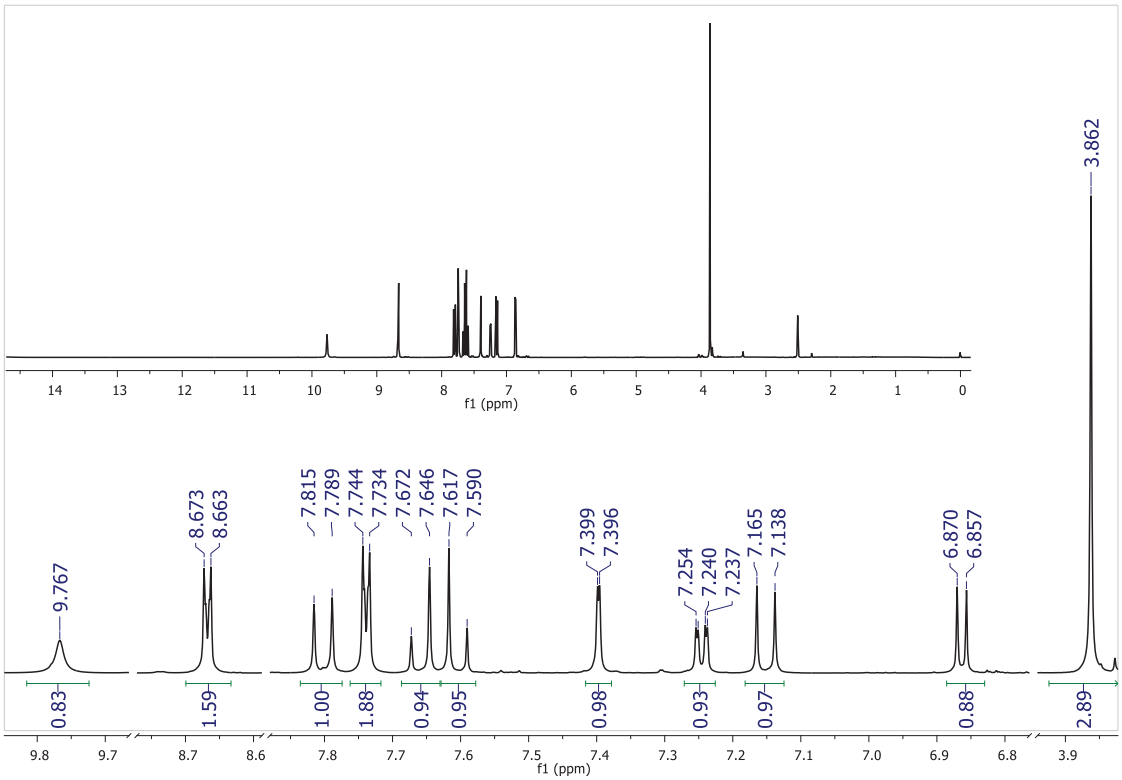

Figure S26. ii) ^{13}C NMR spectrum of compound **25**

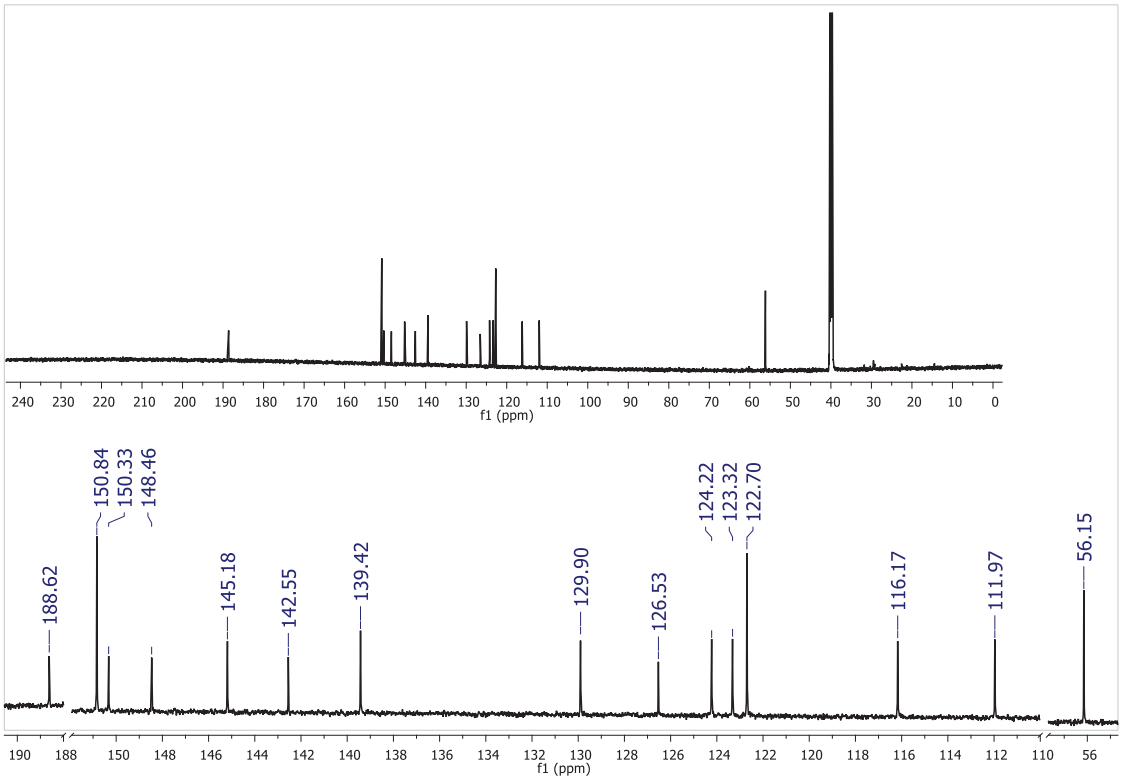

Figure S26. iii) UV-Vis spectrum of compound **25**

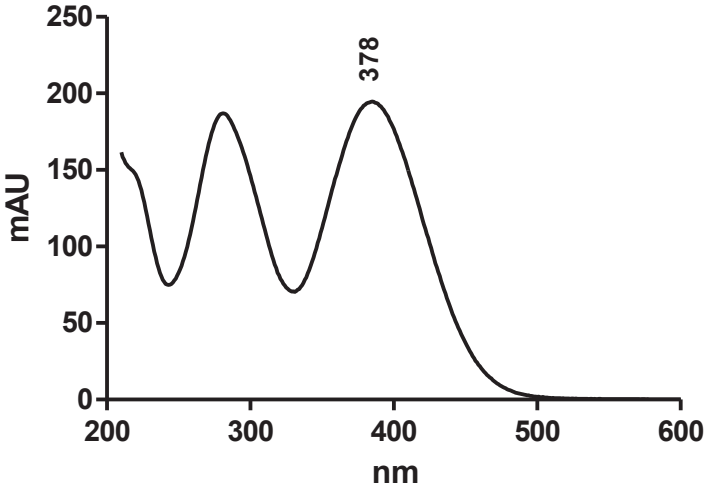

Figure S26. iv) HPLC chromatogram of compound **25**

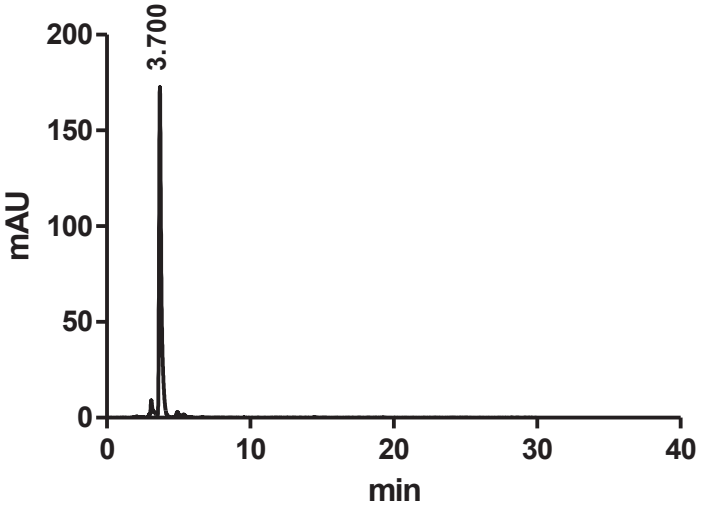

Figure S27. i) ^{1}H NMR spectrum of compound **26**

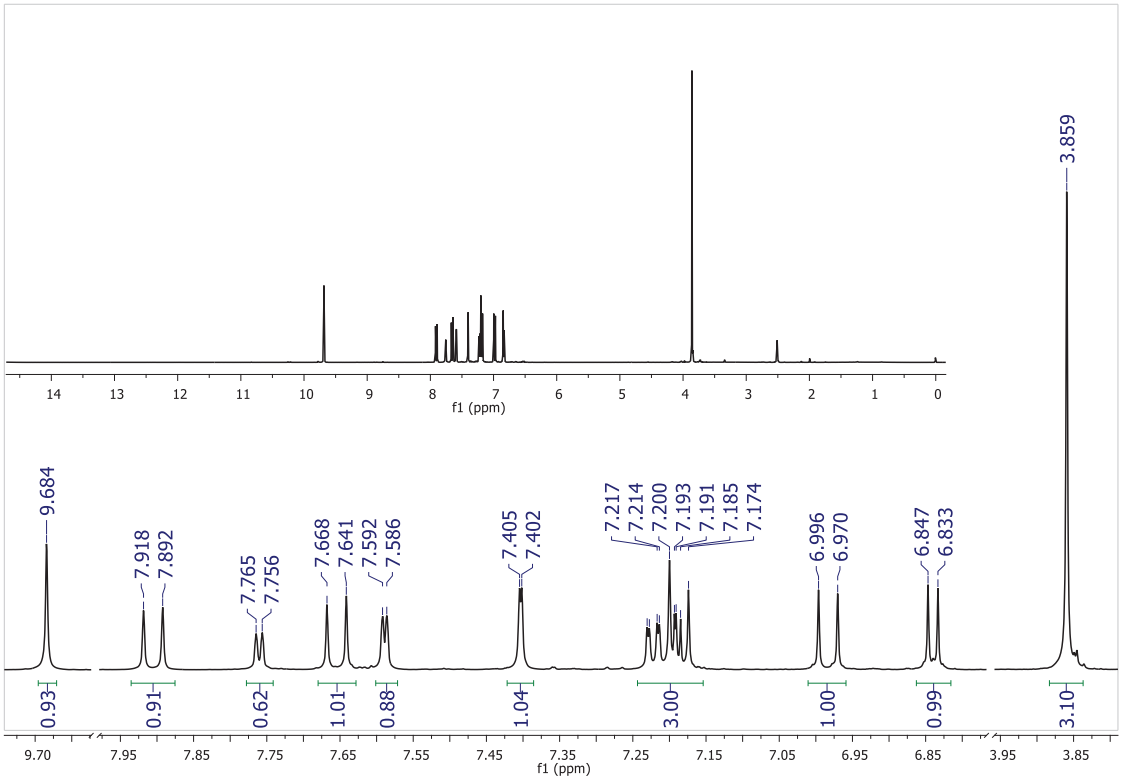

Figure S27. ii) ^{13}C NMR spectrum of compound **26**

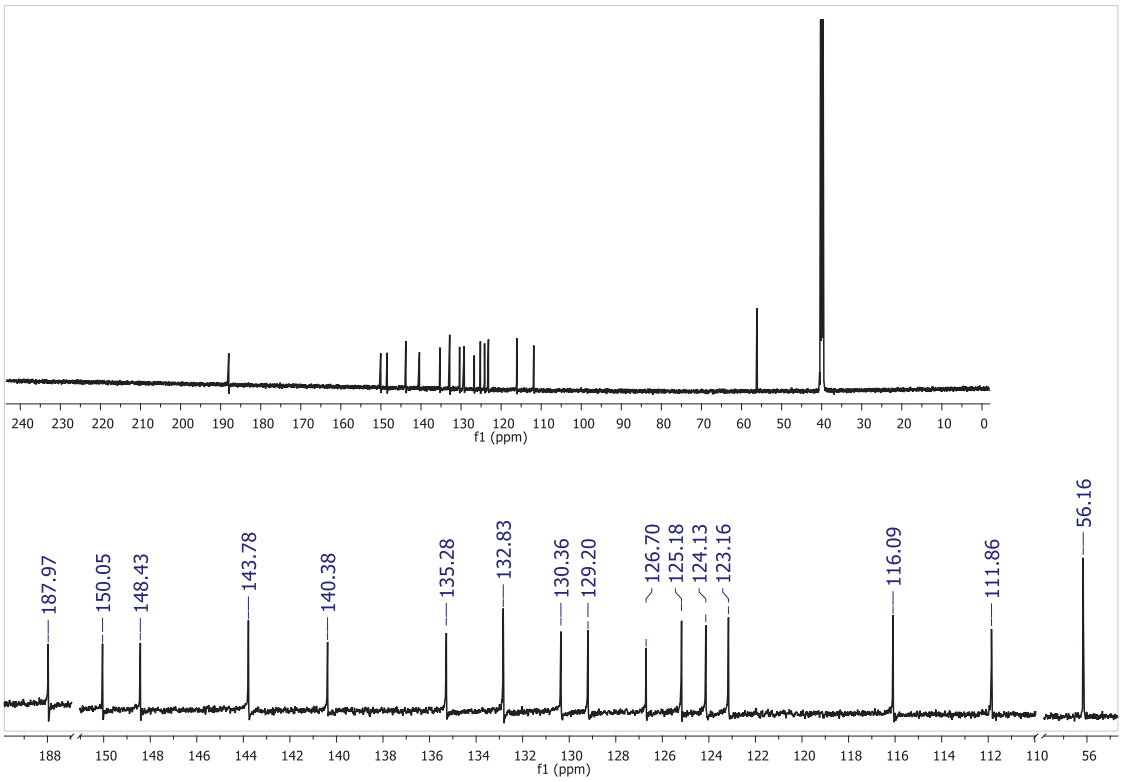

Figure S27. iii) UV-Vis spectrum of compound **26**

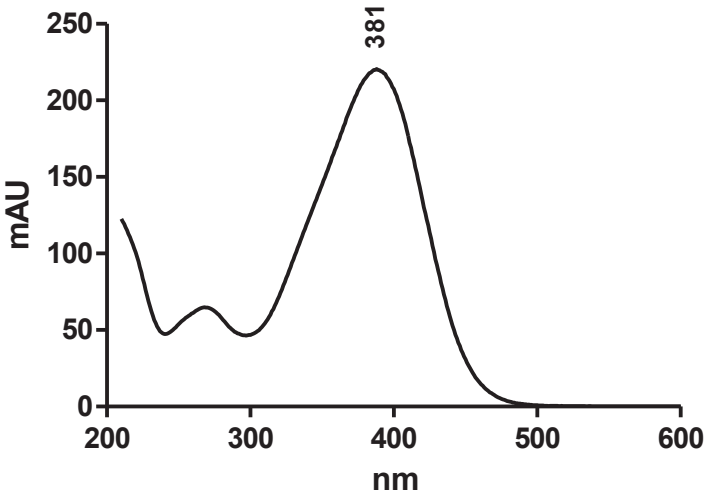

Figure S27. iv) HPLC chromatogram of compound **26**

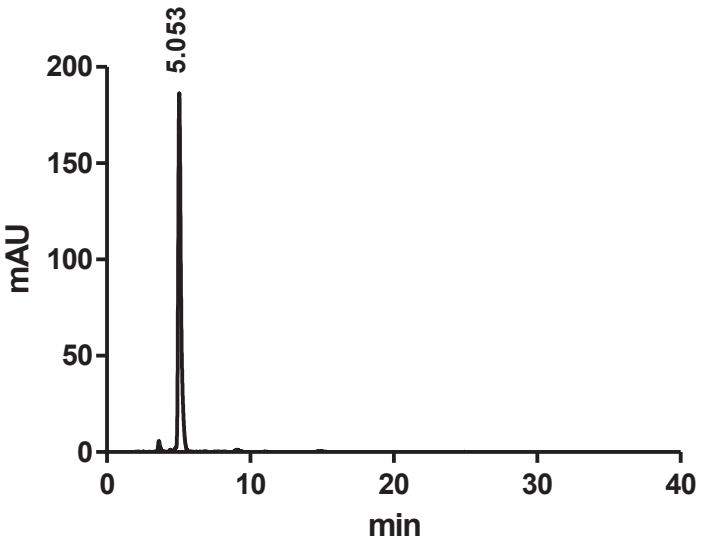

Figure S28. i) ^{1}H NMR spectrum of compound **27**

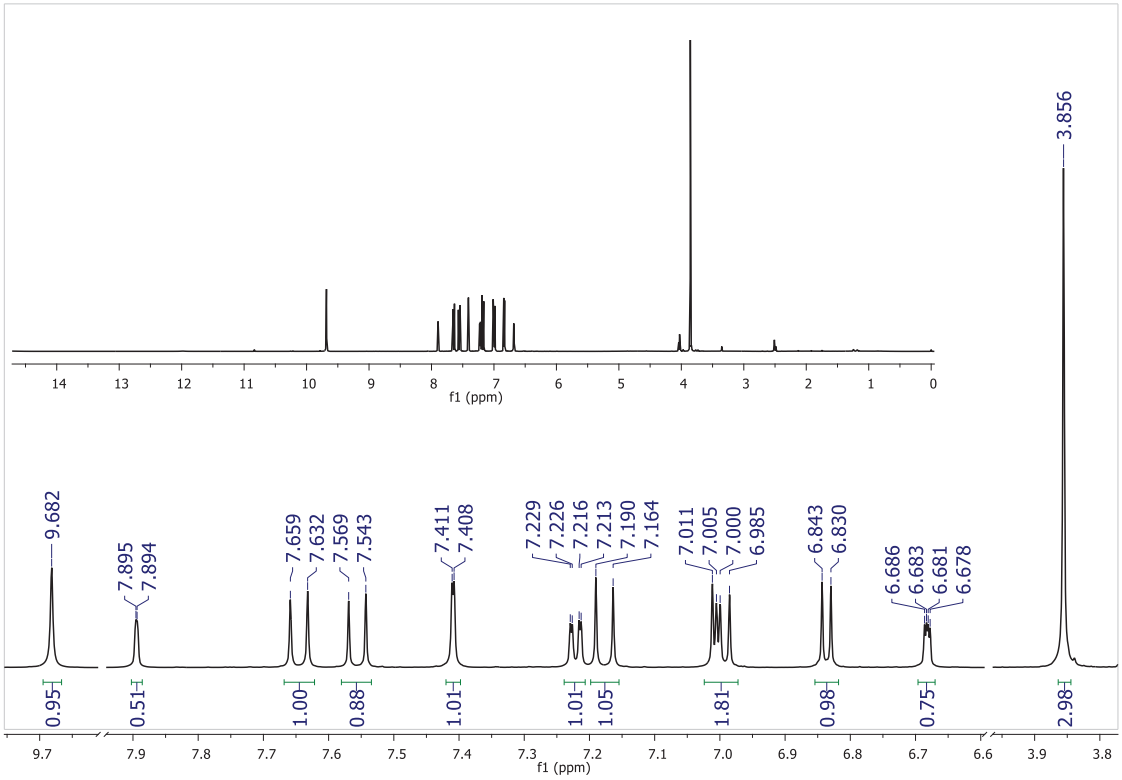

Figure S28. ii) ^{13}C NMR spectrum of compound **27**

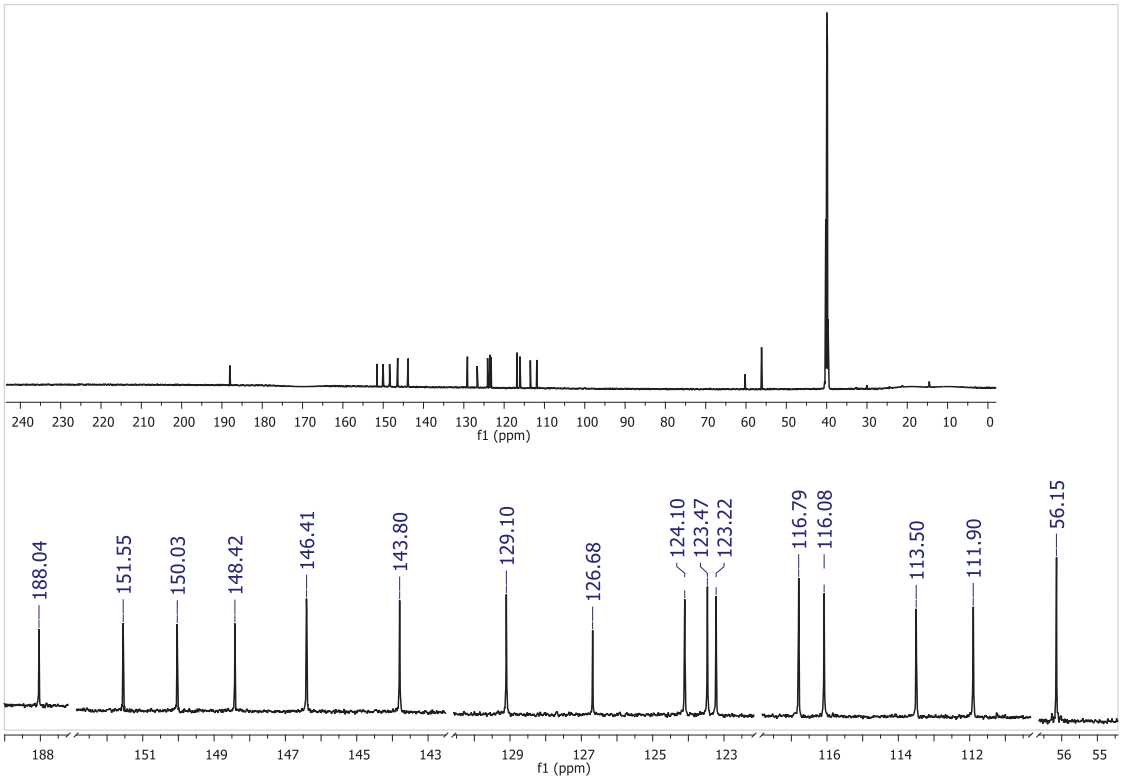

Figure S28. iii) UV-Vis spectrum of compound **27**

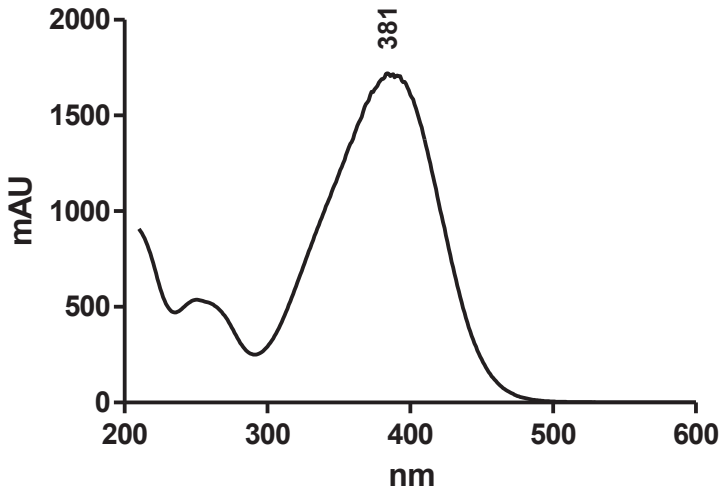

Figure S28. iv) HPLC chromatogram of compound **27**

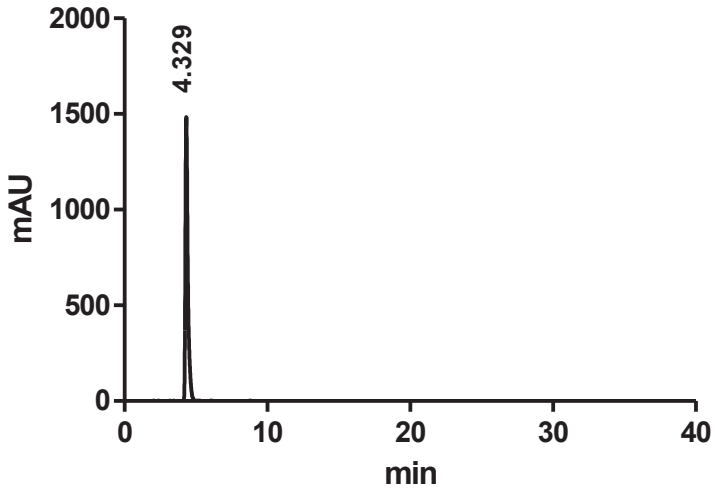

Figure S29. i) ^{1}H NMR spectrum of compound **28**

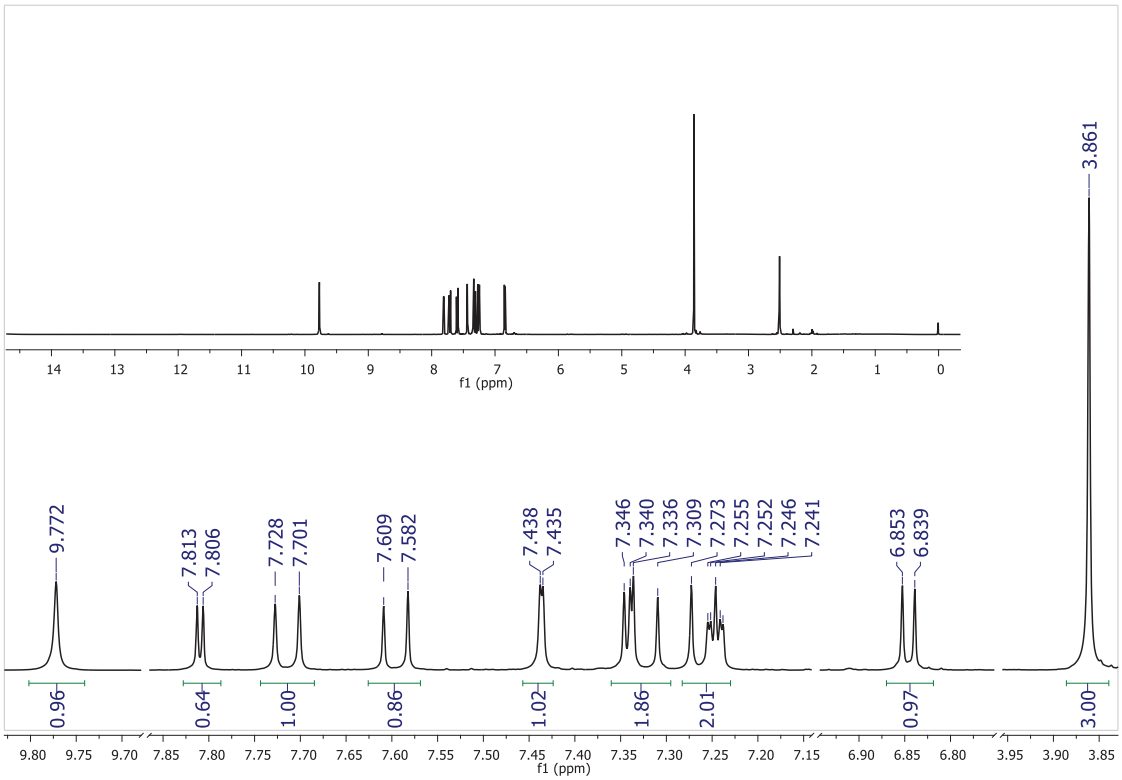

Figure S29. ii) ^{13}C NMR spectrum of compound **28**

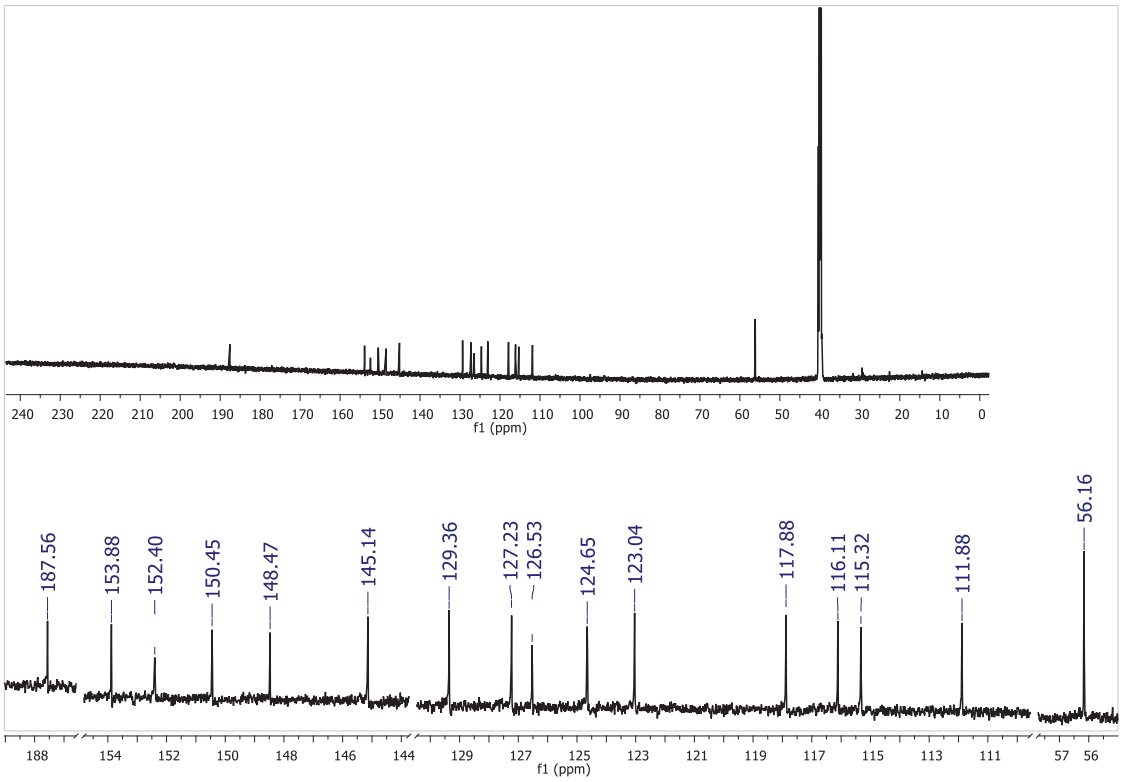

Figure S29. iii) UV-Vis spectrum of compound **28**

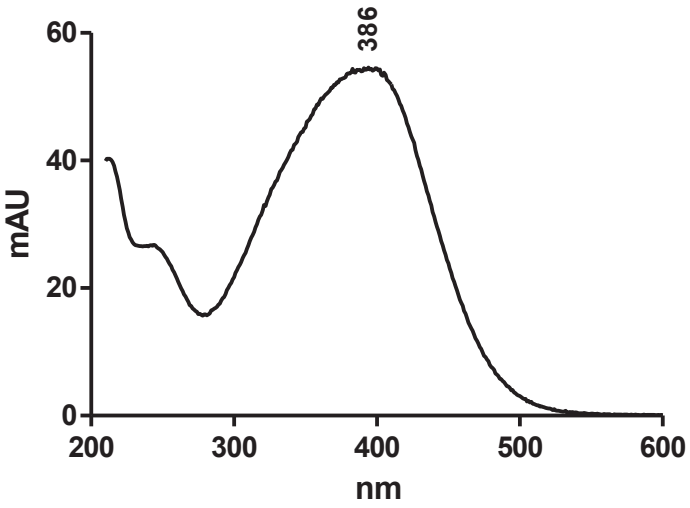

Figure S29. iv) HPLC chromatogram of compound **28**

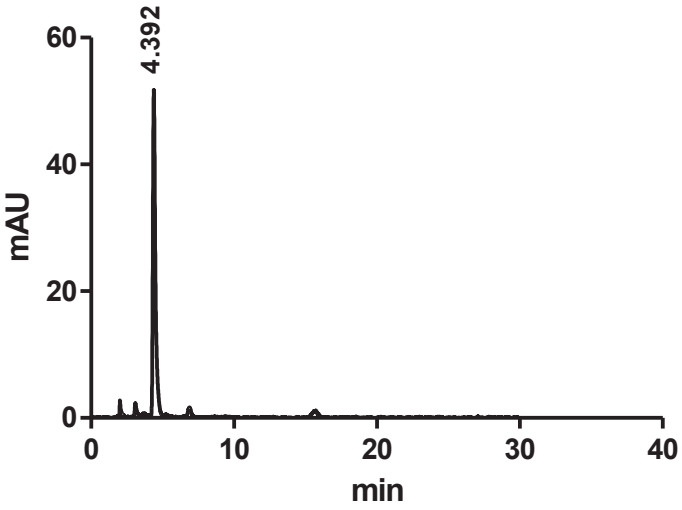

Capítulo III

1. CONCLUSÕES

A) Duas séries de análogos de curcumina com a subunidade β-dicêtonica substituída por um grupo monocarbonílico foram sintetizadas e comprovadas estruturalmente. Enquanto a série I constituiu-se de análogos com o anel B substituído por grupos eletroatratores/eletrodoadores e lipofílicos/hidrofílicos, a série II foi composta por análogos com bioisósteros do grupo fenila (anel B). Os análogos foram obtidos com rendimentos variando de 8 a 90%. As substâncias **3**, **4**, **7**, **12**, **15-18**, **21-23**, **25**, **27** e **28** são inéditas na literatura.

B) A substituição da subunidade β-dicêtonica por um grupo monocarbonílico potencializou o efeito contra *M. tuberculosis* H37Rv. Em relação à série I, os dados ressaltaram a relevância de substituições no anel aromático B por grupos eletroatratores e lipofílicos (log $P_{o/a} \geq 3,0$) bem como da posição dos substituintes para a atividade antimicobacteriana. A comparação dos valores de CIM_{90} das substâncias das séries I e II demonstrou que a presença de heteroátomos e do grupo nitro aumentou a atividade anti-TB contra *M. tuberculosis* H37Rv.

C) De modo geral, os análogos monocetônicos de curcumina demonstraram menor toxicidade e maior seletividade para macrófagos do que fibroblastos de pulmão. Além de apresentar maior atividade antimicobacteriana contra *M. tuberculosis* H37Rv que os demais análogos, a substância **28** foi a mais seletiva para fibroblastos de pulmão e macrófagos.

D) A presença de heteroátomos reduziu a atividade antimicobacteriana contra isolados clínicos de *M. tuberculosis* com resistência a diferentes fármacos anti-TB. A atividade dos análogos **7**, **8**, **13**, **15–17**, **27** e **28** contra três isolados clínicos, inclusive uma cepa XDR, sugeriu que o mecanismo de ação dessas substâncias provavelmente difere dos fármacos utilizados clinicamente no tratamento da TB.

E) O análogo monocetônico de curcumina **28** não apresentou antagonismo com a rifampicina e a moxifloxacina, fármacos de primeira e segunda linha, respectivamente, utilizados na terapia da TB. Além disso, essa substância não demonstrou toxicidade *in vivo* significativa em *G. mellonella*, indicando seu potencial uso seguro em estudos clínicos.

F) Os análogos monocetônicos de curcumina não violaram as regras de Lipinski e Veber e apresentaram alta absorção intestinal *in silico*, sendo potenciais candidatos a fármacos por administração oral. Estudos *in silico* também evidenciaram que essas substâncias penetram com facilidade a barreira hematoencefálica, podendo ser utilizadas no tratamento da meningite tuberculosa.

G) Nosso estudo estabeleceu dados preliminares de relação estrutura-atividade, além de identificar análogos monocetônicos de curcumina como promissores candidatos a fármacos contra a TB.

UNIVERSIDADE ESTADUAL PAULISTA
"JÚLIO DE MESQUITA FILHO"
Campus de São José do Rio Preto

TERMO DE REPRODUÇÃO XEROGRÁFICA

Autorizo a reprodução xerográfica do presente Trabalho de Conclusão, na íntegra ou em partes, para fins de pesquisa.

São José do Rio Preto, 25 / 02 / 2019

Gabriela M. Ayusso

Gabriela Miranda Ayusso